Proceedings of

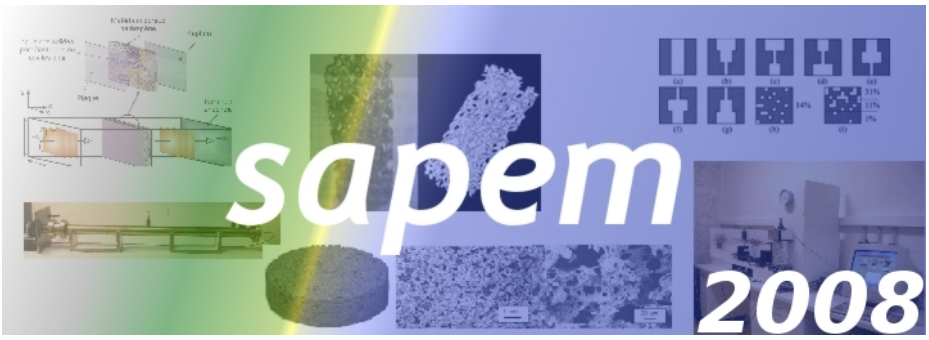

Symposium on the Acoustics of Poro-Elastic Materials

December 17-18-19, 2008

hosted by University of Bradford, UK

Collected by K. Horoshenkov, L. Jaouen, F-X. Bécot

Temperature- and frequencydependence of the elastic properties of porous materials

Jan Descheemaecker, Laurens Boeckx(*), Walter Lauriks
Laboratorium voor Akoestiek en Thermische Fysica, K.U.Leuven, Belgium
(*) Huntsman Polyurethanes, Everberg, Belgium

1 Introduction

The last decades, a lot of research has been done about the propagation of sound in heterogeneous and porous materials. Especially the two-phase nature of the poro-elastic material leads to interesting physical phenomena. During recent year, several measuring methods have been developed to determine the material parameters.
However, a lot of problems aren't solved yet. Because of the visco-elastic behavior of a lot of these materials, the elastic moduli will become frequency dependent (rubberlike behavior at low frequencies and glasslike behavior at high frequencies). Experimental data about the frequency- and temperature dependence of the elastic moduli are scarce because of experimental difficulties. Some results about this subject will be presented in this paper.

2 Measurement method: the burst method

2.1 Measurement setup

The most important elements of the measurement setup are the laser Doppler vibrometer (which will serve as a detector for the displacements caused by the Rayleigh wave), a magnetic transducer (which is used as a source) and a function generator. A detailed description of the measurement setup can be found in [BOE-05]. This whole setup is placed in a temperature-controlled chamber. The setup is showed in figure 1.

Figure 1: Schematic view of the experimental setup of the burstmethod.

2.2 Experimental determination of the phase velocity and damping

The phase velocity and damping of a wave can be determined by detecting the wave at various distances of the source. The phase velocity is the slope of the curve which is obtained by plotting the distances as a function of the arrival times. From the phase velocity, elastic moduli like the shearmodulus can be determined. The entire setup in mounted in a temperature controlled chamber, which allows to obtain data from -40°C to +50°C. The damping can be determined by taking into account that the amplitude decreases with $1/\sqrt{r}exp(\Im(k_R))$, when the distance r to the source increases. A detailed description of the determination of the phase velocity and damping can be found in [BOE-05].

3 Experimental results

In this section, some experimental results about the frequency- and temperature dependence of the elastic moduli will be showed for a porous material. The sample used in this study was Urecom ([DES:07], material of recticel). In figure 2, the phase velocity and damping are shown as a function of the temperature for 2, 3 and 4 kHz.
Globally, when the temperature decreases, the phase velocity increases. At certain temperatures, there is a huge increase in the phase velocity. Obviously, when this happens, there is a peak in the damping at the same temperature. When the frequency increases, this peak shifts to higher temperatures.

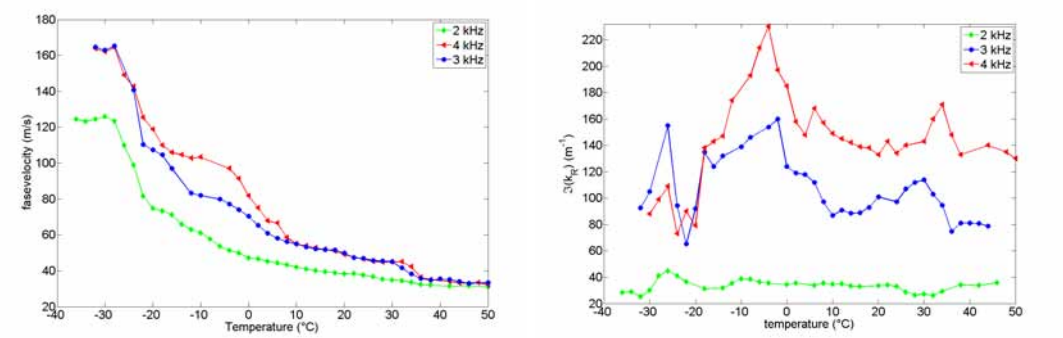

Figure 2: Pase velocity and damping of Urecom as a function of temperature at different frequencies.

The left graph in figure 3 shows the phase velocity as a function of frequency for different temperatures. The full lines are numerical fits of the experimental data taking in account the full Biot theory. From these fits, the shear modulus can be determined (right figure). Numerical simulations show that with a frequency independent shear modulus, the A_0-mode should be in the Rayleigh regime above 1 kHz. But the experimental data show that this isn't the fact. The phase velocity continues to increase and becomes constant at higher frequencies. For some temperatures (for example $0°C$) the phase velocity is constant in a certain frequency domain, and then increases with higher frequencies. This shows that for all the temperatures in figure 3, the material is visco-elastic. The same measurements were done for higher temperatures until $50°C$. Also there the experimental data can only be fitted with a frequency dependent shear modulus. Again, at the temperatures where there is a sudden increas in fasevelocity, a peak in the damping was observed. When the temperature is decreased, this peak shifts to lower frequencies.

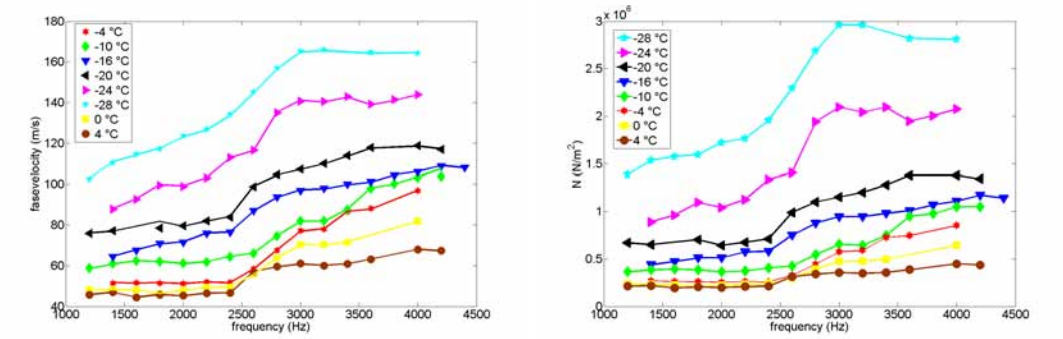

Figure 3: Phase velocity (left) and shear modulus (right) as a function of frequency at different temperatures.

4 References

[BOE-05]: L. Boeckx, "Study of the sound field in and above porous materials-application to characterization of sound absorbing materials",(PhD thesis K.U.Leuven,2005,http://www.kuleuven.ac.be/doctoraatsverde
[BOEb-05]:L. Boeckx, P. Leclaire, P. Khurana, C.Glorieux, W. Lauriks and J.F. Allard, "Guided elastic waves in porous materials saturated by air in Lamb conditions," Accepted for publication in J. Appl. Phys. (2005).
[BOEb-05]: L. Boeckx, P. Leclaire, P. Khurana, C. Glorieux, W. Lauriks and J.F.Allard, "Investigation of the phase velocities of guided acoustic waves in soft porous layers," J.Acoust. Soc. Am., 117, 545-554, (2005).
[DES:07]: J. Descheemaeker, "Oppervlakte en geleide golven in poro-elastische materialen", (Master thesis K.U.Leuven,2007).

Prediction of scattering effects on sound propagation in rigid porous media

C. Boutin

Université de Lyon -Ecole Nationale des Travaux Publics de l'Etat
Laboratoire Géomatériaux - Département Génie Civil et Bâtiment - URA CNRS 1652
Rue M. Audin, 69518 Vaulx-en -Velin Cedex- France.
claude.boutin@entpe.fr

The homogenisation method of periodic media [2, 4, 5, 12] is a multi-scale asymptotic method that enables to determine the macroscopic description from the knowledge of the physics at the microscopic level. By principle, this approach applies provided that a sufficiently good scale separation between macro and micro scale is fulfilled. For this reason, the homogenization procedure is generally restrained to the first significant term that defines the equivalent continuum behaviour. In the case of poor scale separation the macroscopic continuum description has to be enriched by the next order terms that induce non-local effects, see [6] for elastostatic case. For mechanical waves in elastic composite materials [7] it was shown that the so-derived correctors properly describe the Rayleigh scattering. A similar approach was applied to diffusive thermal waves in [8]. Recently, the Darcy's law correctors have been established in [3] for permanent flow and in acoustic regime [9].

These works prove that high order homogenization is an efficient tool to investigate long waves scattering in complex situations where no simplified assumptions can be used. This is the case of acoustic waves in porous media since the intrinsic features of such materials, make inefficient the usual scattering approach for several reasons:

- the strong contrast of properties between fluid and skeleton avoid the simplifying assumptions of quasi-homogeneous material to be used.
- the finite porosity makes irrelevant the simplified modelling based on a weak concentration of heterogeneity,
- the coupling between elastic, viscous and thermal effects induce significant differences with purely elastic or diffusive cases.

In this paper, the Rayleigh scattering of acoustic waves in noise absorbing materials, i.e. made of rigid porous media saturated by air, is investigated. At the pores scale the physics is governed by both mass and heat transfer:

- the harmonic gas motion is governed by the linearized Navier-Stokes equation,
- the heat flux (between gas and isotherm skeleton) is driven by the Fourier equation.

Following the homogenization method, these balance equations are rescaled to describe the frequency range where the viscous and thermal layers are of the order of the pore size, d. Variables are looked as asymptotic expansions according to the scale ratio, $\varepsilon = 2\pi d/\lambda$, where λ is the wavelength. The resolution is performed up to the second order terms.

When the homogenization process is limited to the zero order approximation, the Biot-Allard modelling, [1], is recovered. This modelling, characterized by dynamic permeability and compressibility, captures the main physical effects when the wavelength is significantly larger than the characteristic pore size, ($\varepsilon << 1$). This description leads to a single acoustic wave (similar to the second compressional Biot wave, P_2) presenting a strong frequency dispersion, from a diffusive wave at low frequency, to a damped propagation wave at high frequency.

In the Rayleigh domain, i.e., when focusing on poor scale separation ($\varepsilon < 1$), scattering phenomena occurs and the modelling have to be improved by the first and second order terms.

The corresponding balance equations show that the pressure field of zero order creates a homogenized force density (source) of first order, which induces, in turn, a field of first order. These two fields, through a similar process produce a volume force that radiates a field of order 2, and so on. The correctors involve second and third pressure gradient (i.e. a non-local effect), and tensors (^{i}K, $^{i}\Pi$) depending on the microstructure and the frequency. It is demonstrated that the first order pressure perturbation vanishes, so that the actual corrector is of the order of ε^2. Thus, the enhanced continuum description reads, with usual notations for velocity V, pressure P, temperature T, angular frequency ω, porosity Φ :

$$\mathrm{div}(V^0) + (i\omega\Phi)[P^0/P^e - T^0/T^e] = 0 \quad ; \quad \mu V^0 = -\,{}^0K.\nabla P^0$$
$$; \quad T^0/T^e = {}^0\Pi P^0/P^e$$

$$\mathrm{div}(V^1) + (i\omega\Phi)[-T^1/T^e] = 0 \quad ; \quad \mu V^1 = -\,{}^1K.\nabla\nabla P^0$$
$$; \quad T^1/T^e = {}^1\Pi\nabla P^0/P^e$$

$$\mathrm{div}(V^2) + (i\omega\Phi)[P^2/P^e - T^2/T^e] = 0 \quad ; \quad \mu V^2 = -\,{}^0K.\nabla P^2 - {}^2K.\nabla\nabla\nabla P^0 + (i\omega\mu\Phi/P^e)^2N.\nabla P^0$$
$$T^2/T^e = {}^0\Pi P^2/P^e + {}^2\Pi\nabla\nabla P^0/P^e$$

Using this improved description, the scattering perturbation (in term of velocity and damping) can be derived for any kind of wave. Focusing on plane wave, it is demonstrated that the frequency dependence of the correction is rather complex due to the dispersion of the P_2 wave. As an example, the case of an anisotropic medium made of periodic slits is treated analytically. It clearly shows the anisotropy of the scattering effect, and provides the velocity correction (which may reach 10% in realistic cases) in both diffusive and propagation ranges.

Finally the validity range of this modelling is discussed and the interest for practical applications and explanations of observed deviation between experiments [10] and modelling [11], is evoked.

[1] Allard J.F. 1993. *Propagation of Sound in Porous Media. Modelling Sound Absorbing Materials*, Chapman & Hall, London.

[2] Auriault J.L., 1991. *Heterogeneous medium. Is an equivalent macroscopic description possible?* Int. J. Engng Sci. 29(7): 785-795.

[3] Auriault J.L.,Geindreau C., Boutin C., 2005. *Filtration law in porous media with poor scale separation*. Transport in Porous Media. (60): 89-108

[4] Bakhvalov N., Panasenko G., 1989. *Averaging processes in periodic media. Mathematical problems in mechanics of composite materials*. Kluwer Academic Dordrecht.

[5] Bensssoussan A., Lyons, J.L., Papanicolaou G., 1978. *Asymptotic methods in periodic structures*. North-Holland Amsterdam.

[6] Boutin C., 1996. *Microstructural effect in elastic composite*. Int. J. Solids Structures, 33(7): 1023-1051.

[7] Boutin C., Auriault J.L., 1993. *Rayleigh scattering in elastic composite materials*, Int. J. Eng. Sci., 31(12): 1669-1689.

[8] Boutin C., 1995. *Microstructural influence on heat conduction*. Int. J. Heat Mass Transf., 38(17): 3181-3195

[9] Boutin C., 2007. *Rayleigh scattering of acoustic waves in rigid porous media*. J.A.S.A., 122 (4): 1888-1905.

[10] Leclaire P., Kelders L., Lauriks W., Allard J.F., Glorieux C., 1996. *Ultrasonic wave propagation in reticulated foams saturated by different gases : High frequency limit of the classicial models*. Appl. Physic. letter 69. 18, 2641-2643

[11] Tournat V., Pagneux, V. Lafarge D., Jaouen L. , 2004. *Multiple scattering of acoustic waves and porous absorbing media*. Physical Review E. 70, 026609:1-9

[12] Sanchez Palencia, E. 1980. *Nonhomogeneous media and vibration theory*, Lectures notes in Physics, 127, Berlin: Springer-Verlag.

Experimental study on transmission loss of MPP structures with the air-layer-subdivision technique

M. Toyoda[a] and D. Takahashi[b]
[a]Pioneering Research Unit, B104, Kyoto Univ. Katsura, Nishikyo-ku, 615-8530 Kyoto, Japan
[b]Dept. of Urban and Environmental Eng., C1-4-352, Kyoto Univ. Katsura, Nishikyo-ku, 615-8540 Kyoto, Japan
masahiro.toyoda@kupru.iae.kyoto-u.ac.jp

1 Introduction

A microperforated panel (MPP) was first proposed by Maa [1] and it is now recognized as one of the next-generation sound-absorbing materials. In order to develop a further possibility of a MPP, its sound insulation characteristics were studied theoretically by the authors [2]. It was shown that the insulation performance of a typical MPP structure is not much greater than that of the back wall alone at mid frequencies. However, it was also shown that inserting a partition like honeycomb structure into the air cavity can significantly improve the performance. This air-layer-subdivision technique can create local one-dimensional sound fields in each of the subdivided cells and lead to normal incidence of sound wave into the orifices, which is the most effective condition for Helmholtz-type resonance absorption. However, in the theoretical model proposed by authors, some assumptions and simplifications have been made, and therefore, it should be validated. In this study, some experiments were performed by using a reverberation box and the practical effects of the air-layer-subdivision technique are investigated.

2 Experimental setup

A schematic diagram of the experimental apparatus is shown in Fig. 1. The reverberation box has the opening of dimensions 0.35 m × 0.45 m. Five kinds of samples shown in Fig. 2 were installed at the opening. The sample (a) is composed of a non-perforated panel alone as reference. The panel is made of acryl and the thickness is 1.0 mm. The sample (b) consists of a MPP and an acryl non-perforated panel of thickness 1.0 mm with a cavity of depth 60 mm. Parameters of the MPP, made of acryl, are as follows: the thickness is 0.5 mm; the aperture diameter is 0.5 mm; the distance between apertures is 5.0 mm. As for the sample (c), a paper honeycomb of depth 60 mm was inserted into an air cavity of the same configuration as the sample (b). It means that the subdivision technique is applied to the sample (c). Effects of the subdivision technique depend on whether the partition is glued to the panels or not. In sample (c), the honeycomb was located with slight spaces between the honeycomb and both of two panels so as to avoid stiffening those panels and also avoid the mechanical propagation of vibration. The cell size of the honeycomb is 10 mm, which is sufficiently smaller than one-half wavelength at 8 kHz. The subdivision technique with gluing is applied to the sample (d). A MPP, a paper honeycomb, and a non-perforated panel, which have the same properties as the sample (c), were glued tightly. In this case, the mass and the rigidity are different from those of the samples (a), (b), and (c). Therefore, in order to extract the effects of the subdivision technique, sample (e) was prepared as reference only for evaluation of the sample

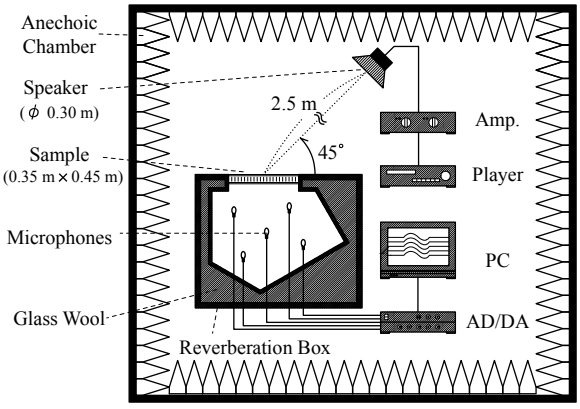

Fig. 1 Experimental setup for measurement of TL.

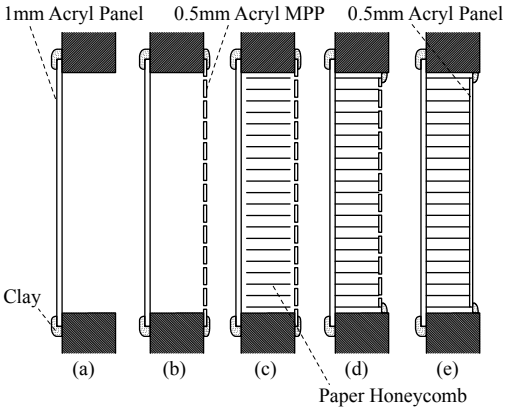

Fig. 2 Five kinds of experimental samples.

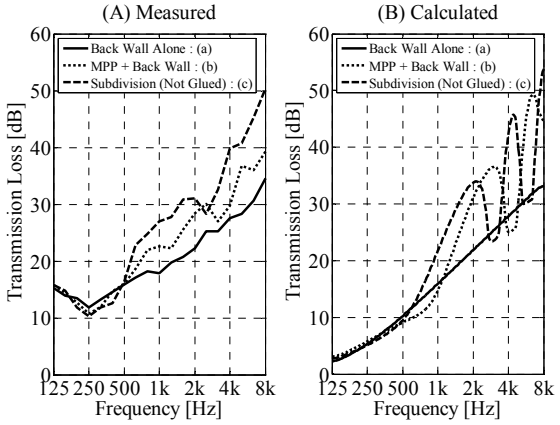

Fig. 3 Results for the cases (a), (b), and (c).

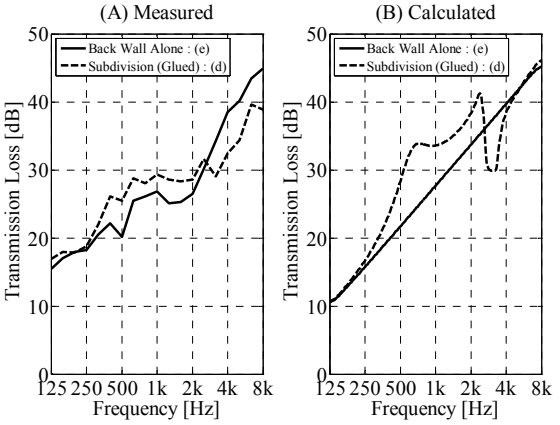

Fig. 4 Results for the cases (d) and (e).

(d). The sample (e) is composed of a paper honeycomb and two acryl non-perforated panels of thicknesses 0.5 mm and 1.0 mm. They were glued tightly so that the sample has almost the same mass and the same rigidity as the sample (d). The incident angle considered here is 45° direction. Pink noise was used for the source signal and spatially averaged sound pressure levels over each 1/3-octave band were measured from five microphones in the reverberation box. To obtain transmission loss, the incident sound pressures at the points, where the samples were supposed to be located, were also measured without both the box and the samples. Transmission loss was obtained from those sound pressures with correction for background noises and reverberation times for each 1/3-octave band.

3 Results

Figure 3 shows the experimental and theoretical results of transmission loss for the samples (a), (b), and (c). The theoretical results are calculated with the infinite-plate model. For the case of the sample (a), the experimental results of transmission loss basically follow the mass law. As for the sample (b), the insulation performance is greater than that of the sample (a). Furthermore, that of the sample (c) is even greater due to the subdivision technique without gluing. Figure 2 shows the experimental and theoretical results for the samples (d) and (e). In comparison between them, adverse effects above 3 kHz can be seen in both theoretical and experimental results. These adverse effects would be caused by resonances in each cell. However, transmission loss from 300 Hz to 3 kHz can be improved by the subdivision technique with gluing. The frequency range where improvement can be obtained is rather lower compared with the subdivision technique without gluing.

4 Conclusion

The characteristics of the experimental results are in good agreement with the theoretical ones. It is shown that the subdivision technique has the practical effects for improving the transmission loss at mid frequencies and its characteristics can be changed by gluing or not. The wide use of these structures for both sound insulation and sound absorption is anticipated.

Acknowledgments

This study was supported by Program for Improvement of Research Environment for Young Researchers from Special Coordination Funds for Promoting Science and Technology (SCF) commissioned by the Ministry of Education, Culture, Sports, Science and Technology (MEXT) of Japan.

References

[1] D. Y. Maa, “Theory and design of microperforated panel sound-absorbing constructions,” *Scientia Sinica* **18**, 55-71 (1975)

[2] M. Toyoda and D. Takahashi, “Sound insulation characteristics of a microperforated panel with a subdivided air layer,” *Proc. of 19th ICA 2007*, RBA-08-006-IP (2007)

Modelling acoustical heterogeneous materials composed of porous inclusions

E. Gourdon[1], M. Seppi[2]

[1]DGCB - URA CNRS 1652
ENTPE, Membre de Université de Lyon
Rue Maurice Audin
69518 Vaulx en Velin Cedex FRANCE

[2] Faculty of Engineering, University of Bologna
c/o Istituto IMAMOTER - CNR
Via Canal Bianco, 28
44100 Cassana (FE) ITALY

This study deals with modelling acoustical heterogeneous materials obtained through a set of poroelastic inclusions. The presented theoretical model is based on the homogenization hypotheses introduced by Boutin [3]. The idea behind the inclusion of a second poroelastic material into the original single porosity material, is to obtain the pressure diffusion effect already observed in the double porosity case, without losing performances in transmission. It is shown in the present study, that this aim can be obtained with heterogeneous materials, made up of periodical inclusions. When compared to the single porosity material, a double porosity material (air perforations) provides an increase of the absorption coefficient, but in general the gain is obtained above a certain frequency value. Therefore, the absorption properties are worsened at low frequency, a range where in general the performances of single porosity materials are already not satisfactory. Then due to the perforations, for problems in which the acoustic transmission is involved, the performance of a double porosity material is worse than the single porosity one. In any case, when a general problem is addressed (e.g. a complex field like in [7] or the case of adjacent cavities) the problem can be significant. Those problems described above for double porosity are faced up by heterogeneous materials. In the case of double porosity, the pressure diffusion effect is obtained through a highly resistive micro- porous material (together with all the problems involved in this case [1]). The same effect can be reproduced in the case of heterogeneous materials, through a high difference in the air flow resistivity between the two involved microporous materials. Details about modelling are described in the following study. An analytical model is described and points out the acoustical and geometrical characteristics, that are necessary to obtain the supposed effects of sound absorption increase and pressure diffusion. Discussions about the validation of the analytical model through the comparison with experimental measurements are carried out. In particular, details are given about the prediction of the pressure diffusion effect. Several geometrical con£gurations have been measured and taken into account for the validation. The different cases of high and low permeability contrast are addressed. The role of geometrical shape factors into the diffusion function is discussed.

References

[1] Olny, X. 1999 Acoustic absorption of porous media with single and double porosity-modeling and experimental solution (in french). *Ph.D. thesis, ENTPE-Institut National des Sciences Appliquées de Lyon.*

[2] Olny, X., Boutin, C. 2003 Acoustic wave propagation in double porosity media. *J. Acoust. Soc. Am.* **114**(1), 73-89.

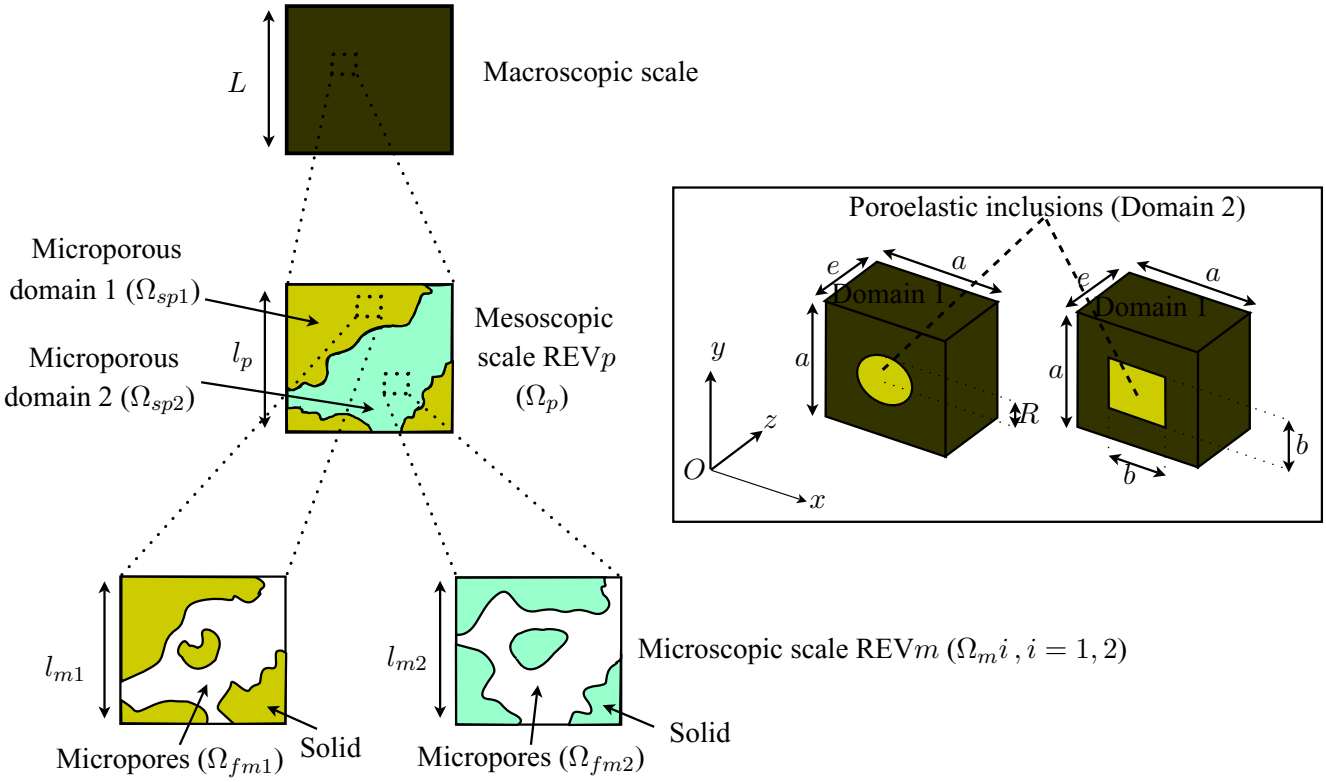

Figure 1: The three scales of the considered heterogeneous medium and Considered periodic cells: circular or square cross-section for the poroelastic inclusion.

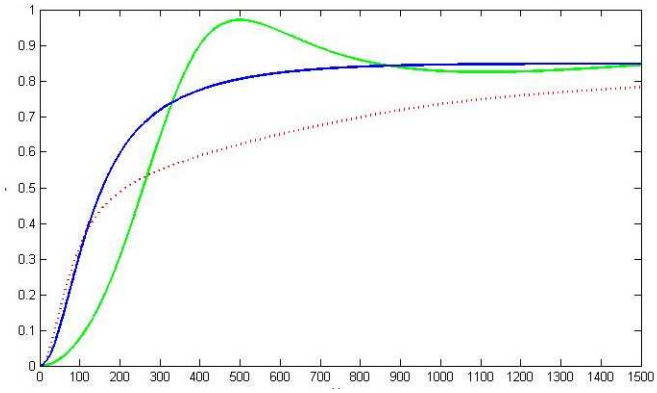

Figure 2: Typical analytical absorption coefficient for a single porosity (red), a double porosity (green) and an heterogeneous (blue) porous material, characterized by the same thickness.

[3] Boutin, C., Royer, P., Auriault, J.-L. 1998 Acoustic absorption of porous surfacing with dual porosity. *Special Issue on poroelasticity, International Journal of Solids and Structures.* **35**, 4709-4737.

[4] Atalla, N., Panetton, R., Sgard, F.C., Olny, X. 2001 Acoustic absorption of macro-perforated porous materials. *J. Sound Vib.* 243(**4**), 659-678.

[5] Sgard, F.C., Olny, X., Atalla, N., Castel, F. 2005 On the use of perforations to improve the sound absorption of porous materials. *Appl. Acoustics* **66**, 625-651.

[6] Groby., J.-P., Wirgin, A., de Ryck, L., Lauriks, W. 2007 Acoustic response of a rigid frame porous medium slab with a periodic set of inclusions *J. Sound Vib.* **arXiv:0705.2754v1**

[7] Amirouche, N. 2008 Dispositifs absorbants a base de materiaux a double porosite dans des champs acoustiques complexes. *These de doctorat, Entpe, France.*

PRESSURE/MASS METHOD TO MEASURE OPEN POROSITY OF POROUS SOLIDS

Yacoubou SALISSOU and Raymond PANNETON
GAUS, Department of mechanical engineering, Université de Sherbrooke, Québec, Canada, J1K 2R1
Yacoubou.Salissou@USherbrooke.ca, Raymond.Panneton@USherbrooke.ca

1. INTRODUCTION

The open porosity of a porous solid is a key parameter in the physical and acoustical modeling of porous media, especially to relate the effective properties of the fluid saturating the interconnected pores to the effective properties of the porous solid.[1,2] In the past, several acoustical indirect methods have been proposed to measure this parameter[3,4] However, direct methods are generally preferred. Examples of direct measurement methods include the pioneer work of Beranek,[5] and its improved version standardized as ASTM D 2856-94. The method relies on the equation of state for ideal gases at constant temperature. However it is time consuming and requires several calibration of the device. Other direct measurement methods include the improvement of Beranek method proposed by Leclaire *et al.*[6] and by Champoux *et al.* [7] and the missing mass method proposed by Panneton and Gros[8].

In this paper, a method is presented to measure the open porosity of porous solids. The method needs only a simple apparatus and its accuracy is predictable from the knowledge of the total bulk volume of the tested porous sample.

2. THEORY

The open porosity of porous solid is expressed as

$$\phi = 1 - V_s / V_t \,, \tag{1}$$

where V_s is the volume of the solid phase, and V_t the total bulk volume of the porous aggregate. In general, V_s is unknown and needs to be determined. To determine its value, the four tests presented in fig.1 are used together with the perfect gas law relation. If the process between and during tests is very slow and room conditions are constant, isothermal condition can be assumed. The volume of the solid phase V_s can then be expressed as [see ref [9]]

$$V_s = \left(\left(M_2 - M_1 \right) / \left(P_2 - P_1 \right) - \left(\left(M_4 - M_3 \right) / \left(P_4 - P_3 \right) \right) \right) RT \tag{2}$$

where R is the specific gas constant, T is the temperature in Kelvin and M_i the different masses measured on the balance.

3. ERROR ANALYSIS

3.1 Applicability of the method

As shown, to apply the proposed method, volume V_s needs first to be evaluated. Usually, the target pressures to use are low pressure P_{lo} and high pressure P_{hi} so that $P_1 \cong P_3 \cong P_{lo}$, and $P_2 \cong P_4 \cong P_{hi}$. Also, it can be easily shown that the difference $M_i - M_{i-1} = m_i - m_{i-1}\big|_{i=2,4}$. Furthermore, $m_2 - m_4$ yields the mass of gas occupied by the solid phase of the porous sample at high pressure (i.e., $\rho_{hi} V_s$, where ρ_{hi} is the mass density of the gas at high pressure), and $m_1 - m_3$ yields the mass of gas occupied by the solid phase at low pressure (i.e., $\rho_{lo} V_s$, where ρ_{lo} is the mass density of the gas at low pressure). Consequently, $M_2 - M_4 - M_1 + M_3 = \left(\rho_{hi} - \rho_{lo} \right) V_s$ and ρ_{lo} corrects for the fact that the low pressure condition is not the perfect vacuum condition. Not accounting for $m_1 - m_3$ would only add a bias error proportional to P_{lo} in the evaluation of V_s and ϕ; however it does not prevent the applicability of the method.

From the previous analysis, the most severe condition that remains for applying the method is the readability of the high pressure mass difference (i.e., $m_2 - m_4 \geq \varepsilon$, where ε is the balance readability). This condition gives the maximum porosity the method can determine for a given set of operation conditions

$$\phi_{\max} = 1 - RT\varepsilon / P_{hi} V_t \,. \tag{3}$$

Figure 2 gives the minimum bulk volume per balance readability as a function of open porosity for different operating conditions. It shows that larger bulk volume, larger high pressure, and gas with larger density are desirable to increase the applicability of the method, and to detect open porosity closer to unity (typical for sound absorbing porous materials).

3.2 Precision of the method

Using the total differential method and assuming that the errors are random and follow a normal distribution, the expected error committed on the open porosity is

$$\delta\phi = \pm \left(1 - \phi \right) \sqrt{\left(\delta T / T \right)^2 + \left(\delta V_t / V_t \right)^2 + \left(\delta Z / Z \right)^2} \,, \tag{4}$$

For a cylindrical test sample, the error on its bulk volume is given by $\delta V_t = \pm V_t \delta_L \sqrt{\left(2/D \right)^2 + \left(1/H \right)^2}$, where D and H are its diameter and height, and δ_L is the uncertainty on the dimension measurement. δZ is the error related to variable Z defined, following Eq.(2), as $Z = V_s / RT$. Considering that the uncertainty relative to the masses and pressures are

given, respectively, by the balance and the manometer readability ε and *p*, and Assuming P_1 and P_3 are approximately equivalent and equal to low pressure P_{lo}, P_2 and P_4 are approximately equivalent and equal to high pressure P_{hi}, and test chamber volume $V>>V_s$, one obtains

$$\delta Z \cong 2\sqrt{\varepsilon^2 + \left(pV/RT\right)^2} \Big/ \left(P_{hi} - P_{lo}\right). \quad (5)$$

The error predicted by the Eq. (4) is valid only if $V_t \le V$. Figure 3 shows the expected absolute error on open porosity as a function of bulk volume per test chamber volume for three different open porosity values (0%, 90%, and 99%). The error generated by the individual uncertainties on the mass and pressure, the bulk volume, and the temperature are also plotted. It is noted that the precision of measurement is better when using larger bulk volume. It is also noted that for the three cases, the error is mostly controlled by the uncertainty on the mass and pressure reading. Since the error is mostly controlled by the uncertainty on the mass and pressure reading, the error on the open porosity can be estimated by the approximated expression given by

$$\delta\phi \cong 2\sqrt{\left(\left(RT\varepsilon\right)^2 + \left(Vp\right)^2\right)} \Big/ V_t\left(P_{hi} - P_{lo}\right). \quad (6)$$

One can observe that it fits well with the global error in the valid range of bulk volume ($V_t/V \le 1$).

4. EXPERIMENTAL TESTS AND RESULTS

To validate the gas porosimeter and its precision, two tests have been performed. The first test consists in applying the method to measure the porosity of high porosity samples (95%) of known solid phase volume V_s. The second test consists to applying the method to measure the porosity of low porosity samples (45%) of known solid phase volume V_s. Details on test setup and procedure can be found in ref[9]. Figure 4a compares the measured standard deviation (i.e., measured error) for each of the ten samples to the theoretical prediction. It is observed that the measured error fits well with the one predicted by Eq.(6). Figure 4b shows the measured mean porosity for 30 individual tests as a function of the bulk volume to test chamber volume ratio to better visualize the scattering of the measurements around the theoretical value. One can clearly observed that the precision on the measurements improves with the bulk volume to test chamber volume ratio.

ACKNOWLEDGEMENTS

N.S.E.**R**.C., **R**EGAL, and ALCAN supported this work.

REFERENCES

[1]Biot, J. Acoust. Soc. Am., 28, 168 (1956).
[2]Allard, Propagation of sound in porous media, Elsevier, NY (1993).
[3]**U**mnova et al., Appl. Acous., 66, 607 (2005).
[4]Fellah et al., J. Appl. Phys., 93, 296 (2003).
[5]L.L. Beranek, J. Acoust. Soc. Am., 13, 248 (1942).
[6]Leclaire et al., **R**ev. Sci. Inst., 74, 1366 (2003).
[7]Champoux et al., J. Acoust. Soc. Am., 89, 910 (1990).
[8]**R**. Panneton and E. Gros, Acta Acustica, 91, 342 (2005).
[9]Salissou and Panneton, J. Appl. Phys. 101, 124913 (2007)

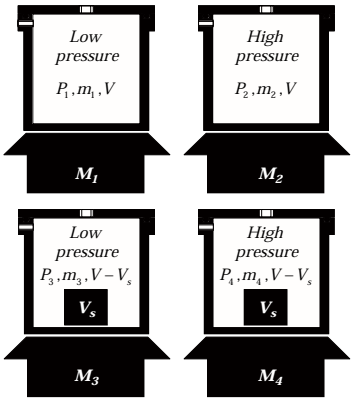

Figure **1:** Measurement procedure. For the four conditions shown in the figure, the mass is measured on the balance.

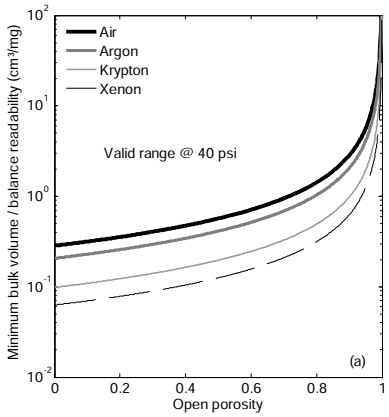

Figure **2:** Minimum bulk volume per balance readability as a function of open porosity.

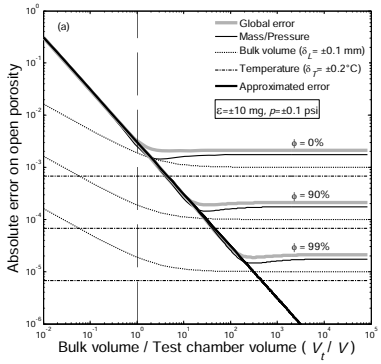

Figure **3:** Theoretical absolute error on open porosity as a function of bulk volume per test chamber volume.

Figure **4** : Experimental tests results

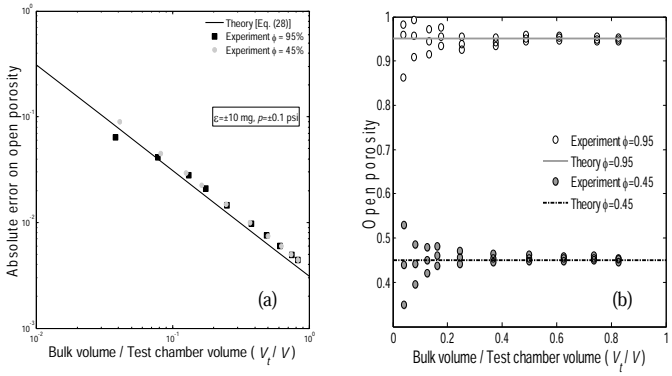

Field acoustic characterization of soil properties.

V.S. Averbakh, A.V. Lebedev, A.P. Maryshev, V.I. Talanov
Institute of Applied Physics Russian Academy of Sciences,
46 Ulyanov Street, Nizhny Novgorod, 603950, Russia.
e-mail: swan@hydro.appl.sci-nnov.ru

The properties of natural media depend strongly on the consolidation degree, pore structure and fluid saturation [1]. Because of that acoustic characterization of natural sediment in situ is of great importance. We discuss the results of acoustic field measurements. Our goal was to develop acoustic methods for the soil properties measuring in the field conditions. The methods are based on the use of portable vibratory source. Two approaches are considered in the paper. The first employs electro-acoustical analogies. This is impedance method of measurements. The second method employs the analysis of phase relations between signals recorded to extract fine characteristics of the soil which are associated with an action disturbing the soil equilibrium.

Consolidation degree influences mainly on shear modulus. Lithology (including mineralogical composition and packing structure) can be evaluated using Pickett's cross-plot [1] where Poisson ratio is a key parameter. Impedance method provides both shear modulus and Poisson ratio measurements. The results presented point to high sensitivity of the impedance method that allows investigating acoustic property changes for a variety of environmental conditions. In particular we showed the influence of weather conditions and the soil integrity on its shear stiffness and Poisson ratio.

Acoustic nonlinearity and radiation stability were studied also. We showed dominating role of the interface area between the vibrator baseplate and the soil beneath. This statement is in a good agreement with theoretical model [2] where this interface area was introduced and analyzed to account observed nonlinear distortions [3]. Although interface region is very small compared with representative soil volume determining the soil reaction, acoustical losses was found compatible with seismic waves radiation losses. It was shown that the losses in the interface region were due to dynamical fracture of the contact between the baseplate and the soil. The criteria of permanent stability of seismoacoustic radiation were determined. Based on these criteria precision phase measurements during several hours became available and were employed to study fine characteristics of the soil in field conditions.

Using precision phase measurements we found slow logarithmic in time relaxation of Rayleigh wave velocity perturbation caused by an impact. Broad-band measurements were made using coherent portable vibratory source and accelerometers mounted at known distance from the source. It is known that Rayleigh wave is exponentially decaying with depth [4]. This feature allows looking deeper inside the soil varying the frequency radiated. Frequency band used in the experiment was from 30 Hz to 500 Hz (higher frequencies were found attenuating rapidly due to random scattering at grass roots). The mean value of Rayleigh wave velocity was found about 150 m/s that corresponded to the depth of penetration from 5 cm at 500 Hz to 1 meter at 30 Hz. Four octaves in frequency and high signal-to-noise ratio enabled very accurate phase measurements for each acoustic snapshot, while criteria of the seismoacoustic signal permanent stability, which were determined in the first experiment, provided absolute phase measurements.

The analysis of data obtained during 3 hours points to an existence of localized (metastable) states inside granular medium. Perturbed region was found localized close to the area subjected to the impact. We estimated the scales associated with observed relaxation characteristics and found these scales were of 25 angstroms. This is

compatible with grain-to-grain interface region size where surface forces of various natures are revealed. An existence of the variety of surface forces acting between the grains in natural soft materials is very typical [5, 6] and small external actions can change internal state of the material. In the paper [5] grains were found separated by 5 angstroms in the equilibrium state and by about 60 angstroms in metastable state. These values are in a good agreement with our experimental results.

In conclusion major results are drawn and future investigations are discussed. Beside interesting physics valuable practical applications are pointed. Simplicity of realization allows using proposed methods of acoustic characterization in engineering, for soil properties monitoring, as supplement technique in complex acoustic measurements where the interaction between air-born sound and the ground is of interest. Unresolved problems are also specified. First, linearity of portable vibratory source should be enhanced. The source is almost linear now but residual nonlinear distortions in actuator system could be reduced to improve the source quality. Second, logarithmic relaxation which was associated with repacking in granular medium should be studied in lab using calibrated granular media under controlled environmental conditions, fluid saturation degree etc.

This investigations were partly supported by Russian Foundation of Basic Research (project nos. 08-02-00670, 06-05- 64925, and 07-02-10014), and the Program of Basic Research of the Division of Physical Sciences of the Russian Academy of Sciences “Coherent Acoustic Fields and Signals”.

REFERENCES

1. K.W. Winkler and W.F. Murphy III, Acoustic Velocity and Attenuation in Porous Rocks // Rock Physics and Phase Relations. A Handbook of Physical Constants. T.J. Ahrens, Editor. AGU Reference Shelf 3. P. 20–34. American Geophysical Union, 1995.
2. A.V. Lebedev and I.A. Beresnev, Nonlinear distortion of signals radiated by Vibroseis sources // Geophysics, 2004. V. 69(4). P. 968–977.
3. B.P. Jeffryes, Far-field harmonic measurement for seismic vibrators: 66th Annual International Meeting, SEG, Expanded Abstracts. 1996. P. 60–63.
4. L. D. Landau, E. M. Lifshitz, A. M. Kosevich and L. P. Pitaevskii, Theory of elasticity. Pergamon Press, 1986.
5. M.M. Sharma and A.N. Tutuncu, Grain contact adhesion hysteresis: A mechanism for attenuation of seismic waves // Geophys. Research Letters. 1994. V. 21(21). P. 2323–2326.
6. M. Kleman and O.D. Lavrentovich, Soft matter physics, Springer, 2003.

Influence of the pore sealing on the acoustic Transition Terms of a water-saturated porous plate obeying Biot's theory.

Serge Derible, Hervé Franklin.

Laboratoire Ondes et Milieux Complexes, Groupe Ondes Acoustiques

LOMC FRE 3102 CNRS

IUT Place Robert Schuman 76610 Le Havre, FRANCE.

We investigated the theoretical acoustic behaviour of a water-saturated porous plate under different sealing conditions imposed to the pores of its faces. The derivation of *R* and *T*, the reflection and transmission coefficients of the plate, is achieved in the frame of Biot's theory introducing a new impedance parameter κ in the boundary conditions in order to characterize the permeability of a given water/plate interface [1,2]. The possibility of the propagation of a slow wave in the plate largely hinges on the value this impedance parameter is given. When all the pores communicate with the surrounding water $\kappa \to \infty$, while they are sealed $\kappa = 0$.

The transition terms TT_{sym} and TT_{asym} are linear expressions in *R* and *T* directly connected with the symmetry of the displacement of the faces of the porous plate [3].

We recorded the reflected and the transmitted signals from the same water-saturated porous plate under the following different boundary conditions.

1°) The pores of both the faces were open.

2°) The pores of one face were sealed by means of an application of a very thin layer of quick-setting cement, able to harden on the immersed plate. The reflection coefficient of each one of the faces was measured and the two transmission coefficients of the plate as well.

3°) The pores of the second face of the plate were sealed in the same manner.

The 5mm thick plate was always normally insonified by an acoustic pulse. The wide band apparatus chain made possible an experimental frequency range from 0.1 to 2MHz (0.5 to 10 MHZmm).

There is a good agreement between the theoretical and experimental transition terms when all the pores are sealed. For the other cases, the agreement is good in the low frequency range, while a discrepancy raises as frequency increases. This work suggests that a loss frequency power law should be introduced in Biot's theory to obtain a better fitting of the relevant curves.

[1] M. A. Biot, “Theory of propagation of elastic waves in a fluid saturated porous solid: I Low frequency range, II Higher frequency range”, J. Acoust. Soc. Am **28** (2) 168-191, (1956).

[2] H. Deresiewicz, “The effect of boundary conditions on wave propagation in a liquid-filled porous solid: IV. Surface wave in half-space”, Bull. Seism. Soc. Am. **52**, 627-638 (1962).

[3] F. Belhocine, S. Derible and H. Franklin, “Transition term method for the analysis of the reflected and the transmitted acoustic signals from water-saturated porous plates”, J. Acoust. Soc. Am **122** (3) 1518-1526, (2007).

Poroelastic plate theories of arbitrary order

Loris Nagler, Martin Schanz

Institute of Applied Mechanics
Graz University of Technology
Technikerstraße 4/II, 8010 Graz, Austria

Abstract

The numerical treatment of noise insulation of solid walls has been of interest in scientific research for many years. In problems of sound absorption, the main noise source is given by the bending vibration of the walls excited by acoustic pressure. Walls are often modelled as elastic plates despite their porous structure. Especially, if an effective porous sound insulator has to be modelled, a poroelastic plate theory is advantageous.

Poroelastic plate theories as extensions of the classical Kirchhoff theory have been presented by Theodorakopoulos and Beskos [3] and, with some additional assumptions, by Leclaire et al. [1]. A Mindlin based theory has been developed by Schanz et al. [2]. In the book by Cederbaum et al. [4] beside a plate theory also other poroelastic structural elements are presented. All these formulations are based on Biot's theory for porous media [5].

Plate theories rely on a reduction of the 3-d continuum to a 2-d structure by means of some assumptions regarding the strain and stress distribution in thickness direction. Whereas in elasticity the intuitive Kirchhoff or Mindlin assumptions are accepted and verified, for a poroelastic plate theory it is questionable whether these assumptions can be transferred also to the pore pressure and the flux of the interstitial fluid.

That is why here a more mathematical motivated approach is chosen which is based on the work of Kienzler [7] for elastic plates. Due to the unknown dependency of the variables on the thickness coordinate x_3 a power series expansion with respect to this coordinate is introduced. Now an integration in thickness direction becomes possible and hence the reduction from 3-d to 2-d can be performed. According to where the series is truncated, theories of different order can be obtained. As a consequence of this method, a priori assumptions are not needed anymore.

In view of [6], the three solid displacement variables u_i together with the pore pressure p are sufficient to describe the poroelastic continuum in Laplace domain. The series expansions for those variables are given as

$$u_i(x_1, x_2, x_3) = \sum_{\ell=0}^{\infty} \overset{\ell}{u}_i(x_1, x_2)\; x_3^{\ell} \qquad p(x_1, x_2, x_3) = \sum_{\ell=0}^{\infty} \overset{\ell}{p}(x_1, x_2)\; x_3^{\ell}\;.$$

Kienzler has shown in [7] that by choosing the order of the thickness variable h as criterion for the series expansion, the obtained partial differential equations coincide very well with the classical theories. A 'first order' theory actually leads exactly to the classical Kirchhoff

plate equation. The 'second order' formulation yields a 'Mindlin-like' theory. Mathematically, any desired degree of approximation is imaginable. The physical relevance though would be doubtful, since the thickness variable h must be assumed to be small and hence gets even smaller with increasing order.

One of the convenient properties of the method is the fact that the a priori assumptions required for the classical formulations turn out to be a posteriori results. Hence, besides providing plate theories of arbitrary order, this approach could be used for examining the question of the transferability of assumptions from elastic to poroelastic quantities.

The derivation itself consists in minimizing the total poroelastic potential and inserting in the series expansions. For obtaining consistent theories by means of [7], all terms multiplied by h up to a certain order are collected and the remaining terms are discarded.

The resulting equations are solved using the finite element method.

References

[1] Leclaire P.; Horoshenkov K.V.; Cummings A. Transverse vibrations of a thin rectangular porous plate saturated by a fluid. *Journal of Sound and Vibration*, 247(1):1–18, 2001.

[2] Schanz M.; Busse A. Acoustic behavior of a poroelastic Mindlin plate. In *17th ASCE Engineering Mechanics Conference*, 2004.

[3] Theodorakopoulos D.D.; Beskos D.E. Flexural vibrations of poroelastic plates. *Acta Mechanica*, 103:191–203, 1994.

[4] Cederbaum G.; Li L.; Schulgasser K. Poroelastic structures, 2000.

[5] Biot M.A. Theory of propagation of elastic waves in a fluid-saturated porous solid.I/II. Lower/Higher frequency range. *Journal Acoustic Society of America*, 28(2):168–191, 1956.

[6] Atalla N.; Panneton R.; Debergue P. A mixed displacement-pressure formulation for poroelastic materials. *Journal Acoustic Society of America*, 104(3):1444–1452, 1998.

[7] Kienzler R. On consistent plate theories. *Archive of Applied Mechanics*, 72:229–247, 2002.

A TIME DOMAIN NUMERICAL METHOD FOR THE BIOT MODEL

G. CHIAVASSA, B. LOMBARD, J. PIRAUX

A numerical method is proposed to simulate the propagation of transient poroelastic waves across heterogeneous media, in the low frequency range. A velocity-stress formulation of Biot's equations is followed, leading to a first-order differential system. This system is splitted in two parts: a propagative one discretized by a fourth-order ADER scheme, and a diffusive one that can be solved analytically. Near acoustic sources and media interfaces, a space-time mesh refinement is implemented to capture the small spatial scales related to the diffusive slow compressional wave. Lastly, since the physical parameters are non-homogeneous, an immersed interface method is implemented to accurately model the jump conditions between the different media.
The resulting method allows to investigate the propagation through porous/porous or fluid/porous media with realistic values of physical parameters. Numerical experiments in one and two dimensions and comparisons with exact solutions confirm that the whole set of compressional and shear waves is efficiently modeled.

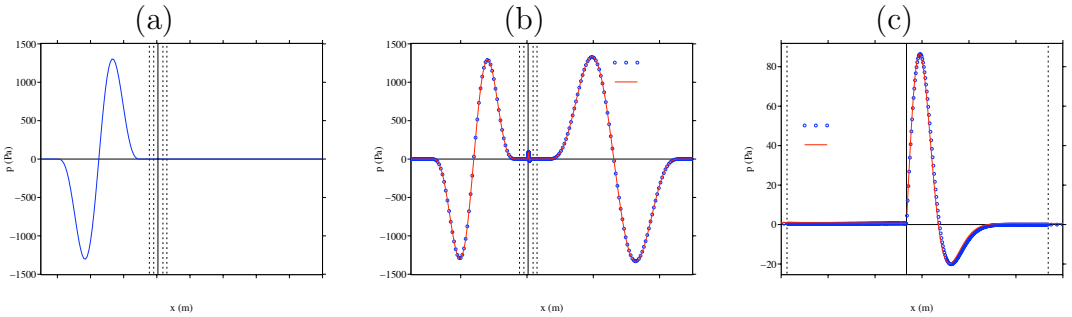

FIGURE 1. Propagation through fluid/porous media (water/sandstone saturated by water). (a) initial right going wave in water; (b): snapshot of pressure after crossing the interface; (c) zoom around interface showing the compressional diffusive slow wave in the porous media. Numerical (•) and exact (–) solutions.

[1] G. CHIAVASSA, B. LOMBARD, J. PIRAUX, *Numerical modeling of 1-D transient poroelastic waves in the low-frequency range*, to appear in J. Comput. Appl. Math., (2008), `http://hal.archives-ouvertes.fr/hal-00193103/fr/`.

A new impedance tube for large frequency band characterization of absorbing materials

Jean Pierre DALMONT [a], Jean Christophe LE ROUX [b]

[a] Laboratoire d'Acoustique de l'Université du Maine, Avenue Olivier Messiaen, 72085 LE MANS, France,
[b] Centre de Transfert de Technologies du Mans, 20 rue Thalès de Milet, 72000 LE MANS, France

The standard two microphones technique does not allow the measurement of absorbing materials characteristics at low frequency. Moreover, to cover a range from 100 to 6000 Hz two experiments have to be done with two different sample diameters. By using a sensor with a known volume velocity source developed by the LAUM together with the CTTM, it is demonstrated that the impedance can be obtained from 10 to 6000 Hz by performing only one measurement with a single material sample. Results showing the behaviour of some materials at low frequency are presented. On the other hand a comparison is done with the classical two-microphone impedance tube method.

1 Introduction

A new impedance setup is presented allowing the measurement of the absorption coefficient of absorbing materials as well as the scattering matrix in a large frequency range.

2 Principle

The impedance measurement setup proposed uses a piezo-electric buzzer as a source. This buzzer is fixed on its back to a closed cavity and is connected to the front to the measured pipe (see figure (1)). The pressure p_2 at the input of the pipe is measured by a microphone (mic 2) and a second microphone (mic 1) measures the pressure p_1 in the back cavity, this pressure being at first order proportional to the volume velocity U delivered by the source. The impedance $Z = p_2 / U$ is thus at first order proportional to the transfer function between the two microphones and it can be written:

$$\frac{p_1}{p_2} = -jC\omega Z \qquad (1)$$

where $C = \frac{V}{\rho c^2}$ is the acoustic compliance of the back cavity of volume V, with ρ the air density and c the speed of sound.

In practice this equation (1) is only valid for low frequencies. Moreover, it is necessary to take the relative sensitivity of the two microphones into account, since the measured transfer function is $H_{21} = \frac{p_2}{p_1}\frac{s_2}{s_1}$ with s_1, s_2 the respective sensitivities of microphones 1 and 2.

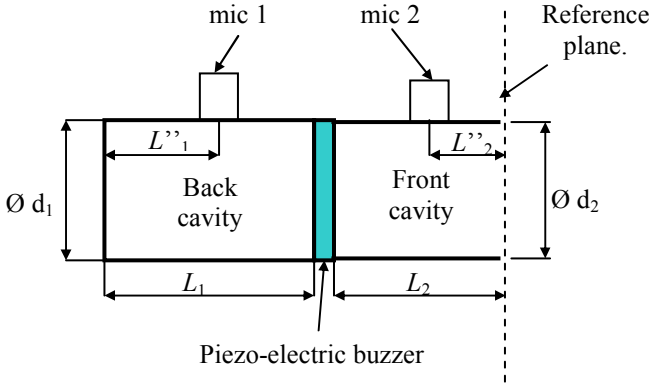

Fig.1 Schematic drawing of the impedance measurement setup and notations

It is also possible to calculate more precisely the expression of the impedance by taking into account the geometrical dimensions of the sensor:

$$Z = \frac{H_{21}/K - \beta}{1 - \delta H_{21}/K} \qquad (2)$$

with $K = -j\frac{1}{Z_{c1}}\frac{s_2}{s_1}\frac{\sin(kL_1)}{\cos(kL_1'')}\frac{\cos(kL_2'')}{\cos(kL_2)}$, $\beta = jZ_{c2}\tan(kL_2'')$ and $\delta = j\tan(kL_2)/Z_{c2}$.

Lengths L_1, L_2, L''_1 et L''_2 are dimensions related to the setup and to the position of the microphones as indicated on figure (1). $Z_{c1} = \frac{\rho c}{S_1}$ and $Z_{c2} = \frac{\rho c}{S_2}$ are the respective characteristic impedances of the front and back cavities ($S_1 = \pi d_1^{\,2}/4$ is the cross section of the back cavity with d_1 its diameter and the same for the front cavity).

It is important to notice that only the relative sensitivity of the sensors is unknown, geometrical quantities being accurately measured with a calibre. The relative sensitivity of the sensors is obtained by doing a calibration with an infinite impedance (i.e a rigid plate) at the input of the impedance head.

3 Application to absorption coefficient measurement

Comparisons are made with the standard two microphones measurement method for the characterization of absorbing materials. With the standard method, the reflection coefficient is then obtained from:

$$R = \frac{Z - Z_c}{Z + Z_c} \qquad (4)$$

with $Z_c = \frac{\rho c}{S}$. From this reflection coefficient the absorption coefficient α can be deduced as:

$$\alpha = 1 - |R|^2 . \qquad (5)$$

4 Application to scattering matrix measurement

For this measurement, the sample holder is replaced by another tube in the middle of which the sample is placed. The end of this tube is closed by a rigid piston in which a third microphone (mic 3) is placed (see figure 2).

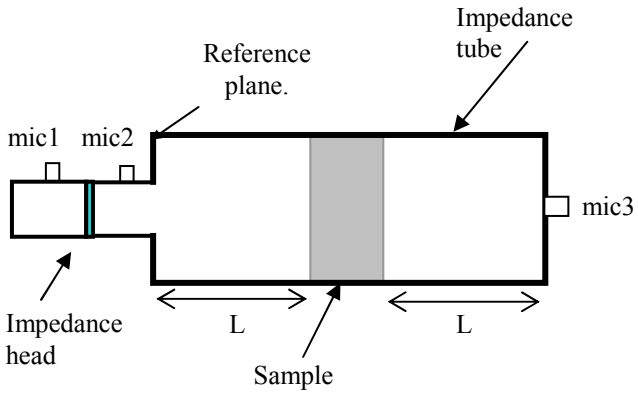

Fig.2 Schematic drawing of the scattering matrix measurement setup

The transfer function H_{31} between the first and the third microphone allows the determination of the transfer impedance $Z_T = p_3 / U$ as it can be shown that:

$$Z_T = \frac{H_{31}}{\delta K_T}(1 + \delta Z), \qquad (6)$$

where $K_T = -\frac{s_3}{s_1}\frac{Z_{c2}}{Z_{c1}}\frac{\sin(kl_1)}{\sin(kl_2)\cos(kl_1'')}$ with s_3 the sensitivity of the third microphone.

The sample being assumed symmetrical the impedance matrix of the whole impedance tube (including the sample) is given by:

$$\begin{pmatrix} Z_{11} & Z_{12} \\ Z_{21} & Z_{22} \end{pmatrix} = \begin{pmatrix} Z & Z_T \\ Z_T & Z \end{pmatrix}, \qquad (7)$$

from which the scattering matrix of the tube and that of the sample can be deduced. From this the effective compressibility and density of the absorbing can be estimated. Note that if the sample is not symmetrical a second measurement in a reversed situation has to be performed.

5 Result: comparison with the standard two microphones method

The measurement of various absorbing material samples has been performed both with the standard two microphones method (BK setup [1]) and the present impedance measurement setup. The same sample holder (29mm diameter) is used for both measurements so that the material is being measured in the same conditions. Results for a 20mm long piece of foam are shown on figure (3).

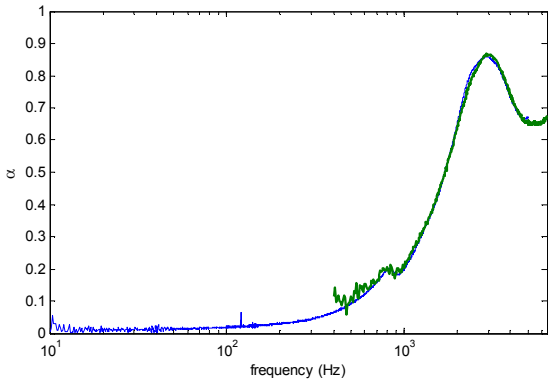

Fig.3 Measured absorption coefficient. Blue line: present impedance measurement setup (range 10-5000Hz). Green line: standard two-microphone impedance measurement tube (range 400-6400Hz)).

It is reassuring to see that both measurement techniques lead to the same result in their common frequency range suggesting that both methods are accurate.

6 Conclusion

Our measurement setup is shown to be able to perform measurements with the same accuracy as the standard two-microphone technique but on a wider frequency range (8 octaves instead of 4). The present setup is actually limited to frequencies above 5kHz. A new setup using slightly smaller cavities with a frequency range extended to 6.4kHz will be presented. Results allowing the determination of absorbing materials parameters will also be presented.

Reference

[1] BRUEL & KJAER 1995 Product data sheet BP 1039-12 Two-microphone impedance measurement tube – Type 4206.

The effect of moisture on the flow resistivity and acoustic admittance of loose granular media.

Kirill V. Horoshenkov, Mostafa H. A. Mohamed and Siow N. Ting

Experiments were carried out to measure the flow resistivity, porosity and acoustic admittance of sand samples at different degrees of water saturation (S_r). Standard instrumentation was used to measure the flow resistivity of samples in accordance with the direct airflow method detailed in the standard ISO 9053 (1991). The acoustic admittance was measured using a standard 100mm diameter Bruel and Kjaer impedance tube Type BK4206. The soil samples for the acoustic and flow resistivity experiments were prepared in two different sample holders, which were specially manufactured to fit the existing experimental setup. The first sample holder used in the flow resistivity experiment was a 100mm diameter PCV cylinder with a calibrated steel mesh that can hold a 50 mm layer of sand with grain size greater than 300μm and has a relatively small effect on the measured values of the flow resistivity. The other sample holder used in the impedance tube experiment was a 50mm high, 100mm diameter steel cylinder with solid bottom. Fully saturated samples of sand were prepared by pouring slowly dry sand into the sample holders which were partially filled with water. In this way any air entrapment can be avoided to ensure that the sand samples were initially fully saturated and that the sand compaction was similar. The samples were dried in an oven at the temperature of 60^oC over fixed time periods and the weight of samples was measured each time when the samples were taken to or from the oven so that the loss of moisture was known at any time in the experiment and hence the degree of saturation can be determined. In this way the degree of water saturation in the range of 0 to 93% was achieved in the acoustic and flow resistivity experiments. The results show that the flow resistivity progressively increases with the increase of the degree of water saturation in the range of $0 < S_r < 35\%$. At higher degrees of water saturation, the behaviour of the flow resistivity is more complex and it can have a maximum at $S_r \approx 70\%$. There is an approximately 20-fold increase in the flow resistivity between the fully dry and 70% saturated samples of sand. This variation in the flow resistivity is reflected in the behaviour of the acoustic admittance which can be predicted using a 2-parameter Attenborough or modified Delany and Bazley models which are studied as a part of this work.

For the past two decades problems concerning the propagation of waves through periodic or finite arrays of scatterers have been widely studied in application to various engineering problems (i.e. sonic crystals, porous materials, photonic crystals etc.). The particular interest lies in the presence of so-called band gaps characterised by the frequencies for which plane waves cannot propagate through the periodic structure. The latter may also be associated with the finite array models. One of the examples can be taken from the acoustics theory, see [5], where sound attenuation peaks relate to appropriate band gaps.

A substantial literature examines the case when boundary conditions on surface of the scatterer are either the Nuemann or the Dirichlet conditions referred to as limiting cases. For such periodic structures it is well-known that the phenomenon of band gaps is related to periodicity (L) of the array. Therefore it is expected that variations in filling fraction, arrangements of the scatterers and properties of host medium may change size of the observed band gaps. However these changes do not significantly affect the general band structure at the low-frequency regime ($kL \ll 1$ or below the first Bragg's frequency). For instance the Nuemann condition is always featured with the dispersion curve emanating at zero frequency, see, for more details, [3]. For the Dirichlet condition, see [4], the first dispersion curve is always bounded away from the zero that makes complete band-gap when $kL \ll 1$.

In our work the application of sonic crystal as a noise barrier is considered. The array of scatterers is embedded into an acoustic medium (index 'o') with the physical property of air that creates a great contrast, in terms of relative acoustic impedance ($\epsilon_{o,c} = \dfrac{c_o\rho_o}{c_2\rho_c}$), with more dense material of solid scatterer. Therefore the scatterer usually takes form of a rigid cylinder (the Neumann condition). This type of boundary conditions, as noted above, cannot be used for effective sound attenuation at the low-frequencies being part of 'noise spectrum'. To resolve this problem more complex form of the scatterer must be employed such as a multi-layer cylinder where 'local' resonances of the layer of thickness h make huge impact on acoustic waves propagating through the array. For this purpose it is assumed that layer thickness is much smaller than typical size of the array ($\eta = h/L \ll 1$). In [1] the case of thin elastic shell is investigated experimentally by the example of balloons. The experiments show existence of 'local' resonances that are independent of the arrangement of scatterers.

The proposed model is analysed using the multiple scattering technique and recurrent relations for elastic/acoustic layers, see [2] and [6]. The solution for the host medium is expressed as a superposition of solutions of the Helmholtz equation solved in conjunction with appropriate boundary conditions; thus

$$p_o \;=\; H_0^{(1)}(kr) + \sum_{n=1}^{N}\sum_{m=-\infty}^{\infty} A_m^n Z_m^n H_m^{(1)}(kr_n)\exp(im\theta_n),$$

where factor Z_m^n is of particular interest. It may be shown for the cylinder having one elastic layer (index 'c') and acoustic core (index 'i') that

$$Z_m^n \;=\; \frac{\epsilon_{o,i}J_m'\left(\kappa_{o,i}kr_n\right)J_m\left(kr_n\right) - \kappa_{o,i}J_m\left(\kappa_{o,i}kr_n\right)J_m'\left(kr_n\right)}{\epsilon_{o,i}J_m'\left(\kappa_{o,i}kr_n\right)H_m^{(1)}\left(kr_n\right) - \kappa_{o,i}J_m\left(\kappa_{o,i}kr_n\right)H_m^{(1)'}\left(kr_n\right)} + \mathcal{O}(\eta), \quad \text{as} \quad \eta \to 0, \qquad (1)$$

where $\epsilon_{o,i} = \dfrac{c_o\rho_o}{c_i\rho_i}$ and $\kappa_{o,i} = \dfrac{c_o}{c_i}$. This approximation may also be transformed to the above-mentioned limiting cases when either $\epsilon_{o,i} = \epsilon \to 0$ or $\epsilon_{o,i} = 1/\epsilon \to \infty$ provided that $\eta/\epsilon = o(\eta)$. Thus, it suggests that to observe 'local' resonances the core must have similar physical parameters to those of the host medium. Moreover next order in (1) requires that elastic layer must be of 'soft' material such as a soft rubber. The dependency of resonance phenomena on the material parameters is illustrated in Figure 1.

Further analysis of 'local' resonances of multi-layer cylinders at the low-frequency regime suggests that neighbouring layers are composed of contrasting materials and thickness of each layer is satisfied to $\eta \ll 1$. This results in 'elastic-acoustic' layer structure of the cylinder where acoustic material is similar to that of the host medium.

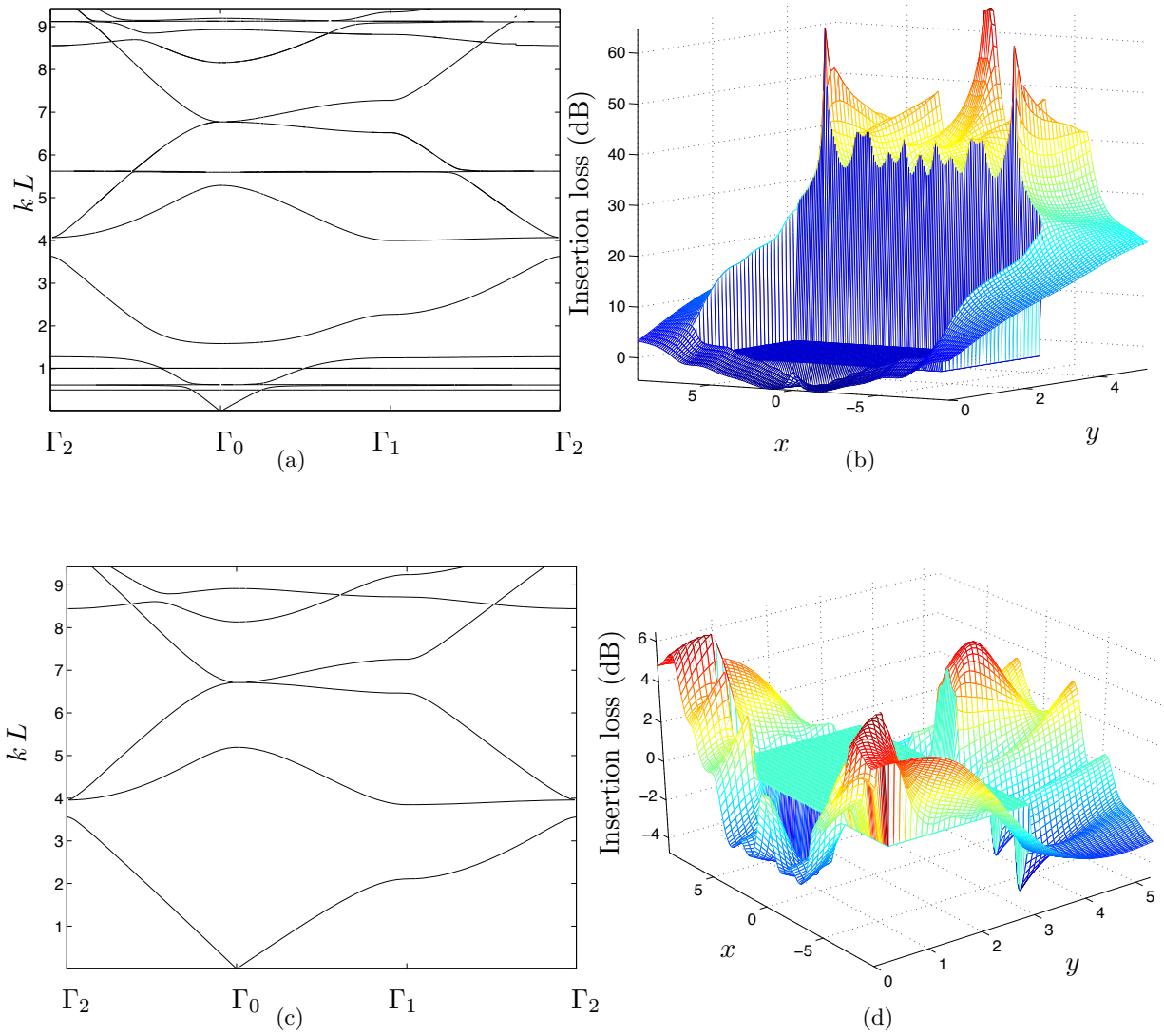

Figure 1: Comparison of the elastic shells (rubber/steel) filled with air and surrounded by air: (a)/(c) band structure of the periodic array, (b)/(d) sound attenuation in Oxy plane for square array of 3×15 elastic shells calculated at $kL = \dfrac{\omega}{c_o} = 1.5$.

References

[1] Fuster-Garcia, E., Romero-Garcia, V., Sánchez-Pérez, J. V. and Garcia-Raffi, L. M., 2007, Targeted band gap creation using mixed sonic crystal arrays including resonators and rigid scatterers. *Applied Physics Letters*, **90**, 244104.

[2] Linton, C.M. and Evans, D.V., 1990, The interaction of waves with arrays of vertical circular cylinders. *Journal of Fluid Mechanics*, **215**, 549-569.

[3] Nicorovici, N.A. and McPhedran, R.C., 1995, Photonic band gaps for arrays of perfectly conducting cylinders. *Physical Review E*, **52**, 1135–1145.

[4] Poulton, C.G., McPhedran, R.C., Nicorovici, N.A., Botten, L.C. and Movchan, A.B., 2001, Asymptotics of photonic band structures for doubly-periodic arrays. *Proceedings of the IUTAM Symposium on Mechanical and Electromagnetic Waves in Structured Media*, held in Sydney, Australia, 18–22 January 1999, 227–238 (Kluwer Academic Publishers).

[5] Sánchez-Pérez, J.V., Caballero, D., Mártinez-Sala, R., Rubio, C., Sánchez-Dehesa, J., Meseguer, F., Llinares, J. and Gálvez, F., 1998, Sound attenuation by a two-dimensional array of rigid cylinders. *Physical Review Letters*, **80**, 5325-5328.

[6] Shenderov, E.L., 1989, *Radiation and scattering of sound*, Sudostrojenie, Leningrad (In Russian).

In recent years interest in time domain models for sound propagation in porous materials has increased substantially. One of their potential applications is finite-difference time-domain (FDTD) simulation of outdoor sound propagation phenomena in the presence of an absorbing surface. It has been shown [1, 2], that in order to take into account wave interactions with the porous surfaces, explicit computations of sound propagation in porous media can be performed using an FDTD scheme. The use of the relaxation model proposed by D.K.Wilson [3] allows analytical formulation of the time domain equations governing sound propagation in porous media. However it satisfies physically correct low and high frequency limits only for materials with viscous and thermal shape factor values close to one. Otherwise it requires the use of different relaxation times in different frequency ranges. Thus, in the general case, the knowledge of the frequency range in which the material is working is important to correctly choose the relaxation time value. This however might be problematic if a broadband signal is used or in the time domain a pulse with most of the energy concentrated in the mid frequency range. In our previous study [4] a semi-empirical model has been formulated which allows an analytical transformation of both momentum and mass conservation equations in the time domain and correctly satisfies both low and high frequency limits for the whole range of shape factor values. Its numerical implementation however was limited to granular materials with shape factor significantly exceeding one and no thermal effects have been taken into account.

The aim of this work is twofold. Firstly, the model for granular materials with large values of shape factors is extended to include thermal effects. Secondly, we show that the suitable discretization of the time domain equations proposed in [4] gives good agreement with the measurements of pulse reflection and transmission for a variety of granular and fibrous materials. Discretization of the equations is based on the approach proposed by Wilson *et al* [2] and has been used in the previous work [5]. Here it is extended to model materials with shape factors significantly lower than one, such as for instance high porosity fibrous absorbers. A vertically installed impedance tube specially designed for pulse transmission measurements has been used for the experiments. The pulse response of different materials has been investigated for long as well as short pulses and the results of FDTD simulations are compared with data.

The equations used in this work are summarized below.

Time domain momentum and mass conservation equations for the materials with viscous and thermal shape factors, M and M' respectively, bigger than one have been formulated in [4, 5].

In case of shape factor values less than one the following set of equations is solved numerically

$$\partial_t v + \frac{v}{2}\sum_{m=1}^{2}\frac{y_m}{\tau_m} + \sum_{m=1}^{2}\frac{y_m}{2\sqrt{\pi\tau_m}}\int_{-\infty}^{t}\frac{v(t')/\tau_m + \partial_{t'}v(t')}{\sqrt{t-t'}}\exp\left(-\frac{t-t'}{\tau_m}\right)dt' = -\frac{\phi\partial_x p}{\alpha_\infty\rho_0},$$

$$(\gamma-1)\phi\partial_t p = \partial_t\left(\gamma\phi p + \rho_0 c^2\partial_x v\right) + \frac{\gamma\phi p + \rho_0 c^2\partial_x v}{2}\sum_{m=1}^{2}\frac{y_m}{N_{pr}\tau_m} +$$

$$+\sum_{m=1}^{2}\frac{y_m}{2\sqrt{\pi N_{pr}\tau_m}}\int_{-\infty}^{t}\frac{\left[\gamma\phi p(t') + \rho_0 c^2\partial_x v(t')\right]/N_{pr}\tau_m + \partial_{t'}\left[\gamma\phi p(t') + \rho_0 c^2\partial_x v(t')\right]}{\sqrt{t-t'}}\exp\left(-\frac{t-t'}{N_{pr}\tau_m}\right)dt'$$

where $y_1 = y$ and $y_2 = 1-y$, with $y\in[0,0.5]$ and $y < M$. Two viscous and two thermal relaxation times, τ_1, τ_2, τ_{e1} and τ_{e2}, are calculated as

$$\tau_1 = \frac{2\alpha_\infty\rho_0}{\sigma\phi}\left(\sqrt{M} + \sqrt{\frac{1-y}{y}(1-M)}\right)^{-2}, \tau_2 = \frac{2\alpha_\infty\rho_0}{\sigma\phi}\left(\sqrt{M} + \sqrt{\frac{y}{1-y}(1-M)}\right)^{-2} \text{ and}$$

$$\tau_{e1} = \frac{2k'N_{pr}}{\nu\phi}\left(\sqrt{M'} + \sqrt{\frac{1-y}{y}(1-M')}\right)^{-2}, \tau_{e2} = \frac{2k'N_{pr}}{\nu\phi}\left(\sqrt{M'} + \sqrt{\frac{y}{1-y}(1-M')}\right)^{-2}.$$

The other parameters are porosity ϕ, the tortuosity α_∞, the static flow resistivity σ, the dynamic viscosity of air ν, the density of air ρ_0, the thermal permeability k', the Prandtl number N_{pr}, the viscous shape factor $M = \frac{8\rho_0\nu\alpha_\infty}{\phi\sigma\Lambda^2}$, the characteristic viscous length Λ, the thermal shape factor $M' = \frac{8k'}{\phi\Lambda'^2}$ and the characteristic thermal length Λ'.

In the previous work [5], simulations under the assumption of constant complex compressibility $C(\omega)$ were performed. At that time, the assumption was justified showing that for the materials used and for the frequency range of interest the imaginary part of the complex compressibility was negligible compared to the real part that was constant and very close to 1. Predictions of reflected pulse by a rigid backed sample of lentils with M=6.72 and thickness of 0.10 m were compared and shown in figure 1 in the case of $C(\omega)=1$ and without this assumption. No important difference between the two simulations is shown confirming that the assumption used in the previous work was exactable. Again in figure 1, comparison between Wilson's model and the two relaxation times model predictions shows an evident improvement given by the latter.

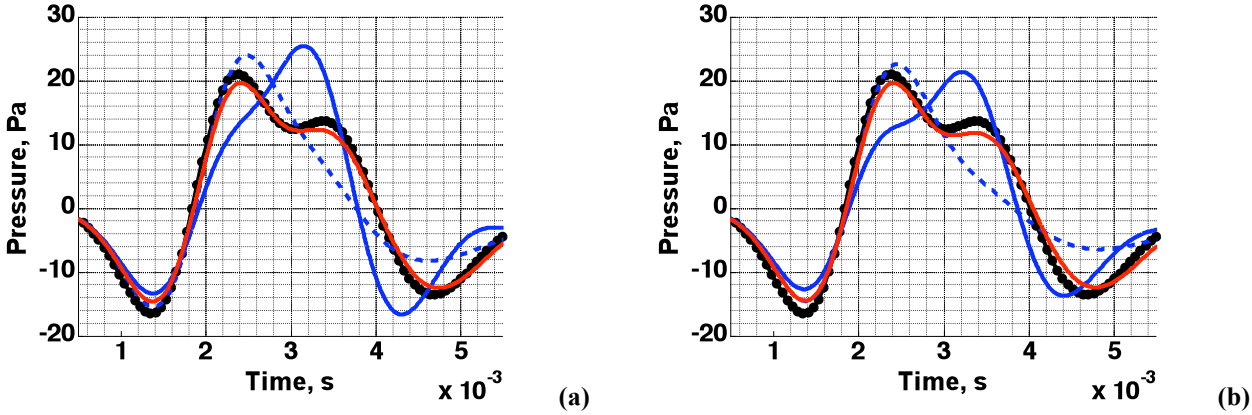

Fig. 1 Reflected Pulse for samples of lentils rigid backed under the assumption $C(\omega)=1$ (a) and without assumption (b).

Data, black line; two relaxation times model, red line; one relaxation time model that satisfies the low frequency limit, solid blue line; one relaxation time model that satisfies the high frequency limit, dash blue line

At the moment only numerical simulations are performed for material characterized by $M<1$ as shown in figure 2. In particular an ideal material composed by straight cylinders with radius of $3\cdot10^{-5}$ m and thickness of 0.20 m has been used for the simulations. The sample is characterized by M=0.204 and once again, from the simulations results it can be seen that the prediction of the two relaxation times model is much different from the ones given by Wilson's model. Future measurements are planed in order to verify the validity of the two relaxation times model predictions.

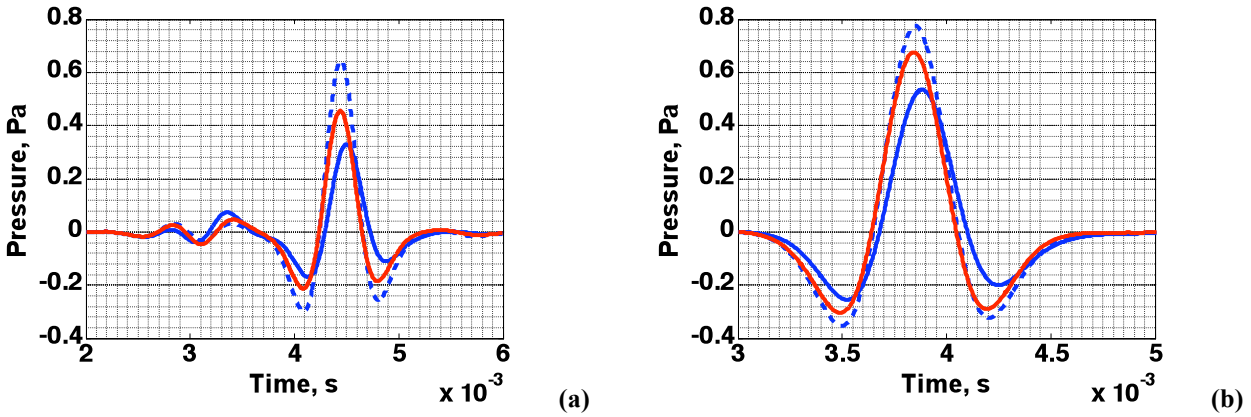

Fig. 2 Reflected Pulse for sample of array of cylinders rigid backed (a) and Transmitted Pulse of the same sample (b).

Two relaxation times model, red line; one relaxation time model that satisfies the low frequency limit, solid blue line; one relaxation time model that satisfies the high frequency limit, dash blue line

References

[1] E.M. Salomons, R Blumrich, D Heimann , "Eulerian time-domain model for sound propagation over a finite-impedance ground surface. Comparison with frequency-domain models", *Acust. Acta Acust.* 88, 483-92 (2002)
[2] D.K. Wilson *et al.*, "Time-domain calculations of sound interactions with outdoor ground surfaces", *Appl. Acoust.* 68, 173-200 (2007)
[3] D.K. Wilson, "Simple, relaxational models for the acoustical properties of porous media", *Appl. Acoust.* 50, 171-8 (1997)
[4] O. Umnova, D. Turo, "Semi-empirical time domain model of sound attenuation in porous materials", *Acoustics'08 Paris.* (2008)
[5] D.Turo, O.Umnova, "Acoustic pulse attenuation and transmission in rigid porous media: Experimental investigation and numerical simulations", *Acoustics'08 Paris.* (2008)

Activated carbon has shown significant additional low frequency absorption [1] in comparison to more common porous absorbers. It is the identification of the causes of this excess acoustic energy dissipation that this paper will attempt to address.

In its granular form, mainly two distinct porous domains characterize the internal structure of activated carbon. The first, defined as the microscopic domain is created by the very large number of interconnected pores of various shapes and sizes, with pore widths ranging from a few nanometers to thousands of nanometers (micro-, meso- and macropores) located within each of the grains [2]. To give an idea of the possible number of pores in the microporous domain, an activated carbon particle $1mm^3$ in size can have up to 10^{11} pore entrances per $1mm^2$ of surface [3]. The second domain, called the macroscopic domain is shaped from pores of widths in the region of hundreds of microns, created by the intragranular voids resulting from the random packing of grains. However, for acoustic waves propagating through its structure at normal conditions of pressure and temperature, the smallest pores in the microporous domain are inaccessible and the effective internal porous structure changes dramatically. The internal 'open' structure of the carbon reduces to the intergranular pores plus some of the larger pores within the grains. This happens because the micro- and mesopores will be almost completely filled with adsorbed and condensed substances [4], held to the pores through weak physical attraction or condensation forces, known as *van der Waals'* forces. This is evident from experiments performed by E. L. Fuller Jr. [4] on the adsorption of nitrogen onto activated carbons, the results of which are presented in the figure below.

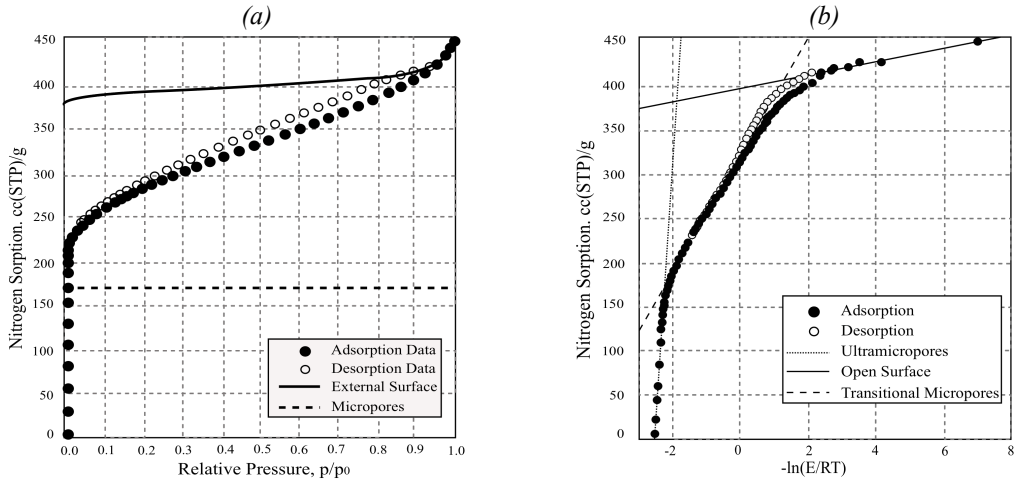

Figure 1 Part *(a)*, Nitrogen sorption on activated coconut-shell charcoal at 77.2 °K as a function of relative pressure. Part *(b)*, sorption process as defined by the Autoshield Potential.

The results shown in part *(a)* of the above figure give the sorption isotherm of the activated carbon sample for a relative pressure range between 0 and 1, where the relative pressure is the pressure normalised by atmospheric pressure. A clear hysteresis phenomenon can be observed between the adsorption and desorption curves. This data is usually obtained using a gravimetric analyzer. Part *(b)* of the figure shows another representation of the same data as in part *(a)*, now plotted using the Autoshield potential method in order to evaluate, from the slope of the linear regions in the plot, the volume of adsorbate in each of the pore ranges in the microporous domain. Fuller has calculated, from the adsorption isotherm results shown in the above figure that most of the adsorbed substance is found in the micropores (~90%) and mesopores (~9%) while the remaining 1% can be found on the surface of the carbon. However, in order to evaluate an adsorption isotherm for activated carbon as related to acoustic pressure perturbations, an experiment similar to the one described by Fuller will be performed for the adsorption of humid air onto activated carbon at 293°K, firstly for the complete pressure range, $0<p/p_0<1$ where $p_0=P_0+dP$, secondly for the pressure region P_0 to P_0-dP and thirdly for the range P_0 to P_0+dP (P_0=101325Pa, dP=5000Pa). This will help quantify the adsorption and desorption effects in the case of a series of static compression and rarefaction pressure steps and aid derive the sorption rate constants at those conditions. Results from the adsorption isotherm experiments will also provide clear indication of the rates of adsorption and desorption, the presence of hysteresis, as well as the integral heat of adsorption at the small compressed and rarefied pressures present in acoustic waves. This will help quantify the influence of such effects on the propagation of sound waves through materials exhibiting sorption properties.

Another likely effect causing the energy loss at low frequencies could be due to the presence of a large number of pores of micron and sub-micron dimensions, evident from the PSD plot in part *(a)* of *Figure 2* below. At this small scale the mean-free molecular path (~60nm) becomes comparable to the pore dimensions and a slip boundary condition on the pore walls is necessary for a correct representation of the fluid flow [5]. Results from an analytical model, based on work by Umnova *et al.* [6] studying the influence of slip boundary condition on dynamic flow perpendicular to a regular array of rigid cylinders are presented below. The predicted surface impedance for such an array, 2.42cm thick of porosity equal to 75% and cylinder radius equal to 100nm is presented in part *(b)* of the figure below and compared to measurements on a sample of activated carbon of the same thickness with a grain size distribution between 0.30 and 0.42mm.

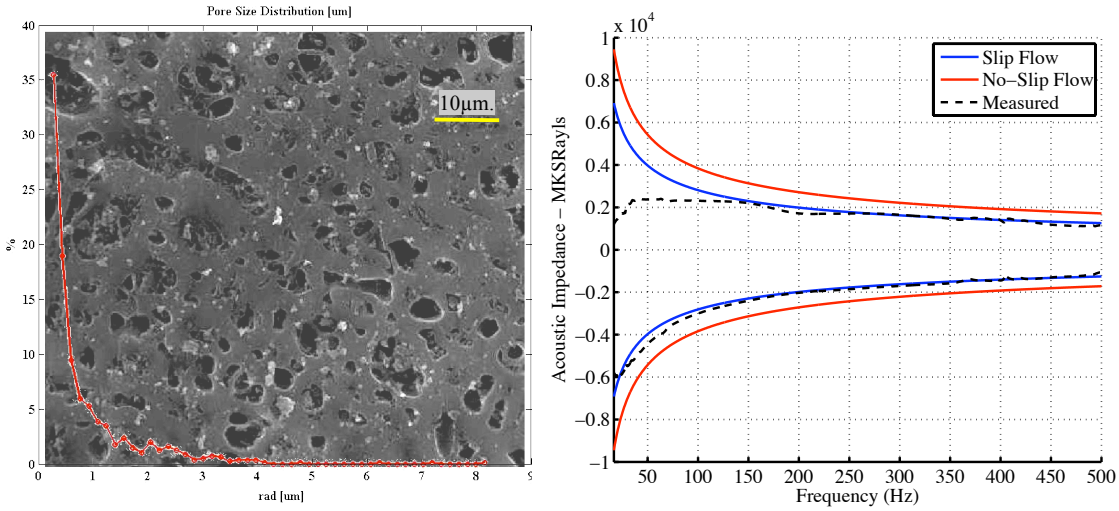

Figure 2 Part *(a)*, pore size distribution derived from a SEM image of a granule of activated carbon. Part *(b)*, measured and predicted surface impedance results, based on the model described by Umnova *et al* [6].

References

[1] F. Bechwati, O. Umnova and T. J. Cox, "New semi-empirical model for sound propagation in adsorbing microporous solids (activated carbon)", on the CD ROM: *19th International Congress on Acoustics Madrid,* September 2007.

[2] IUPAC Manual of Symbols and Terminology, Appendix 2, Part I, "Colloid and surface chemistry"*, Pure and Appl. Chem.,* 31, 578, 1972.

[3] H. Marsh and F. Rodriguez-Reinoso, "Activated Carbon", *Elsevier Science & Technology Books*, 2006.

[4] G. Horvath, "Energetic interactions in phase and molecular level pore characterization in the nano-range", *Colloids and Surfaces*, 141:295, 1998.

[5] V. F. Kozlov and A. V. Federov, "Acoustic properties of rarefied gases inside pores of simple geometries", *J. Acoust. Soc. Am.,* 117 (6), 2005.

[6] O. Umnova, D. Tsilklauri and R. Venegas, "Influence of boundary slip on acoustical properties of fibrous porous materials", on the CD ROM: *Proceedings of the Acoustics '08 Paris,* July 2008.

SECOND SYMPOSIUM ON THE ACOUSTICS OF PORO-ELASTIC MATERIALS
UNIVERSITY OF BRADFORD, ENGLAND, DECEMBER 17-19, 2008

A Novel Cold Extrusion Process to Tailor a Porous Structure from Plastic, Rubber and Fibre Particulate Waste

A. Khan, K.V. Horoshenkov, H. Benkreira, R. Patel, M.J. Swift
School of Engineering, Design and Technology, University of Bradford, UK

EXTENDED ABSTRACT

INTRODUCTION

This work is based on a novel cold extrusion process that has been developed to tailor a porous structure from polymeric waste. The extruder conveys and mixes the particulates with a reacting binder. The end result is the continuous production of bound particulates through which the amount of carbon dioxide gas that is evolved during the reaction is controlled to give the desired acoustic properties.

The tailoring of acoustic materials from polymeric waste poses a broad challenge that is perhaps best appreciated by considering the range of applications where specific types of new porous materials are needed for use in devices or systems that perform specific functions for example in buildings, automotives, white goods etc. These applications will require tailoring of the polymeric waste not only on the molecular size scale, the area of chemical synthesis, but also on the meso and macroscopic size scale, the domain of the waste material type and processing. Tailoring porous materials from recycled polymeric waste raises the question of how porosity can be tailored in a controlled manner. In general, the creation of porosity within the structure requires study at a molecular level, the use of chemistry to organise the waste material into a porous material, with possibly improved mechanical properties by allowing the grains/fibres to be securely bonded together to achieve a porous product. It is possible in this fashion to achieve tailored materials from waste that have a specific absorbance to serve a specific function.

THE COLD EXTRUSION PROCESS

Granular media has been studied extensively in the past; Horoshenkov et al have studied the properties of granular media extensively [1-7] using the batch mixing of the waste with a binder followed by pressing and drying. Based on the results obtained by Horoshenkov et al and given the wide variety of granular waste material that is available, it is surprising that recycled granular waste is not being directed more to make acoustic materials. Work done by Swift [8] has shown that lorry tyre granules can be recycled to make materials for impact damping giving similar performance compared with commercial products.

In this research work an entirely new approach to the tailoring of porous materials will be presented. For acoustic applications the pore size distribution plays a major role, how this is controlled will be presented. The knowledge gained in batch process mixing will be applied to develop a continuous extrusion process that will not require heat. The extruder will be used as a solid conveyor and a solid mixer.

The granules are mixed in the barrel of the extruder, water and binder is injected from the top of the barrel. At the end of the barrel a die is attached to give the mixture a shape, the mixture falls onto the conveyer for curing.

THE PRODUCTS

The materials made using the cold extrusion technology (Figure 1) are compared with commercial materials for sound absorption (Figure 2). As it can be seen in Figure 2, the recycled material shows high absorption.

Figure1: Picture of products made from recycled polymeric waste

Figure2: Showing a comparison of recycled materials performance with commercial products (thickness = 25mm)

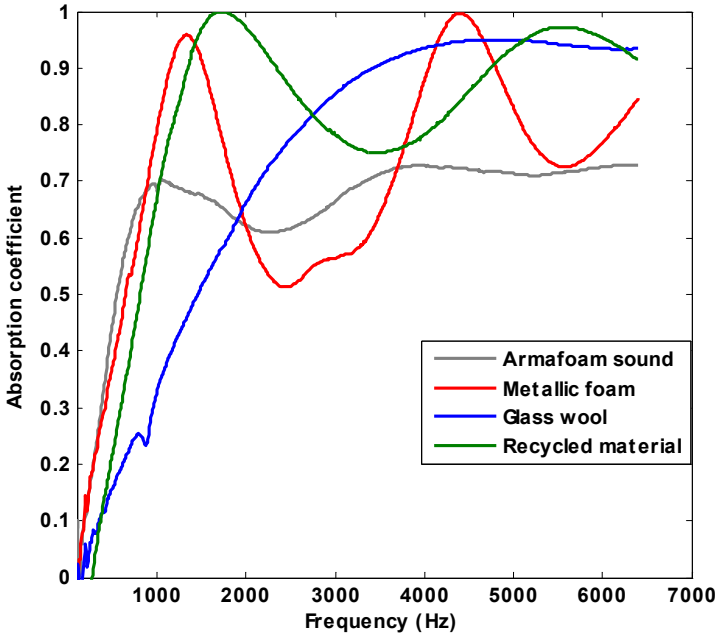

CONCLUSION

A novel cold extrusion process has been developed to structure acoustic structures using polymeric waste. In this work, two distinct models are applied and compared to predict the intrinsic acoustic properties of extruded samples aiming at identifying an engineering tool for correlating the process parameters and the performance of complex materials. Particular attention was paid to the relations between the non-acoustic characteristics of the extruded

materials in an attempt to fully characterise the materials using the Pade approximation and the Johnson Champoux Allard models [9].
As the extrusion is carried out cold and has the advantage of being a continuous process, this new production process requires 4-5 times less energy in comparison with that used for conventional commercial products.

REFERENCES

1. Horoshenkov K. V and Swift M. J, "The acoustic properties of granular materials with pore size distribution close to log normal", Journal of the Acoustical Society of America, volume 110, number 5, November 2001.
2. Voronina V. V, and Horoshenkov K. V, "Acoustic properties of unconsolidated granular mixes", Applied Acoustics, volume 65, 2004, p 673-691.
3. Leclaire P, Swift M. J, Horoshenkov K. V, "Determining the specific area of porous acoustic materials from water extraction data", Journal of Applied Physics, volume 84, number 12, December 1998.
4. Horoshenkov K. V and Swift M. J, "Acoustical properties of consolidated rubber granulates", 5th International Symposium, Transport noise and vibration, St. Petersburg, Russia, June 2000.
5. Miraftab M, Rushforth I, Horoshenkov K. V, "Acoustic underlay manufactured from carpet tile wastes", Autex Research Journal, volume 6, number 1, March 2006.
6. Rushforth I, Horoshenkov K. V, Swift M. J, Miraftab M, "Acoustic damping properties of recycled carpet waste", Euronoise conference, Naples 2003.
7. Miraftab M, Horrocks R, Woods C, "Carpet waste, an expensive luxury we must do without", Autex research journal, volume 1, number 1, 1999.
8. Swift M, "Physical properties of porous recycled materials", PhD Thesis, University of Bradford, 2000.
9. A. Khan et al, "A novel cold extrusion process for making vibro-acoustic products from recycled raw materials", Internoise 2008, Shanghai, China, Conference CD proceedings.

Estimating effective elastic properties of heterogeneous porous media using time-domain finite element modelling

Fabian Wenzlau, Johannes B. Altmann and Tobias M. Müller

July 22, 2008

Abstract

Attenuation and dispersion of seismic waves are often observed within fluid-saturated reservoirs. An important relaxation mechanism causing these signatures is the so-called wave-induced flow of fluids in the pore space. This mechanism is always important when small-scale heterogeneities such as cracks or gas inclusions are present within the medium and porosity and permeability are sufficiently high to allow fluids to flow during the wave cycle. The effective elastic properties of such heterogeneous rocks are described by the Biot theory of poroelasticity at low frequencies. Using a finite element scheme, the relaxation of heterogeneous poroelastic structures is investigated and attenuation and velocity dispersion are inferred. The accuracy of the approach is demonstrated by comparison with an analytical solution.

1 Introduction

The wave-induced flow of pore fluids is considered as one of the most prominent loss mechanism for seismic waves. An explanation for this effect is that in heterogeneous rocks, a passing wave induces pore pressure differences across internal interfaces that drive fluid flow to equilibrate the pore pressure disturbance. Since the flow of a viscous pore fluid is associated with friction, energy is withdrawn from the propagating wave which causes frequency-dependent attenuation. Typically, the scale of the pore pressure equilibration process is several centimetres and the process is therefore mesoscopic for seismic waves.

White et al. (1975) theoretically modelled the effect of wave-induced flow in partially saturated rocks with periodic stratification or with spherical inclusions. More recently, new models have been presented that account for the random distribution of pore fluids (Toms et al., 2007; Müller et al., 2008). In order to verify new theoretical models and to further develop the understanding of waves in porous media, numerical modelling tools are necessary. Usually, dispersion and attenuation are estimated from numerical wave propagation experiments by using the spectral ratio or frequency shift method (e. g. Rubino et al., 2007, and references therein). A different approach was suggested by Masson and Pride (2007) who simulate quasistatic experiments based on a finite differences solver for the dynamic Biot equations. Using their approach, the model size is considerably reduced to only one representative elementary volume (REV).

In this paper, we further develop the idea of Masson and Pride (2007) and propose a new and simple strategy for estimating effective elastic moduli from quasistatic relaxation experiments. From the moduli, velocity dispersion and attenuation are derived straightforward. The simulations are carried out using the commercial Abaqus finite element solver, a package that allows to calculate consolidation processes based on the Biot theory. A synthetic rock model consisting of two porous layers serves as a benchmark test for our approach.

2 Quasistatic relaxation experiments

For the sake of clarity, we confine ourselves to the one-dimensional case, although it is easy to extend the idea to the 2-D and 3-D case. Consider a heterogeneous, fluid saturated, porous rock sample with the height L that is confined laterally, sealed

hydraulically and representing an REV of a porous rock. Initially, a vertical uniaxial strain $\langle \varepsilon_{zz} \rangle$ is imposed instantaneously on the sample, resulting into an initial stress state σ^0_{zz} within. The following pore pressure diffusion process governs the relaxation of the whole sample.

The simulations are carried out in the time domain. In order to transform the results to the frequency domain, we calculate the creep function ϕ commonly used in the context of viscoelastic materials (Aki and Richards, 1980). We calculate the P-wave modulus H according to

$$H(t) = \sigma_{zz}(t)/\langle \varepsilon_{zz} \rangle. \tag{1}$$

and obtain the creep function ϕ by

$$\phi = H_0/H(t) - 1, \tag{2}$$

where H_0 is the initial P-wave modulus at time $t = 0$. The complex, frequency-dependent, effective P-wave modulus is then

$$\tilde{H}(\omega) = \frac{H_0}{1 + \int_0^\infty \dot{\phi}(\tau)\, \exp(i\omega\tau)\, d\tau}. \tag{3}$$

Here, the dot denotes the time derivative. P-wave velocity and attenuation are obtained from the effective modulus $\tilde{H}$ and bulk density ρ by

$$v = \sqrt{\mathrm{Re}\, \tilde{H}/\rho} \quad \text{and} \quad Q^{-1} = -\mathrm{Im}\, \tilde{H}/\mathrm{Re}\, \tilde{H}. \tag{4}$$

3 Example for a partially saturated rock sample

In order to exemplify the applicability and accuracy of the proposed method, we show results for a porous rock with given diffusivity D, saturated with two fluids, 50% water and 50% gas. We assume typical values of the rock and fluid properties and a periodically layered fluid distribution with spatial period L. For this case, an analytical solution is provided by White et al. (1975). Results for the velocity dispersion and attenuation of a P-wave are shown in Figure 1. We find that our numerically obtained estimates are in excellent agreement with the predicted values.

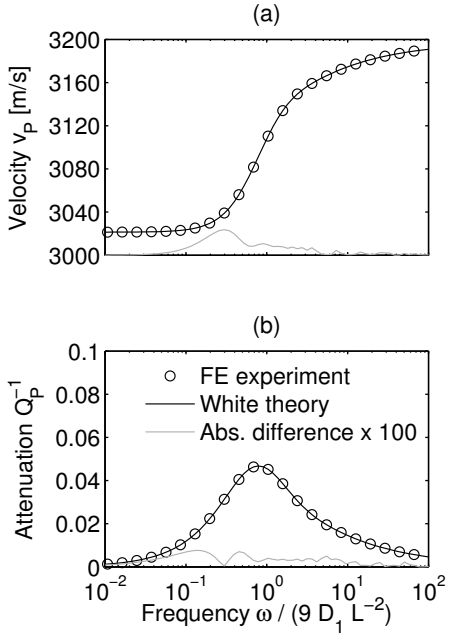

Figure 1: Velocity dispersion (a) and attenuation (b) for a partially saturated rock sample. Frequencies are normalised using the diffusivity D and spatial scale L.

References

Aki, K. and Richards, P. (1980). *Quantitative Seismology: Theory and Methods*. WH Freeman.

Masson, Y. J. and Pride, S. R. (2007). Poroelastic finite difference modeling of seismic attenuation and dispersion due to mesoscopic-scale heterogeneity. *Journal of Geophysical Research*, 112(B3).

Müller, T. M., Toms-Stewart, J., and Wenzlau, F. (2008). Velocity-saturation relation for partially saturated rocks with fractal pore fluid distribution. *Geophysical Research Letters*, 35:L09306.

Rubino, J. G., Santos, J. E., Picotti, S., and Carcione, J. M. (2007). Simulation of upscaling effects due to wave-induced fluid flow in Biot media using the finite-element method. *Journal of Applied Geophysics*, 62(3):193–203.

Toms, J., Müller, T. M., and Gurevich, B. (2007). Seismic attenuation in porous rocks with random patchy saturation. *Geophysical Prospecting*, 55:671–678.

White, J. E., Mikhaylova, N. G., and Lyakhovitskiy, F. M. (1975). Low-frequency seismic waves in fluid saturated layered rocks. *Physics of the Solid Earth*, 11:654–659.

Acoustic propagation in bubbly viscoelastic materials

V. Leroy (1), A.L. Strybulevych (2), M.G. Scanlon (3), J.H. Page (2),
(1) Laboratoire MSC, Université Paris Diderot-Paris 7, CNRS, Paris, France
(2) Department of Physics & Astronomy, University of Manitoba, Winnipeg, Canada
(3) Department of Food Science, University of Manitoba, Winnipeg, Canada

It is well-known that the presence of bubbles in a *liquid* has a tremendous impact on its acoustic properties. For example, the injection of air in water with a volume fraction of Φ=0.4 % is enough to reduce the velocity of sound, at low frequencies, to roughly 200 m/s, a value which is even lower than the velocity of sound in the air that comprises the bubbles. This surprising property is well established [1], has been thoroughly checked experimentally [2, 3] and can easily be demonstrated with the everyday life experiment of the "hot chocolate effect" [4].

Bubbly liquids exhibit other surprising behaviors when one inspects their properties at higher frequencies. Indeed, bubbles are very special acoustic scatterers because they experience a very low frequency resonance, known as the Minnaert resonance [5]. Typically, a 0.1-mm radius air bubble in water has a Minnaert resonance at 30 kHz, which corresponds to an acoustic wavelength in water of 5 cm, thus 500 times larger than the bubble radius. As a consequence of this long wavelength resonance, the large acoustic effects due to the bubbles can still be described by an effective medium theory. Figure 1 shows the prediction of Foldy's model[1] [6] for the effective velocity (Fig. 1a) and the attenuation (Fig. 1b) of sound in water with a 0.4% volume fraction of 0.1-mm radius bubbles. Three different regimes of propagation can be seen, as functions of the frequency ranges. At low frequency (i.e. below the Minnaert frequency), the medium is non dispersive with a low velocity (Wood's approximation) and an attenuation mainly due to thermal losses. At the intermediate frequencies, the medium becomes very dispersive, with a sharp increase of the velocity to very high values (20 000 m/s), and highly attenuating (2000 m^{-1}). At higher frequencies -as a rule of thumb, when the wavelength is comparable to or smaller than the typical distance between two bubbles- the phase velocity becomes close to the velocity of sound in the water, and the attenuation, mostly due to radiative losses, attains much lower values.

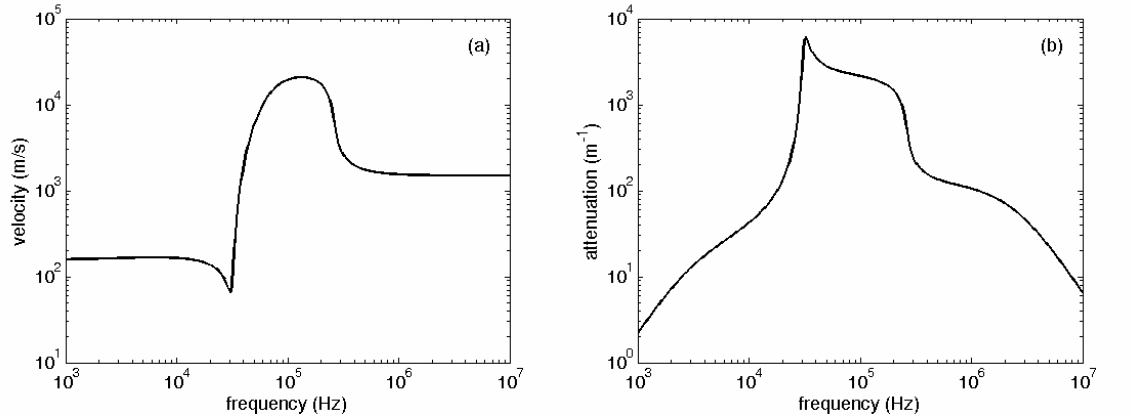

FIG. 1: *Prediction of Foldy's model for the phase velocity (a) and the attenuation (b) of sound in water with a 0.4% volume fraction of 0.1-mm radius bubbles.*

Foldy's model has been experimentally validated for bubbly liquids with gas fractions below 0.01% [3,7]. For these very dilute media, an ultrasonic technique for measuring the

[1] Foldy's model is equivalent to the ISA (independent scattering approximation).

size of the bubbles has been developed [8]. But for higher concentration in bubbles, there is a lack of experimental data and a theoretical controversy exists about how Foldy's model should be corrected for taking into account the coupling between the bubbles [9-12].

In the talk, we will present recent experimental data obtained with *concentrated* bubbly *viscoelastic* liquids. Indeed, most bubbly materials of practical interest are viscoelastic rather than Newtonian, and have a concentration of bubbles significantly higher than 0.01%. We investigated several concentrated bubbly samples whose matrix had increasing shear moduli: hair gel, agar gel, bread dough, and reticulated PDMS.

For bubbly hair gels and agar gels, the real part of the shear modulus is smaller than the atmospheric pressure. In this case, the Minnaert frequency of the bubbles was not affected and we found good agreement between the experimental data and Foldy's model, even at the highest concentration of 1% we managed to measure [13]. We also demonstrated that ultrasound was a good tool for measuring the size distribution of both air bubbles and polystyrene beads incorporated in the same agar matrix [14].

In the cases of bread dough and reticulated PDMS, the shear modulus was large enough to significantly affect the properties of the bubbles: the Minnaert resonance was shifted to a higher frequency. The effects of he bubbles on the phase velocity and the attenuation of sound was still strong, and their behaviors similar to the ones depicted in Fig. 1. However, agreement with Foldy's model was poor: the size distribution of bubbles needed to fit the data was significantly different from the one observed optically (for the PDMS) or by X-ray tomography (for the bread dough) [15]. Thus Foldy's model needs to be corrected for viscoelastic bubbly media. A possible correction will be discussed.

References

[1] A.B. Wood, *A Texbook of Sound* (Bell, London, 1932)
[2] M. Nicholas, R.A. Roy, L.A Crum, H. Oguz, and A. Prosperetti, *J. Acoust. Soc. Am.* **95** (1994)
[3] P.S. Wilson, R.A. Roy, and W.M. Carey, *J. Acoust. Soc. Am.* **117** (2005)
[4] F.S. Crawford, *Am. J. Phys.* **50** (1982)
[5] M. Minnaert, *Phil. Mag.* **16** (1933)
[6] L.L. Foldy, *Phys. Rev.* **67** (1945)
[7] E. Silberman, *J. Acoust. Soc. Am.* **29** (1957)
[8] R. Duraiswami, S. Prabhukumar, and G.L. Chahine, *J. Acoust. Soc. Am.* **104** (1998)
[9] Z. Ye and L. Ding, *J. Acoust. Soc. Am.* **98** (1995)
[10] C. Feuillade, *J. Acoust. Soc. Am.* **99** (1996)
[11] F.S. Henyey, *J. Acoust. Soc. Am.* **105** (1999)
[12] S.G. Kargl, *J. Acoust. Soc. Am.* **111** (2002)
[13] V. Leroy, A.L. Strybulevych, M.G. Scanlon, and J.H. Page, *J. Acoust. Soc. Am.* **123** (2008)
[14] A.L. Strybulevych, V. Leroy, M.G. Scanlon, J.H. Page, *Soft Matter* **3** (2007)
[15] V. Leroy, Y. Fan, A.L. Strybulevych, G.G. Bellido, J.H. Page, M.G. Scanlon, *Bubbles in Food 2: Novelty, Health and Luxury* (Eagan, St. Paul, 2008)

Acoustical properties of disordered arrays of circular cylinders

Rodolfo Venegas and Olga Umnova
Acoustics Research Centre, University of Salford, United Kingdom.
r.g.venegascastillo@pgr.salford.ac.uk
To be presented at SAPEM 2008. December 17-18-19, 2008, Bradford, UK.

Acoustics of porous media has been comprehensively studied by using different approaches that mainly fall into three categories, i.e. empirical models, semi-phenomenological models and direct simulations based on a micro-structural approach. Empirical models are based on fitting experimental data and proposing empirical laws [1]. The main drawback of this approach is given by the non-general nature of the proposed fitted functions and the range of applicability limited to the physical characteristics of the materials measured. Semi-phenomenological models are based on proposing scaling functions, which depend on macroscopical independently measurable parameters to describe viscous and thermal behaviour of the medium. Within this category, one of the most important contributions has been made by Johnson et al. [2], who introduced the concept of dynamic tortuosity to describe frequency-dependent viscous interactions between the pore fluid and the frame. It depends on dc viscous permeability, porosity, tortuosity and viscous characteristic length, all of which can be independently measured. The complete acoustic characterization however should also consider the thermal behaviour of the porous medium. The work by Champoux and Allard [3] further complemented by Lafarge et al. [4] serves this purpose. They introduced another scaling function, complex compressibility, which depends on dc thermal permeability, porosity and thermal characteristic length. The main disadvantage of this approach is the difficulty in measuring all the parameters involved in the modelling. The approach to be used in this work corresponds to the direct numerical simulation based on homogenization theory [5,6]. This theory provides a rigorous method of deducing empirical laws, such as for example the dynamic Darcy's law [6]. Homogenization theory gives the governing equations at different levels. The main hypothesis behind this theory is the separation of scales, which in the context of porous media acoustics, is usually valid when sound wavelength exceeds the characteristic size of the medium. The equations at the respective level are solved in a representative elementary volume (REV) of the porous medium geometry by using an appropriate analytical or numerical method. The main drawback of this approach is the computational time and the use of relatively simplistic inner structure to represent the porous medium. This approach has been applied to model the acoustic properties of various regular structures, such as periodic arrays of cylinders with different cross-section shapes [7], metallic foams represented by a hexagonal array of cylinders [8] and cubic centered sphere packing [9].

In this work the acoustics of the disordered arrays of cylinders is studied numerically. The introduction of the disorder gives a more realistic approximation of the inner structure of fibrous materials widely used for the purpose of sound insulation. The disordered array of cylinders, which corresponds to the REV, is constructed using a Monte Carlo procedure [10, 11] considering periodic boundary conditions and porosities within the range [0.6, 0.95]. Dc viscous permeability k_0, tortuosity α_∞, viscous characteristic length Λ, viscous shape factor M, Biot viscous characteristic frequency ω_{vc}, dc thermal permeability k_0', thermal characteristic length Λ', thermal shape factor M' and thermal characteristic frequency ω_{tc} of the random arrays are computed by solving the steady forced Stokes problem, limiting oscillatory viscous flow problem for the high-frequency regime and the static heat transfer one in the REV and compared to the ones for regular array of cylinders [7]. More details of the numerical procedure, definitions and equations to be solved can be found in [7]. Figure 1 shows the static vertical fluid velocity of random configurations for porosities 0.7, 0.8 and 0.9 (left to right). The gradient of pressure was applied from top to bottom.

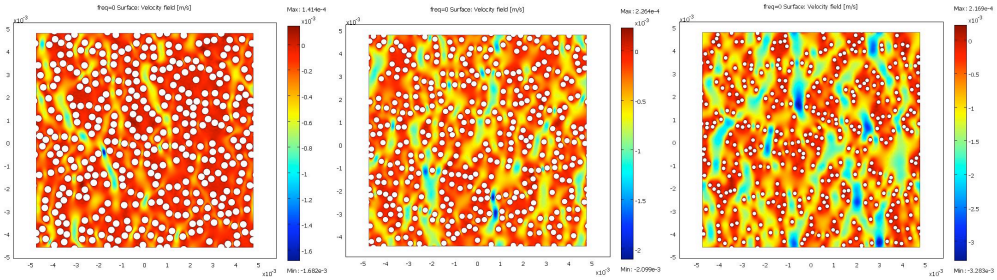

Fig 1. Vertical component of the static fluid velocity for porosities 0.7, 0.8 and 0.9 (left to right)

It has been found that mean values of tortuosity, thermal permeability, viscous and thermal shape factors of random arrays always exceed those of the regular arrays of the same porosity while the characteristic viscous length is always lower for random arrays. An interesting behaviour of dc viscous permeability was found similar to that mentioned in [11] and references therein. Below the critical porosity $\phi < \phi_c$, its mean value for random configurations is smaller than the permeability of the regular square array of cylinders $mean(k_0^{ran}) < k_0^{reg}$, while for porosities higher than critical, $\phi > \phi_c$, the random configurations have higher permeability. Biot viscous characteristic frequency shows the opposite trend. We are exploring the meaning of the critical porosity ϕ_c. Finally, the acoustical behaviour of the disordered configurations is investigated. The predictions of the Johnson-Champoux-Allard-Lafarge model [2,3,4] are compared to direct numeric simulations of sound propagation in randomly selected disordered configurations. It is also shown that dc viscous permeability behaviour influences the prediction of acoustical quantities such as speed of sound, attenuation coefficient, and characteristic impedance, mainly at low frequencies. Figure 2 shows frequency dependence of speed of sound where two distinctly different behaviors can be observed for porosities lower and higher than the critical one. Figure 3 displays absorption coefficient of a rigidly terminated layer of porous material, with thickness $d = 0.1\,\text{cm}$. It has been noted that the spatial distribution considerably affects acoustical quantities in general. However, this influence seems to be less important when predicting sound absorption.

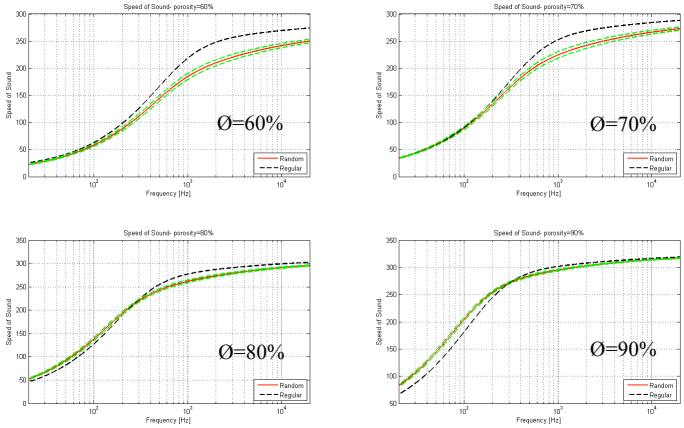

Fig 2. Speed of sound, regular square array of cylinder (dashed black line), mean value and standard deviation of speed of sound for random configurations (red line and green lines respectively).

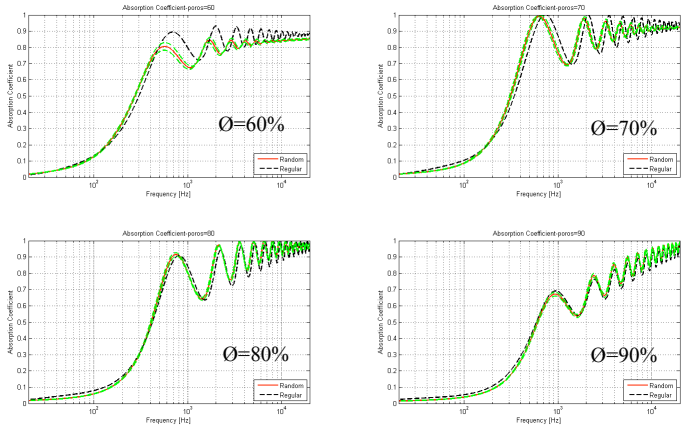

Fig 3. Absorption coefficient, regular square array of cylinder (dashed black line), mean value and standard deviation of absorption coefficient for random configurations (red line and green lines respectively)

References

[1] Delany, M. E. and E. N. Bazley. "Acoustical properties of fibrous absorbent materials", Applied Acoustics 3(2): 105-116 (1970).
[2] Johnson, D. L., Koplik, J. and Dashen, R., "Theory of dynamic permeability and tortuosity in fluid-saturated porous media", J. Fluid Mech. 176, 379-402. (1987).
[3] Champoux,Y. and Allard, J.F., "Dynamic tortuosity and bulk modulus in air-saturated porous media", J. Appl. Phys. 70, 1975-1979 (1991).
[4] Lafarge. D., Lemarinier, P., Allard. J. F. and Tarnow, V., "Dynamic compressibility of air in porous structures at audible frequencies", J. Acoust. Soc. Am 102 (4), 1995-2006 (1997).
[5] Sanchez-Palencia, E., "Nonhomogeneous Media and Vibration theory". Lect. Notes in Physics, vol. 127, Springer Verlag. Berlin (1980).
[6] Auriault, J.-L., Borne, L. and Chambon, R., "Dynamics of porous saturated media, checking of the generalized law of Darcy." J. Acoust. Soc. Am,77(5): 1641-1650 (1985).
[7] Venegas, R. and Umnova, O., "On the influence of the micro-geometry on sound propagation through periodic array of cylinders", Proc. Acoustics'08. June 29-July 4, 2008. Paris, France.
[8] Perrot, C., Chevillotte, F. and Panneton, R., Dynamic viscous permeability of an open-cell aluminum foam: Computations versus experiments, J. Appl. Phys. 103, 024909 (2008).
[9] Gasser, S. and Paun, F., Absorptive properties of rigid porous media: Application to face centered cubic sphere packing, J. Acoust. Soc. Am. 117 (4), Pt. 1, (2005).
[10] Torquato, S., Random Heterogeneous materials, Microstructure and Macroscopic properties, Interdisciplinary Applied Mathematics, Vol. 16 Springer Verlag, 2001. pp-270-278.
[11] Chen, X. and Papathanasiou, T. D., The transverse permeability of disordered fiber arrays: a statistical correlation in terms of the mean nearest interfiber spacing, Transp. Porous Med., Vol. 71, No 2, pp 233-251, (2008).

Linking polyurethane foam cell morphology to acoustical performance using X-ray tomography and Computational Fluid Dynamics.

Mark Brennan, Laurens Boeckx, Kristof Verniers, Jan Vandenbroeck
Huntsman Polyurethanes, CoreScience
Everslaan 45,
BE-3078, Everberg,
Belgium.

Camille Perrot
Groupe D`Acoustique de l`Universite de sherbrooke (GAUS, Department of Mechanical Engineering,
Universite de Sherbrooke, Quebec J1K 2R1, Canada

The acoustic performance of sound absorbing foams is determined by a large number of processes and parameters. Molecular dynamics (10^{-9} m), polymer chain properties (10^{-7} m), reptation (10^{-6} m), surface/interface tensions (10^{-5} m) and multiphase dynamics (10^{-4} m) all influence the bulk wave propagation through a sound absorbing foam. These bulk material properties combined with the exact boundary conditions and geometry of an acoustic component influence the final acoustical performance of a sound package. Numerous authors[1-6] have presented a study of the parameters that influence the bulk wave propagation in a foam. Direct and indirect measurement methods for flow resistivity, open cell porosity, tortuosity, viscous and thermal characteristic lengths have been described by P. Leclaire, among others[7-9]. Direct measurement methods for the wave number through porous materials by the use of a transmission loss tube have been presented by Song and Bolton[10]. Recently[11] a first step has been made relating the foam microstructure to the acoustical behaviour of aluminum foams by defining an equivalent 2D periodic unit cell representative for the 3D structure as determined by a μCT-scan.

This work will focus on the reconstruction of the full 3D structure of a PU foam from a μCT-scan. The reconstruction is then used to numerically solve the Navier-Stokes equations and to perform a structural FEA in order to investigate the influence of the 3D microstructure on different flow regimes, relate those to Biot-Allard parameters, and to the wave propagation throughout the porous structure. Ultimately this could lead to an increased understanding on how the foam morphology influences the acoustical performance of the material.

As a first step to validate, ideal foam structures are constructed and examined. A Kelvin[12] cell and Weaire-Phelan[13] structure are numerically constructed and the Navier-Stokes equations were solved for a steady state and a transient flow regime.

Geometrical data describing cell size distribution, Plateau border thickness and cell orientation were also derived from μCT-scan data using full 3D image processing algorithms. The automated full 3D approach provides information regarding anisotropy, cell formation, cell opening and more accurate estimates, compared to 2D image processing, of the geometrical data such cell size distribution.

The data from the μCT-scan are then directly converted to a structure which can be numerically handled. CFD and structural FEA are performed on a full 3D model of a real PU foam. Different flow regimes are applied at acoustically interesting frequencies providing estimates of the flow resistivity, porosity, the complex density, the complex compressibility and the sound absorption of a semi-infinite layer of idealised. Validations are provided by measuring the flow resistivity according to the ISO-9053, sound absorption is measured using the standing wave tube. The other parameters are determined either by inversion or by ultrasound.

References:

1. D.L. Johnson, J. Koplik and R. Dashen, J. Fluid. Mech., 176, 379 (1987).
2. Y.Champoux, J.F. Allard, J. Appl. Phys., 70, 1975, (1991).
3. J. F. Allard, Propagation of sound in Porous Media: Modeling Sound Absorbing materials , Edited by Elsevier applied Science, (Elsevier, New York, 1993).
4. D. Lafarge, P. Lemarinier, J.F. Allard and V. Tarnow, J. Acoust.Soc. Am. , 102, 1995, (1997).
5. S.R. Pride, F.D. Morgan and A.F. Gangi, Phys. Rev. B. 47, 4964 (1993).
6. D. Keith Wilson, J. Acoust. Soc. Am., 94, 1136-1145, (1993).
7. P. Leclaire, L. Kelders,W. Lauriks, M. Melon, N. Brown, B. Castagnede, J. Appl. Phys. 80, 2009-2012, (1996).
8. X.Only, R. Panneton, J. Acoust. Soc. Am. 123, 814, (2008).
9. Y. Champoux, M.R. Stinson, G.A. Daigle, J. Acoust.Soc.Am., 89, 910 (1991)
10. Bryan H. Song, J. Stuart. Bolton, J. Acoust.Soc. Am. 107, 1131. (2000)
11. C. Perrot, R. Panneton, X. Only, J. Appl. Phys. 101, 113538, (2007).
12. Lord Kelvin (Sir William Thompson), Philos. Mag. 24, 5033 (1887).
13. D.Weaire and R. Phelan, Philos. Mag. Lett. 69, 107, (1994).

Prediction and measurement of sound intensities and energy densities inside porous layers

Nicola Prodi, Paolo Bonfiglio
Dipartimento di Ingegneria, Università di Ferrara, Italia

1. Introduction

The use of sound intensity to investigate the surface properties of materials has gained increasing interest in the past as a complement to the conventional use of the acoustic impedance [1]. The main merit of the intensimetric approach is its direct link with the flow of sound energy, and thus with the dissipative characteristics of the material. This work stems from the theoretical framework presented recently [2] which demonstrated how the active sound intensity and the sound energy density obey a diffusion equation inside a porous layer. Thanks to this equation the local internal dissipative properties of the material, known as "sinks" of energy, are easily formalized. Moreover a differential formulation for the behavior of the energetic quantities is derived and solved. The theory is able to predict all of the second order energetic quantities inside the layer provided that a plane wave propagation is considered. Here the experimental validation of the theory is fully described involving the problems related with sound intensity measurements inside porous materials. The experimental data measured inside a porous sample placed in a plane wave tube fully validate the theory which is also consistent with the conventional transfer matrix approach.

2. Theoretical background

It has been shown recently [1] that, inside a porous layer, a diffusion expression can be written involving the active sound intensity (I) and the sound energy density (E) which reads $I = -D_T \nabla E$ (eq. 1) where $D_T = \frac{\omega}{2\,\alpha\,k} \left[\frac{m^2}{s}\right]$ is called the *sound transfer coefficient*. Physically speaking D_T accounts for the attitude of the material to host or not the sound transfer or, in other words, to be permeated by sound. It is directly proportional to frequency and inversely to the double of the product of the real and imaginary parts of the complex propagation constant of the material (α and k respectively).

Based on eq. (1) a differential formulation is also developed. The sink terms for the sound energy in the material (Q) and the source terms for the reactivity (R) are made explicit respectively as $Q = -2\omega\left[\mathrm{Im}(\tilde{\chi})|p(x)|^2 + \mathrm{Im}(\tilde{\rho})|v(x)|^2\right]$ and $R = -2\omega(E_P - E_K)$. Then an analytical solution for the course of the sound energies inside the material layer is achieved in the form $E_d(x) = C_1\cosh(2\alpha\,x) + C_2\sinh(2\alpha\,x) + C_3\cos(2k\,x) + C_4\sin(2k\,x)$ and finally the courses of the active and reactive sound intensities can be predicted too. The four $C_{1,2,3,4}$ constants are obtained from the values at the porous layer boundaries and the related first order derivatives.

3. Experimental validation

The measurements were taken inside a 12cm layer of melammine foam which was inserted in a plane wave tube and backed either with a rigid termination or with an anechoic one. The measurement positions were fixed in air in front of the material, inside the material (spaced 1cm

apart) and on the rigid backing. Impulse responses were measured by means of swept sine technique with a single pressure microphone at each position. All of the relevant quantities and corrections were elaborated off line via FFT analysis. Direct measurement of characteristic impedance and propagation constant of the material was also pursued. As regards the sound intensity measurements, the p-p technique was adopted to obtain the particle velocity and specific corrections were elaborated to account for the finite difference and for the material. An accurate estimate of the error was developed too [3].

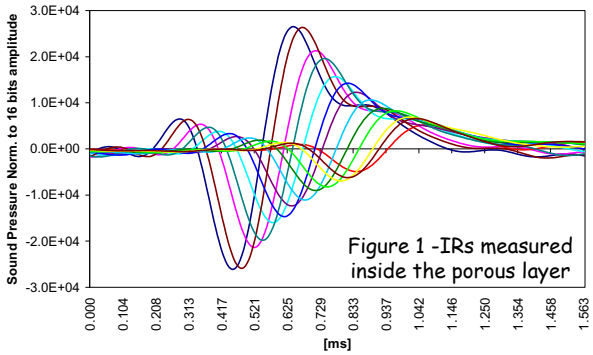

Fig 1 shows the impulse responses measured from the outside to the inside of the material. After sound intensities and sound energy densities were calculated, also the relevant theoretical curves were achieved by two methods: the former is the conventional impedance matrix formulation and the latter is the analytical solution of the diffusion equation presented above. In Fig. 2 and 3 two comparisons between measures and theories are reported showing typical results for active sound intensity (I) and potential sound energy density (E_P).

It is seen that the match of the experimental data with the diffusion theory is quite good since it is always within the experimental error. Furthermore the analytical solution and the transfer matrix approach show negligible discrepancies.

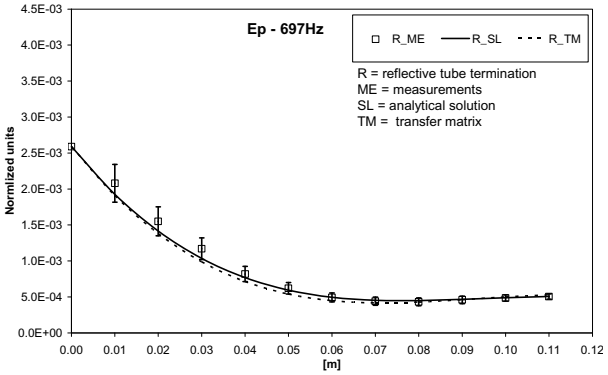

Figure 3 – Plot of results for E_P

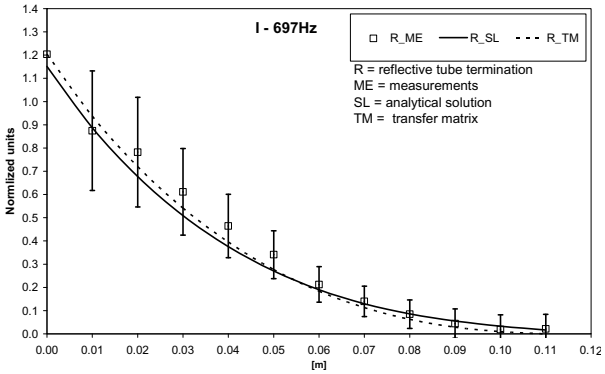

Figure 4 – Plot of results for I

4. Concluding remarks

In this work the analogy of the time averaged sound transfer inside a rigid frame porous materials with a diffusion process was experimentally validated. The active intensity inside a porous layer was demonstrated to obey a diffusion equation which is driven by the gradient of the sound energy density. The time averaged net transfer of energy is not affected by the local oscillations of energy described by the reactive intensity. The experimental data gave a robust validation to the above theory. The main applications are expected in the design and optimization of sound absorbing packages.

References

[1] P. Bonfiglio, N. Prodi, A. Farina, F. Pompoli, *On the use of a p-u sound intensity probe for the qualification of complex surface properties*, Proc. of 13 Inter. Conf. on Sound and Vib. – ICSV13, Wien, July 2-6 2006.

[2] N.Prodi, *On the diffusion of sound energy in porous materials*, Proc. of Acoustics08 Conference, Paris, June 28th – July 5th 2008.

[3] J.R.Taylor, *Introduzione all'analisi degli errori*, Zanichelli Editore, 2nd Ed., 2000.

Technical Requirements for Recycled Noise Control Materials

SAPEM 2008

There have been only very small changes in the development of acoustic insulation materials over the last 30 years. Mineral fibre and flexible foam insulation materials remain widely used across a range of industry sectors. Recent developments in recycling technologies have lead to a wealth of new possibilities for the creation of high performance and sustainable alternatives to these 'traditional' types of insulation. Driven by the desire to find alternative uses for our material waste, these developments, coupled with an increase in tougher noise legislation, offers a new commercial opportunity for insulation material producers.

Although acoustic properties are a fundamental consideration, care should be taken to fully understand the non-acoustic technical requirements for each market segment and application area. Whether it is for use in a building, or automotive, white goods or the marine/offshore environment, key considerations will usually include: fire and smoke/toxicity performance, mechanical integrity, chemical and UV resistance, resistance to fluid ingress, weight, handling and application details, thermal performance, temperature resistance, etc. Manufacturing costs are also a crucial consideration and many technologies, although technically excellent, are currently very expensive. Without due regard to all these issues, many producers of recycled acoustic materials will struggle with product positioning and ultimately, commercial realisation.

This presentation serves as a quick overview on some of these key considerations and provides an example of a product developed jointly by Bradford University and Armacell, which is successful within many industry segments throughout the world.

Dr. Mark Swift
Segment Manager Acoustic Products
Armacell UK Ltd.

Comment to Editor: There will be several slides with pictures and charts and these have to be finalised. I hope that you will allow me not to send these at this stage.

Generalized Variational Principle for Dissipative Hydrodynamics and its Application for Description of Generalized Biot's Models of Multiphase Media

German A. Maximov

The generalization of the Hamilton's and Osager's variational principles for dissipative hydrodynamical systems is represented in terms of the mechanical and thermal displacement fields [1-3]. A system of equations for these fields is derived from the extreme condition for action with a Lagrangian in the form of the difference between the kinetic and the free energies minus the time integral of the dissipation function. The generalized hydrodynamic equation system is then evaluated on the basis of the generalized variational principle. At low frequencies this system corresponds to the traditional Navier – Stokes equation system and in the high frequency limit it describes propagation of acoustical and thermal modes with the finite propagation velocities.

Based on the generalized variational principle [1-3] the system of the generalized Biot's equations is derived for consistent account of fluid shear relaxation. Account of shear viscosity relaxation leads to existence of a couple shear propagation modes additionally to a couple of longitudinal modes as in the Biot's approach [4]. At this the one shear mode is an acoustical one, while the other shear mode has a diffusive behavior at low frequencies. Phase velocity and attenuation factor for the second shear mode linearly depend on frequency in the low frequency limit that is different from analogous behavior of diffusive longitudinal mode with the root frequency behavior of analogous values.

The system of generalized Biot's equations, describing waves propagation in a multi-phase or multi-component medium in the presence of heat exchange between phases, is derived on the basis of generalized variational principle [1-3]. It is shown that in the presence of N phases 2N propagating eigen-modes can exist in this medium. At high frequencies N modes are of the acoustical type and N modes are of the diffusive (thermal) type of propagation. At low frequencies there is the single acoustical (wave) mode and the rest 2N-1 modes possess the diffusion (thermal) type of behavior. For a two-component medium without temperature exchange the developed approach is reduced to the well known Biot's model. The account of the temperature field yields the generalized Biot's model for two components medium [5].

1. Maximov G.A. On the variational principle for dissipative hydrodynamics. // Preprint 006-2006. Moscow. MEPhI, 2006. – 36p. (in Russian)
2. Maximov G.A. On the variational principle for dissipative hydrodynamics and acoustics. // Proc. XVIII session of RAS. –Moscow, GEOS, -2006. V.1. pp. 5-8. (in Russian)
3. Maximov G.A. On the variational principle in dissipative hydrodynamics. // Proc. Of International Conference "Days on Diffraction" 2006. May 30 – June 2, 2006, St.Petersburg, Russia, p.173-177.
4. Biot M.A. Theory of propagation of elastic waves in fluid-saturated porous solid. I. Low-frequency range. // J. Acoust. Soc. Am., 1956, V.28, N2, p.168-178.
5. Maximov G.A. Biot's equations for multiphase media with temperature gradient on the basis of generalized variational principle. // Proc. Of International Conference "Days on Diffraction" 2007. May 30 – June 1, 2007, St.Petersburg, Russia, p.109-111. ISBN 5-9651-0118-x

QUANTIFYING THE THROUGH-THICKNESS ASYMMETRY OF SOUND ABSORBING POROUS MATERIALS

Yacoubou SALISSOU and Raymond PANNETON
GAUS, Department of mechanical engineering, Université de Sherbrooke, Québec, Canada, J1K 2R1
Yacoubou.Salissou@USherbrooke.ca, Raymond.Panneton@USherbrooke.ca

1. INTRODUCTION

Sound absorbing porous materials are widely used in noise-control applications. When the material behaves as an equivalent fluid[1,2], its acoustic behaviour is completely defined by two intrinsic dynamic properties: its equivalent acoustical characteristic impedance ($\tilde{Z}_{eq}$) and complex wave number ($\tilde{k}$), or alternatively by its equivalent dynamic density ($\tilde{\rho}_{eq} = \tilde{Z}_{eq}\tilde{k}/\omega$) and bulk modulus ($\tilde{K}_{eq} = \tilde{Z}_{eq}\omega/\tilde{k}$), where ω is the angular frequency. Established acoustical impedance tube methods have been developed for measuring these dynamic properties[3,4,5,6]. All those methods assume the porous material to be a single layer with symmetrical acoustic properties. However, common porous materials are usually subjected to some variations in their microstructure during manufacturing. This may lead to macroscopic asymmetrical behaviours[7]. Unfortunately, there is no mean of simply quantifying the level of asymmetry (or symmetry) of a single porous layer.

In this paper, a method to quantify the through-thickness asymmetry of a sound absorbing porous material is proposed and discussed. The method only requires impedance tube measurements (ASTM E1050, ISO 10534) of the acoustical surface impedance performed on both sides of the tested material.

2. INDEX OF ASYMMETRY

Let P be a given bulk property (e.g., absorption coefficient, acoustical surface impedance, acoustical characteristic impedance or complex wave number) measured with an impedance tube. For the two-layered porous material shown in Fig.1, let P_{AB} be the value of P when the impedance tube measurement is performed when side A of the material is facing the incident sound wave (normal configuration), and P_{BA} the value of P when side B is now facing the incident sound wave (inverted configuration).

For each angular frequency, the asymmetry can be quantified by the relative difference between P_{AB} and P_{BA} expressed as

$$RD(\omega) = \left|P_{AB}(\omega) - P_{BA}(\omega)\right| \Big/ \max\left(\left|P_{AB}(\omega)\right|, \left|P_{BA}(\omega)\right|\right). \quad (1)$$

From Eq. 1, the average relative difference (*ARD*) of the bulk property P is defined as

$$ARD = \sum_{i=1}^{n} RD(\omega_i) \Big/ n, \quad (2)$$

where n is the number of discrete frequencies in the considered frequency range.

To verify if *RD* is a good basis for quantifying the asymmetry of a porous material, let consider a two-layered porous system. The first layer is made up from identical oblique circular cylindrical pores of radius $r = 0.1$ mm. Their inclination with respect to the surface normal is $\theta = 10°$. The geometrical properties of the second layer are $\theta' = (1+x)\theta$ and $r' = (1+x)r$, where x is their relative variation compared to the first layer. Each layer has a thickness $H = 12.5$ mm, and a surface pore density of $N = 30 \times 10^6$ pores/m². Simulated measurements of the normal incidence impedance tube problem shown in Figure 1 are conducted to obtain the sound absorption coefficient (α), acoustical surface impedance ($\tilde{Z}_s$), $\tilde{Z}_{eq}$ and $\tilde{k}$ on the two-layered porous system for different values of x. The simulations are made for both normal and inverted configurations and over the frequency range [300-4000 Hz]. Also, the effect of random noise is included in the simulations in order to better reflect real measurements. The simulation method is explained in the ref.[8].

Figure 2 shows the *ARD* values for α, $\tilde{Z}_s$, $\tilde{Z}_{eq}$, and $\tilde{k}$ as a function of the variation x. This result indicates that *ARD* (hence, *RD*) is consistent with the composition of each sample. Indeed, the *ARD* increases as the change in the geometrical properties increases. Also, it indicates that $\tilde{k}$ and α are less sensitive to the asymmetry of the material compared to $\tilde{Z}_{eq}$ and $\tilde{Z}_s$. Therefore, *ARD* (or *RD*) of $\tilde{Z}_{eq}$ and *ARD* (or *RD*) of $\tilde{Z}_s$ are both good candidates for studying the asymmetry of the material..

Contrary to $\tilde{Z}_{eq}$, $\tilde{Z}_s$ is not an intrinsic acoustical property of the sample (i.e., it depends on the thickness, rear boundary condition, and excited side). It has always a physical meaning even when the material is asymmetric – its determination does not require the symmetry property. This

is not the case with $\tilde{Z}_{eq}$. Because of that, $\tilde{Z}_{eq}$ looses its physical meaning when the material is asymmetric. For these reasons, it is not likely to quantify the asymmetry of a porous material from $\tilde{Z}_{eq}$; the most suitable indicator of the asymmetry should be defined from $\tilde{Z}_s$ (i.e. from RD of $\tilde{Z}_s$).

3. CRITERION FOR ASYMMETRY

Let us analyze how *RD* of $\tilde{Z}_s$ varies with the reduced frequency ϖ and x ($\varpi = \omega/\omega_v$ with the viscous transition frequency $\omega_v = 8\eta\cos\theta/\rho_0 r^2$, where ρ_0 and η are the density and viscosity of air). From the results of the simulations shown in Fig. 3(a), one can observe the following: **(i)** the typical evolution of *RD* as a function of x and ϖ from the low frequency ($\varpi < 1$) to high frequency ($\varpi > 1$) regime; **(ii)** at $\varpi \to 0$, and for *RD* lower than 10 %, *RD* is a good estimate of the overall variation of the geometrical properties (i.e., $x \approx RD$ at $\varpi \to 0$); **(iii)** at $\varpi = 1$, and for *RD* lower than 30%, *RD*/2 is a good estimate of the overall variation of the geometrical properties (i.e, $x \approx RD/2$ at $\varpi = 1$). From these observations, assuming that 5 % variation in the geometrical properties of the material is tolerable, and assuming that the same behaviour would be observed for any porous materials, the following criterion of asymmetry could be used over the frequency range of analysis: $\max\left(RD(\omega)\right) \geq 10\%$.

4. EXPERIMENTAL TESTS

Three real materials (a 50-mm thick melamine foam, a 30-mm thick fiber material and a 24-mm thick of another fiber material) were experimentally tested with a 44.5-mm diameter impedance tube. From the measurements, the *RD* curves are computed and plotted in Fig. 3(b) in function of the frequency. One can observe that the typical behaviour previously discussed is observed for the real materials. From these curves, it is clear that the melamine foam is acoustically symmetric (*RD* always smaller than 5 %). Also, the 24-mm thick fiber material can be considered acoustically symmetric ($\max\left(RD(\omega)\right) \prec 10\%$). However, the 30-mm thick fiber material seems to suffer from a slight asymmetry ($\max\left(RD(\omega)\right) \succ 10\%$).

ACKNOWLEDGEMENTS

N.S.E.R.C., REGAL, and ALCAN supported this work.

REFERENCES

[1]Allard, Propagation of sound in porous media, Elsevevier, NY (1993).
[2]R. Panneton, J. Acoust. Soc. Am. 122, EL217-EL222 (2007).
[3]R.A. Scott, Proc. Phys. Soc. London 58, 358-368 (1946).
[4]Utsuno et al., J. Acoust. Soc. Am. 86, 637-643 (1989).
[5]Iwase et al., Proc. Inter-Noise, New Zealand (1998).
[6]B.H. Song, J.S. Bolton, J. Acoust. Soc. Am. 107, 1131-1152 (2000).
[7]De Ryck et al., J. Appl. Phys. 102, 024910 (2007).
[8]Salissou and Panneton, JASA EL, accepted for publication

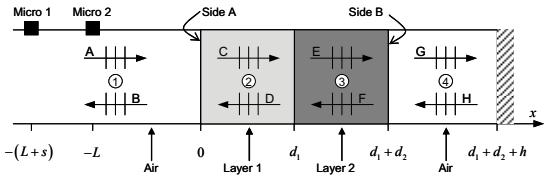

Figure 1: A schematic view of the impedance tube configuration with the two-layered porous material backed by a plenum of air and a hard termination.

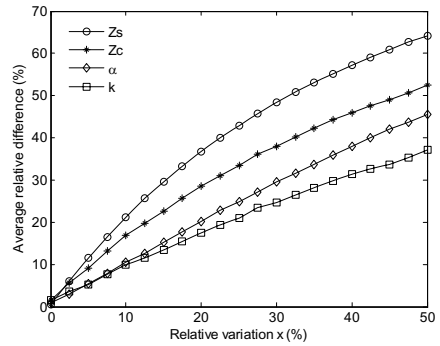

Figure 2: *ARD* of *Zs*, *Zc*,α and *k* plotted as a function of the relative variation *x*.

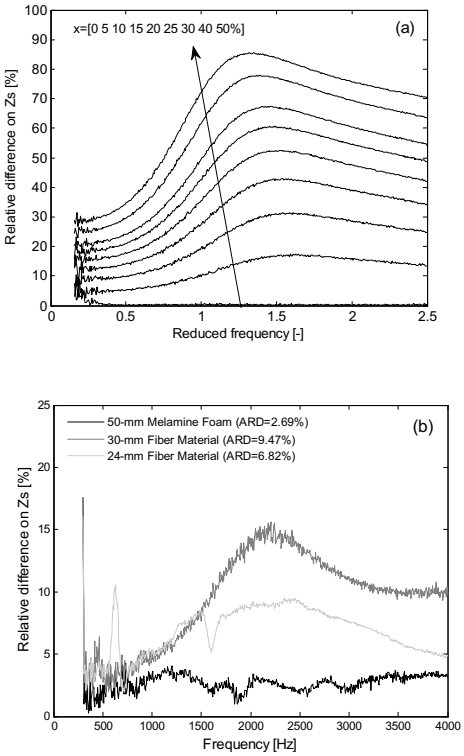

Figure 3: RD curves computed (a) from simulations on the two-layered porous system having oblique circular cylindrical pores with different values of the relative variation *x*, (b) from experimental measurements on melamine foam and two fiber materials.

Recent developments free field PU impedance technique

Emiel Tijs[1], Hans-Elias de Bree[1, 2]
[1]*Microflown Technologies, Zevenaar, The Netherlands, tijs@microflown.com, www.microflown.com*
[2]*HAN university, dpt. Vehicle Acoustics, Arnhem, The Netherlands*

Introduction

Current standard techniques to measure the acoustic material impedance have limitations. The Kundt's method requires a sample to be cut out and put in a fully reflective tube. Many materials including some porous materials are not locally reacting, meaning the impedance depends on the angle of incidence. With the Kundt's tube it is only possible to measure at perpendicular sound incidence. The walls of the tube can influence the behavior especially if the material has a high flow resistivity [15] like some foams or multi-layer materials. Some samples cannot be cut and leakage effects are observed when the tube is put highly porous surfaces (eg. road asphalt or some aircraft engine liners).
With a reverberant room it is possible to measure the diffuse absorption but it requires large and expensive facilities and samples of several square meters.
There is a need to measure samples in the free field, or better in situ, without sample cut-out or large amounts of material. The free field PU impedance technique was tested successfully for the first time in 2004 [4]. A so-called PU probe makes use of a dedicated velocity sensor combined with a microphone. Directly the impedance can be measured close to the material. This paper gives an overview of recent developments of this method.

PU free field principle

The PU free field surface impedance technique makes use of a Microflown velocity sensor and a sound pressure microphone. Both sensors are mounted in one probe that is positioned close to the material and a sound source is positioned at a certain distance. The impedance can be derived from the ratio of pressure and velocity [4-12]. From this, material reflection and absorption can be calculated. The probe is able to measure in the whole audible range but the lower frequency limit of the method at this moment is 100~300Hz. This is due to the low sound pressure emission from the loudspeaker at low frequencies (and the limited dimensions of the sample).

Fixed distance probe-source

A PU probe can be calibrated with a spherical source in an anechoic room [13]. A model is used to calculate the plane wave sensitivity. The spherical surface impedance can be measured with the same source and has to be converted to the plane wave impedance with e.g. a F-term correction [5]. If the source-probe distance is kept constant the measurement results are similar on several materials when no corrections are applied at all. The calibration model and the measurement model seem to cancel each other. This has to be supported by theory and more measurements in the future.

Figure 1. Handheld PU free field impedance setup

A simple point source model can be used to allow for the measurement distance [9]. Due to this simple model measurement results can be produced in real time.
A fixed probe-source distance is now possible because the setup in Figure 1 is made in such a way that vibrations from the loudspeaker are isolated from the sensor support. This is especially important when the impedance of the sample is high.
A typical calibration takes 5 seconds and again 5 seconds for the material measurement. So it is common to calibrate before each measurement session.

Low influence of reflections

The distance between the probe and the source is only 26cm so reflections at some distance are less dominant than the signal of the direct source. The calibration and measurement can be done in a regular office, but even in a strong reverberant environment like a car interior, see Figure 2 [9].

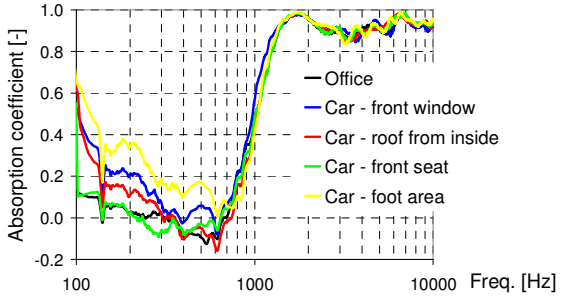

Figure 2. Absorption measurements in a car

A moving average in the frequency domain gives a result similar an anechoic measurement. A time windowing technique can also be used but the moving average is more robust [9]. The smoothed result should follow the actual impedance however when the actual impedance has a sharp change this averaging should not be applied, so some care is required.

Small spatial resolution
Because the method makes use of an ultra miniature PU probe the measurements can be done very close to the material. Much smaller samples are required than with other free field techniques. The measurement resolution is in the order of millimeters. Figure 3 shows the absorption calculated from the local impedance measured every 5mm above a sample with a quarter lambda tube [10]. To obtain the effective absorption of the whole sample the average impedance of the whole surface should be taken.

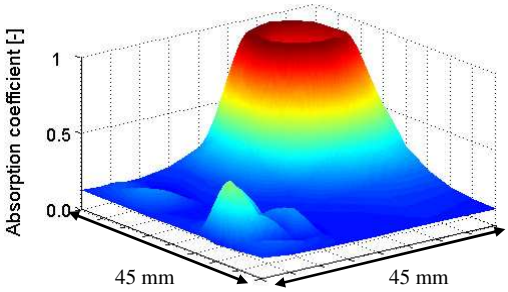

Figure 3. Absorption quarter lambda resonator at 1330Hz

Kundt's tube comparison
Results similar to the Kundt's tube are measured when the sample is measured in exactly the same conditions. Figure 4 shows certain samples can have totally different behavior when the sample size is increased, showing a limitation of the Kundt's method, [9]. In this figure also can be seen an absorption value lower than zero is measured. The reason for this is still unknown.

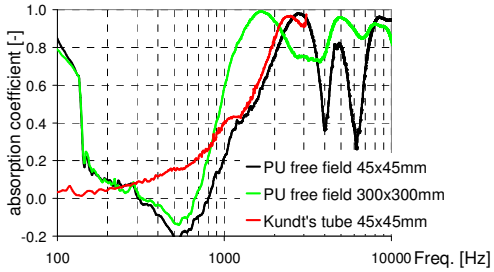

Figure 4. Influence of sample size

Moving samples and wind
Measurements are done on moving samples and it is possible to determine the absorption coefficient when the measurement time above an area of constant impedance is 0.05 seconds or larger [16]. This would for instance mean that the measurement area would be 1,1m if the speed would be 80km/h. These high speeds are necessary for impedance measurements on roads not to disturb traffic.
The acoustic behavior of materials may change after installation if the material is glued, mounted on a surface that is not fully reflective, etc. and needs to be checked. During production or time materials might vary. In line testing becomes feasible now.
Acoustic properties change when there is a flow over the material. Measurements are already successfully taken at relative low wind speeds of 7 m/s [16,17]. A goal is to measure aircraft engine liner material simultaneously at 0.5 mach, 500 deg Celsius and at high sound levels.

Measurements under an angle
It is possible to measure an acoustic sample under an angle [4,5,9]. The probe is rotated on the fixture and calibrated in this position. Measurements can now be taken with the probe in the normal direction. With this procedure the angle does not have to be modeled because the rotated calibration allows for this.

Conclusions
The handheld PU free field surface impedance technique has several benefits compared to established standard techniques that measure the acoustic material behavior. Due to a fixed probe-source distance corrections for the sound field during the calibration and the material measurement have become easier which reduced calculation power for the computer. Real time measurements on moving samples are possible. Measurements can be taken in situ, under an angle, even under difficult conditions like inside a car. The spatial resolution is in the order of millimeters, which could provide researchers extra insights in material behavior.
Further research will be focused on extending the method to lower frequencies to find the reason for absorption values lower than zero and measuring not only reflection, but also material transmission. The method shows the potential to measure with high flow speeds, high temperatures and at high sound levels. For utilization in a production environment the influence of very loud background noise needs to be investigated.

Special thanks goes out to W. Lauriks from the university of Leuven who contributed to the content of this paper.

References
[1] H-E de Bree et al, The Microflown; a novel device measuring acoustical flows, Sensors and Actuators: A, Physical, volume SNA054/1-3, pp 552-557, 1996
[2] H-E de Bree: The Microflown: An acoustic particle velocity sensor, Acoustics Australia 31, 91-94 (2003)
[3] M. A. Nobile and S. I. Hayek, Acoustic, propagation over an impedance plane, J.Acoust. Soc. Am. 78(4), 1325–1336, 1985.
[4] R. Lanoye et al, a practical device to determine the reflection coefficient of acoustic materials in-situ based on a Microflown and microphone, ISMA, 2004.
[5] R. Lanoye, G. Vermeir, W. Lauriks, R. Kruse, V. Mellert, Measuring the free field acoustic impedance and absorption coefficient of sound absorbing materials with a combined particle velocity-pressure sensor, JASA, May 2006
[6] Roland Kruse, Volker Mellert, In-situ Impedanzmessung mit einem kombinierten Schnelle- und Drucksensor, Daga 2006, Germany
[7] HE de Bree et al., Two complementary Microflown based methods to determine the reflection coefficient in situ, ISMA 2006
[8] J.D. Alvarez, F. Jacobsen, In-situ measurements of the complex acoustic impedance of porous materials, INTER-NOISE 2007
[9] HE de Bree, M. Nosko, E. Tijs, A handheld device to measure the acoustic absorption in situ, SNVH, GRAZ, 2008
[10] Tijs et al, Non destructive and in situ acoustic testing of inhomogeneous materials, ERF33, Kazan, Russia, 2007
[11] JD Alvarez and F Jacobsen, In-situ measurements of the complex acoustic impedance of porous materials, INTER-NOISE 2007
[12] H-E de Bree et al, Broad band method to determine the normal and oblique reflection coefficient of acoustic materials, SAE 2005
[13] Finn Jacobsen et al, A note on the calibration of pressure-velocity sound intensity probes, Jasa, 2006
[14] Yang Liu and Finn Jacobsen, Measurement of absorption with a p-u sound intensity probe in an impedance tube, ASA, 2005
[15] T.E. Vigran et al., Prediction and measurements of the influence of boundary conditions in a standing wave tube, Acta Acustica, 83, 419-423 (1997).
[16] Acoustic absorption measurements of moving structures and under influence of flow,E. Tijs et al, ISMA 2008
[17] PU surface impedance measurements on liner materials in the presence of a grazing flow, E. Tijs et al, CEAS 2008

Comparison of three measurement techniques of normal absorption coefficients in free field method using boundary element method

K. Hirosawa, H. Nakagawa, M. Kon and A. Yamamoto

System division, Nittobo Acoustic Engineering Co.,Ltd.
1-21-10 Midori, Sumida-ku, Tokyo 130-0021, Japan

1 Introduction

There are several in-situ measurement techniques of absorption coefficient in free field. A typical method is called the transfer function method using the sound pressures at two microphones[1]. Recently PU-Probe was developed [2], since it can measure the sound pressure and the particle velocity simultaneously, it is called “surface impedance method” which measures the acoustic impedance at one point near by an absorbing material[3].

Since the particle velocity is vector, it can be expected that the particle velocity has robustness to avoid the influence of the edge effect or extra reflected waves by objects. Therefore the new measurement technique can be thought to use the particle velocities at two points. In this paper, surface impedance method, two-microphone method and two particle velocities method are compared in regard to in-situ measurement technique of normal absorption coefficient. Here, surface impedance method is called “PU-method”, two-microphone method is called “PP-method” and two particle velocities method is called “UU-method”. The investigation uses boundary element method (BEM) in stead of physical experiments because of eliminating extra reflected waves and realizing ideal S/N ratio.

2 Analysis model

Fig.1 shows three dimensional hemi free field, xy plane is the rigid infinite plane. There is the absorbing surface F which has L[m]×L[m] area, and the center of the absorbing area is the origin. The distance between the source and the absorbing area is r[m].

The mirror image method is applied to the analysis model. The field is calculated by BEM for the sound pressure and the particle velocity[4]. In this paper, the quadrilateral constant element is used in BEM, maximum element length is less than 1/8 wavelength at the frequency. The formulation of BEM in frequency domain includes the whole edge effect.

The absorbing surface F is modeled as a locally reacting plane with the acoustic impedance of a 25 mm glass wool (flow resistivity 55000 Ns/m^4) at normal incidence. The normal acoustic impedance is estimated by the empirical equation proposed by J.F.Allard et.al.[5].

3 Measurement techniques

It assumes that the distance r_1 and r_2 are sufficiently large compared to the wavelength and F is locally reacting surface in Fig.2.

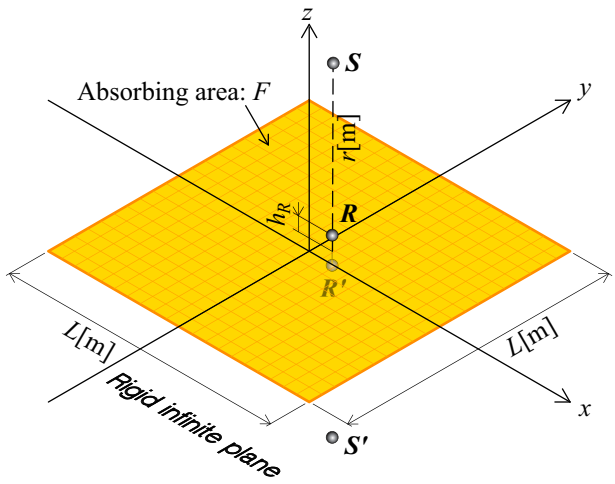

Fig. 1: Analysis model. $\boldsymbol{S}$: Real source, $\boldsymbol{S}'$: Imaginary source, $\boldsymbol{R}$: Real receiver, $\boldsymbol{R}'$: Imaginary receiver, h_R: Receiver height.

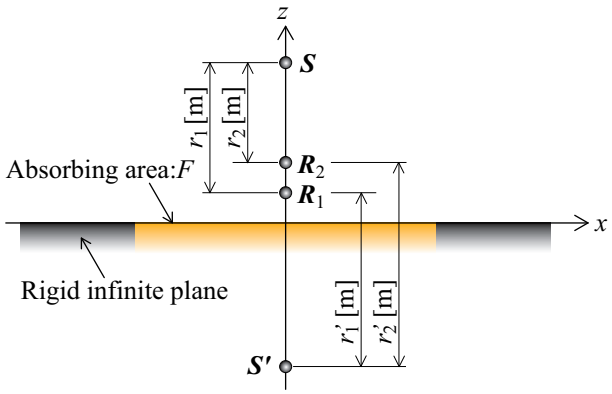

Fig. 2: Geometry of the sources and the receivers

3.1 PU-method

In Fig.2, $\boldsymbol{R}_1$ is the receiver position. Since the specific acoustic impedance $Z_n(\boldsymbol{R}_1)$ is the ratio of the sound pressure $p(\boldsymbol{R}_1)$ to the particle velocity $u(\boldsymbol{R}_1)$, the plane wave reflection coefficient R_p is given by[3]

$$R_p = \frac{\dfrac{\exp(-jkr_1)}{r_1}\cdot\left(Z_n(\boldsymbol{R}_1)\dfrac{1+jkr_1}{jkr_1'}-\rho c\right)}{\dfrac{\exp(-jkr_1')}{r_1'}\cdot\left(Z_n(\boldsymbol{R}_1)\dfrac{1+jkr_1'}{jkr_1'}+\rho c\right)}. \qquad (1)$$

3.2 PP-method

The ratio of the sound pressures at the receivers $\boldsymbol{R}_1$ and $\boldsymbol{R}_2$ is the transfer function $H(\omega) = p(\boldsymbol{R}_2)/p(\boldsymbol{R}_1)$, the plane wave reflection coefficient R_p is given by[1]

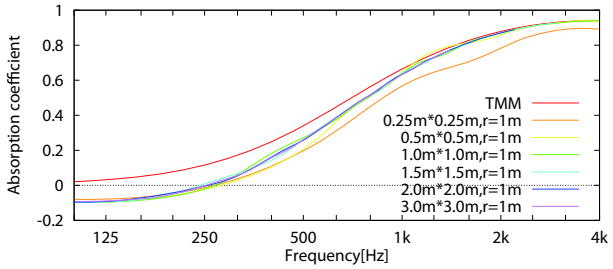

Fig. 3: PU-method, r = 1m

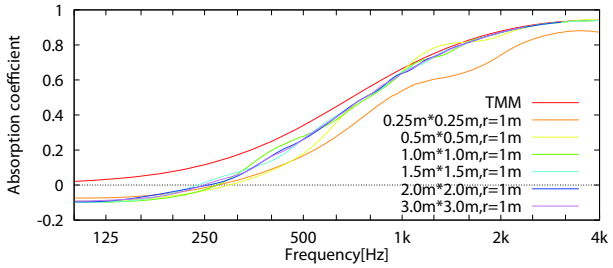

Fig. 4: PP-method, r = 1m

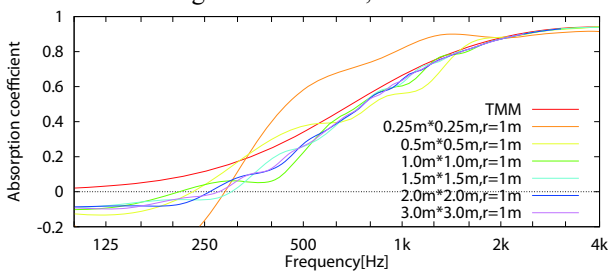

Fig. 5: UU-method, r = 1m

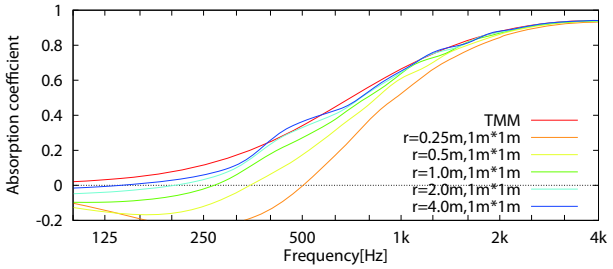

Fig. 6: PU-method, area: 1m×1m

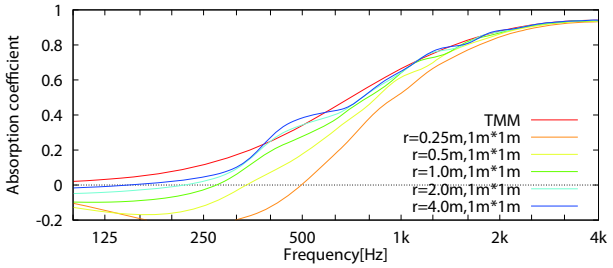

Fig. 7: PP-method, area: 1m×1m

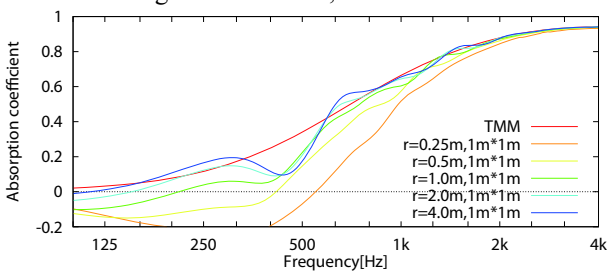

Fig. 8: UU-method, area: 1m×1m

$$R_p = \frac{\dfrac{\exp(-jkr_2)}{r_2} - H(\omega)\dfrac{\exp(-jkr_1)}{r_1}}{H(\omega)\dfrac{\exp(-jkr'_1)}{r'_1} - \dfrac{\exp(-jkr'_2)}{r'_2}}. \tag{2}$$

3.3 UU-method

The ratio of the particle velocities at the receivers $\boldsymbol{R}_1$ and $\boldsymbol{R}_2$ is the transfer function $H'(\omega) = u(\boldsymbol{R}_2)/u(\boldsymbol{R}_1)$, the plane wave reflection coefficient R_p is given by

$$R_p = \frac{\dfrac{1+jkr_2}{r_2}\dfrac{\exp(-jkr_2)}{r_2} - H'(\omega)\dfrac{1+jkr_1}{r_1}\dfrac{\exp(-jkr_1)}{r_1}}{\dfrac{1+jkr'_2}{r'_2}\dfrac{\exp(-jkr'_2)}{r'_2} - H'(\omega)\dfrac{1+jkr'_1}{r'_1}\dfrac{\exp(-jkr'_1)}{r'_1}}. \tag{3}$$

4 Calculated results

Fig.3 ~ Fig.5 show the normal absorption coefficients in the cases of different absorbing areas with $\boldsymbol{R}(0.1, 0.05, 0.01)$ and $\boldsymbol{S}(0.1, 0.05, 1.0)$. A legend "TMM" in the figures means the absorption coefficient calculated by transfer matrix method[6]. The absorption coefficients of PU-method and PP-method tend to converge with area is more than 1.5m×1.5m. However those of UU-method do not tend to converge, it is more sensitive in edge effect than PU-method and PP-method.

Fig.6 ~ Fig.8 show the absorption coefficients in the cases of different source heights r with fixed absorbing area 1m×1m, $\boldsymbol{R}(0.1, 0.05, 0.01)$ and $\boldsymbol{S}(0.1, 0.05, r)$. The source is higher, the absorption coefficient of finite absorbing area is closer to that of infinite area described by "TMM". Namely the major cause for variation of the absorption coefficient is the source height rather than the specimen area.

5 Conclusions and further studies

In this paper, three measurement techniques have been compared by BEM. As a result, it has found that PU-method is more stable against the influence of the edge effect than other methods, against original expectation. In the future, it will be also compared with the solution for the infinite absorbing area, and the elimination of the edge effect will be investigated by numerical analysis and physical experiments.

6 Acknowledgement

This research got useful advices from Prof. Walter Lauriks in Katholieke Universitet Leuven, to whom the authors are very grateful.

References

[1] J.F.Allard and Y.Champoux, *Noise Contr. Eng. J.* 32(1), pp.15-23 (1989)

[2] H-E. de Bree, *Acta Acustica* 89, pp.163-172 (2003)

[3] R.Lanoye, et al., *J.A.S.A.* 119(5), pp.2826-2831 (2006)

[4] T.Terai, *J.S.V.* 69(1), pp.71-100 (1980)

[5] J.F.Allard, et al., *J.A.S.A.*,91(6), pp.3346-3353 (1992)

[6] B.Brouard, et al., *J.S.V.*, 183(1), pp.129-142 (1995)

Some Historical Milestones in Modelling Sound Propagation in Porous Media

Keith Attenborough
Department of Design, Development, Environment and Materials,
The Open University, Milton Keynes MK7 6AA, UK

1. Introduction

Although the focus of SAPEM is the acoustical behaviour of materials used in building acoustics and noise control, the acoustical properties of porous media are of interest over a wide range of contexts including geophysics, underwater sediment acoustics, sound absorber design and ultrasonic monitoring of bone. Different contexts have given rise to specific idealisations for the purpose of analytical modelling. Particular interest is taken in the applicability of analytical approaches developed for concentrated suspensions to predicting the acoustical properties of rigid-porous media. Although key cross-context developments are well known there are other less noticed but important contributions relevant to specific applications and these are highlighted. The extent to which the resulting parameters are independently measurable and the roles of 'slow' waves in the various contexts are discussed.

2. Models for Rigid-Porous Media

2.1 Phenomenological models

The classical analytical approach to characterising sound propagation in a rigid-porous medium used modified equations of motion and continuity of the air within the pores [1,2]. If the material is supposed to be isotropic, then, in addition to the volume porosity of connected pores, this requires the introduction of two bulk parameters viz. flow resistivity and structure factor. To agree with data it was found necessary to allow these parameters to be frequency-dependent or 'effective'. Even frequency-dependence of 'porosity' has been suggested as a way of allowing for frame flexibility [3]. However, this would lead to parameters that have to be deduced from acoustical data. This is an inherent limitation of the phenomenological approach. A low frequency/high flow resistivity approximation of microstructural models (see 2.2) enables the structure factor to be identified as tortuosity [1]. A recent development of the phenomenological approach due to Berengier *et al* [4] includes frequency-dependent thermal effects. This model is cited in the HARMONOISE prediction scheme [5].

2.2 Microstructural models

A classical idealised microstructure is that of parallel cylindrical pores. The cross-sectionally averaged velocity in a circular capillary pore can be expressed in terms of a dimensionless parameter equal to the product of the pore radius and the viscous wave number [2]. This parameter can be expressed in terms of the ratio of frequency to the steady state flow resistivity of the bulk medium which is the basis for the widely-used semi-empirical model due to Delany and Bazley [6]. As long as viscous and thermal effects can be treated separately then the pore-based approach leads to explicit expressions for complex density and compressibility. The complex density function can be substituted by the viscosity correction function derived by Biot [7]. Comparison of the high-frequency asymptotic forms of the viscosity correction functions for circular capillaries and for parallel slit-like pores enabled Biot [7] to suggest a pore shape factor based essentially on the functional forms (involving Bessel or Kelvin functions of complex argument) for cylindrical pores. Subsequently work by Champoux *et al* [8, 9] has resulted in complex density (or viscosity) functions also for pores with triangular and rectangular cross sections. Borrowing from models for underwater sediment acoustics, the pore-based approach can be extended to pore size distributions [9, 10]. Consideration of low and high frequency asymptotes of a viscosity function for an arbitrary pore structure leads to the formulation proposed by Johnson *et al* [11] introducing the viscous characteristic dimension, subsequently incorporated along with an analogous thermal characteristic dimension in the well-known Johnson – Allard model [12]. It has been found possible also to characterise viscous and thermal effects in arbitrary microstructures using relaxation models [13]. Another microstructure that has been analysed using multiple scattering [14] and external flow [15-17] approaches is that of an array of parallel rigid fibres. A parallel elastic fibre microstructure has been used in

modelling ultrasound propagation in cancellous bones [18]. Stinson [19] has derived a powerful relationship between the complex density and complex compressibility functions by considering the similarity between the equations governing viscous effects and heat transfer effects in narrow tubes of uniform arbitrary cross section filled with ideal gas. This has been used in the derivation of an 'external' flow model for propagation in stackings of spheres [19].

3. Models for poroelastic media and slow wave contributions

Theories for rigid-framed porous media predict the sound propagation in the pore fluid. Biot theory [7], which has been confirmed by a rigorous homogenisation approach, predicts two dilatational waves ('fast' and 'slow' propagating mainly in solid and fluid respectively) and a shear wave in a poroelastic medium. Originally developed in the context of geophysical prospecting, it has been used extensively in underwater acoustics [20]. Important precursors to Biot theory, were the contributions, for example by Kosten et al [21], concerned with materials used in building acoustics. Despite the fact that the 'slow' wave is the predominant mode of propagation in air-filled porous media excited by airborne sound, there was controversy in the underwater acoustics community concerning the existence of the 'slow' wave for many years. The existence of 'slow' waves in water saturated materials has been demonstrated in the laboratory [22] and has been shown to have an important influence on attenuation in sediments where there are multiple layers. A similar role for 'slow' waves has been predicted at the interface between air- and water-filled layers in the propagation of groundborne vibration from underground railways [23]. 'Slow' waves have been found to have an influence on ultrasonic transmission through marrow-filled cancellous bones [24].

References

[1] Attenborough K. Acoustical characteristics of porous materials. Physics Reports **82**(3) 179-227 (1982)
[2] Attenborough K and Umnova O. Acoustics of Rigid-Porous Materials. Ch. 8, *Lecture Notes on the Mathematics of Acoustics*, ed. MCM Wright, Imperial College Press, 2005.
[3] Morse P M and Bolt R H. Sound waves in rooms. Rev. Mod. Phys. **16** 69 (1944)
[4] Bérengier M, Stinson M, Daigle G, Hamet J-F. Porous road pavements: Acoustical characterization and propagation effects. J. Acoust. Soc. Am. **101** 155-162 (1997)
[5] HARMONOISE contract funded by the European Commission IST-2000-28419, (http://www.harmonoise.org, 2000)
[6] Delaney M E and Bazley E N. Acoustical properties of fibrous absorbent materials. Applied Acoustics **3** 105-116 (1970)
[7] Biot M A. Theory of elastic waves in a fluid-saturated porous solid. Parts I and II. J. Acoust. Soc. Am. **28** 168-191 (1956)
[8] Champoux Y and Stinson M R. On acoustical models for sound propagation in rigid frame porous materials and the influence of shape factors. J. Acoust. Soc. Am. **92** (2) 1120-1131 (1992)
[9] Attenborough K. Models for the acoustical characteristics of air-filled granular materials. Acta Acustica **1** 213-226 (1993).
[10] Horoshenkov K V and Swift M J. The acoustic properties of granular materials with pore size distribution close to log-normal. J. Acoust. Soc. Am. **110** 2371-2378 (2001)
[11] Johnson D L, Koplik J and Dashen R. "Theory of dynamic permeability and tortuosity in fluid-saturated porous media", J.Fluid.Mech. **176**, 379-402 (1987)
[12] Allard J-F. *Propagation of Sound in Porous Media*. Elsevier Applied Science. London. 1993
[13] Wilson D K. Simple relaxation models for the acoustical properties of porous media. Applied Acoustics **50** 171—188 (1997)
[14] Attenborough K and Walker J A. Scattering theory for the absorption of sound in fibrous media. J. Acoust. Soc. Am. **49** 1331-1358 (1971).
[15] Mechel F. Eine Modeltheorie zun Faserabsorber [Parts I and II]. Acustica **36** (2) 53 – 89 (1976/77)
[16] Tarnow V. Calculation of the dynamic air flow resistivity of fiber materials. J. Acoust. Soc. Am. **102** 1680-1688 (1997)
[17] Wear K.A. Recent developments in modelling and measuring scattering from trabecular bone. Proc. Acoustics '08. (2008)
[18] Stinson M R. The propagation of plane sound waves in narrow and wide circular tubes and generalization to uniform tubes of arbitrary cross-sectional shape. J. Acoust. Soc. Am. **89** 550-558 (1989)
[19] Umnova O. Attenborough K. and Li K. M. A cell model for sound propagation in stackings of spheres. Acustica combined with Acta Acustica. **87** 226 – 235 (2001)
[20] Stoll R D. Theoretical aspects of sound transmission in sediments, J. Acoust. Soc. Am. **68**(5): 1341-1350 (1980)
[21] Kosten C W and Janssen J H. Acoustic properties of flexible and porous materials. Acustica **7** 372 (1957)
[22] Plona T J. Observation of a second bulk compressional wave in a porous medium at ultrasonic frequencies. Appl. Phys. Lett. **36** 259 (1980)
[23] Thornely-Taylor, R. Numerical modelling of groundborne noise and vibration from underground railways: geotechnical considerations. Proc. 12th ICSV Lisbon (2005)
[24] Hosokawa A and Otani T. Ultrasonic wave propagation in bovine cancellous bone. J. Acoust. Soc. Am. **101**, 558–562 (1997)

Recent developments free field PU impedance technique

Emiel Tijs[1], Hans-Elias de Bree[1, 2]
[1]*Microflown Technologies, Zevenaar, The Netherlands, tijs@microflown.com, www.microflown.com*
[2]*HAN university, dpt. Vehicle Acoustics, Arnhem, The Netherlands*

Introduction

Current standard techniques to measure the acoustic material impedance have limitations. The Kundt's method requires a sample to be cut out and put in a fully reflective tube. Many materials including some porous materials are not locally reacting, meaning the impedance depends on the angle of incidence. With the Kundt's tube it is only possible to measure at perpendicular sound incidence. The walls of the tube can influence the behavior especially if the material has a high flow resistivity [15] like some foams or multi-layer materials. Some samples cannot be cut and leakage effects are observed when the tube is put highly porous surfaces (eg. road asphalt or some aircraft engine liners).
With a reverberant room it is possible to measure the diffuse absorption but it requires large and expensive facilities and samples of several square meters.
There is a need to measure samples in the free field, or better in situ, without sample cut-out or large amounts of material. The free field PU impedance technique was tested successfully for the first time in 2004 [4]. A so-called PU probe makes use of a dedicated velocity sensor combined with a microphone. Directly the impedance can be measured close to the material. This paper gives an overview of recent developments of this method.

PU free field principle

The PU free field surface impedance technique makes use of a Microflown velocity sensor and a sound pressure microphone. Both sensors are mounted in one probe that is positioned close to the material and a sound source is positioned at a certain distance. The impedance can be derived from the ratio of pressure and velocity [4-12]. From this, material reflection and absorption can be calculated. The probe is able to measure in the whole audible range but the lower frequency limit of the method at this moment is 100~300Hz. This is due to the low sound pressure emission from the loudspeaker at low frequencies (and the limited dimensions of the sample).

Fixed distance probe-source

A PU probe can be calibrated with a spherical source in an anechoic room [13]. A model is used to calculate the plane wave sensitivity. The spherical surface impedance can be measured with the same source and has to be converted to the plane wave impedance with e.g. a F-term correction [5]. If the source-probe distance is kept constant the measurement results are similar on several materials when no corrections are applied at all. The calibration model and the measurement model seem to cancel each other. This has to be supported by theory and more measurements in the future.

Figure 1. Handheld PU free field impedance setup

A simple point source model can be used to allow for the measurement distance [9]. Due to this simple model measurement results can be produced in real time.
A fixed probe-source distance is now possible because the setup in Figure 1 is made in such a way that vibrations from the loudspeaker are isolated from the sensor support. This is especially important when the impedance of the sample is high.
A typical calibration takes 5 seconds and again 5 seconds for the material measurement. So it is common to calibrate before each measurement session.

Low influence of reflections

The distance between the probe and the source is only 26cm so reflections at some distance are less dominant than the signal of the direct source. The calibration and measurement can be done in a regular office, but even in a strong reverberant environment like a car interior, see Figure 2 [9].

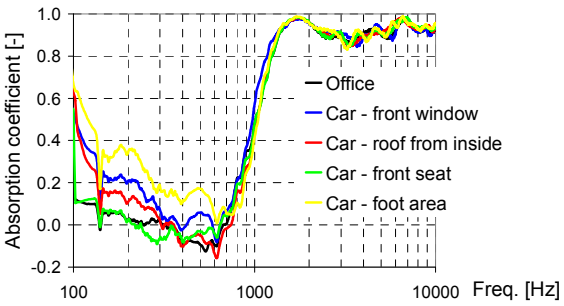

Figure 2. Absorption measurements in a car

A moving average in the frequency domain gives a result similar an anechoic measurement. A time windowing technique can also be used but the moving average is more robust [9]. The smoothed result should follow the actual impedance however when the actual impedance has a sharp change this averaging should not be applied, so some care is required.

Small spatial resolution

Because the method makes use of an ultra miniature PU probe the measurements can be done very close to the material. Much smaller samples are required than with other free field techniques. The measurement resolution is in the order of millimeters. Figure 3 shows the absorption calculated from the local impedance measured every 5mm above a sample with a quarter lambda tube [10]. To obtain the effective absorption of the whole sample the average impedance of the whole surface should be taken.

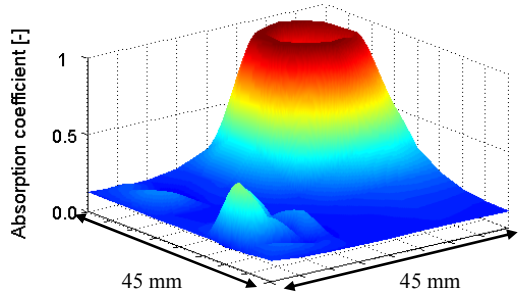

Figure 3. Absorption quarter lambda resonator at 1330Hz

Kundt's tube comparison

Results similar to the Kundt's tube are measured when the sample is measured in exactly the same conditions. Figure 4 shows certain samples can have totally different behavior when the sample size is increased, showing a limitation of the Kundt's method, [9]. In this figure also can be seen an absorption value lower than zero is measured. The reason for this is still unknown.

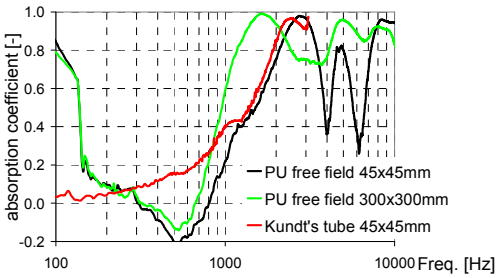

Figure 4. Influence of sample size

Moving samples and wind

Measurements are done on moving samples and it is possible to determine the absorption coefficient when the measurement time above an area of constant impedance is 0.05 seconds or larger [16]. This would for instance mean that the measurement area would be 1,1m if the speed would be 80km/h. These high speeds are necessary for impedance measurements on roads not to disturb traffic.

The acoustic behavior of materials may change after installation if the material is glued, mounted on a surface that is not fully reflective, etc. and needs to be checked. During production or time materials might vary. In line testing becomes feasible now.

Acoustic properties change when there is a flow over the material. Measurements are already successfully taken at relative low wind speeds of 7 m/s [16,17]. A goal is to measure aircraft engine liner material simultaneously at 0.5 mach, 500 deg Celsius and at high sound levels.

Measurements under an angle

It is possible to measure an acoustic sample under an angle [4,5,9]. The probe is rotated on the fixture and calibrated in this position. Measurements can now be taken with the probe in the normal direction. With this procedure the angle does not have to be modeled because the rotated calibration allows for this.

Conclusions

The handheld PU free field surface impedance technique has several benefits compared to established standard techniques that measure the acoustic material behavior. Due to a fixed probe-source distance corrections for the sound field during the calibration and the material measurement have become easier which reduced calculation power for the computer. Real time measurements on moving samples are possible. Measurements can be taken in situ, under an angle, even under difficult conditions like inside a car. The spatial resolution is in the order of millimeters, which could provide researchers extra insights in material behavior.

Further research will be focused on extending the method to lower frequencies to find the reason for absorption values lower than zero and measuring not only reflection, but also material transmission. The method shows the potential to measure with high flow speeds, high temperatures and at high sound levels. For utilization in a production environment the influence of very loud background noise needs to be investigated.

Special thanks goes out to W. Lauriks from the university of Leuven who contributed to the content of this paper.

References

[1] H-E de Bree et al, The Microflown; a novel device measuring acoustical flows, Sensors and Actuators: A, Physical, volume SNA054/1-3, pp 552-557, 1996

[2] H-E de Bree: The Microflown: An acoustic particle velocity sensor, Acoustics Australia 31, 91-94 (2003)

[3] M. A. Nobile and S. I. Hayek, Acoustic, propagation over an impedance plane, J.Acoust. Soc. Am. 78(4), 1325–1336, 1985.

[4] R. Lanoye et al, a practical device to determine the reflection coefficient of acoustic materials in-situ based on a Microflown and microphone, ISMA, 2004.

[5] R. Lanoye, G. Vermeir, W. Lauriks, R. Kruse, V. Mellert, Measuring the free field acoustic impedance and absorption coefficient of sound absorbing materials with a combined particle velocity-pressure sensor, JASA, May 2006

[6] Roland Kruse, Volker Mellert, In-situ Impedanzmessung mit einem kombinierten Schnelle- und Drucksensor, Daga 2006, Germany

[7] HE de Bree et al., Two complementary Microflown based methods to determine the reflection coefficient in situ, ISMA 2006

[8] J.D. Alvarez, F. Jacobsen, In-situ measurements of the complex acoustic impedance of porous materials, INTER-NOISE 2007

[9] HE de Bree, M. Nosko, E. Tijs, A handheld device to measure the acoustic absorption in situ, SNVH, GRAZ, 2008

[10] Tijs et al, Non destructive and in situ acoustic testing of inhomogeneous materials, ERF33, Kazan, Russia, 2007

[11] JD Alvarez and F Jacobsen, In-situ measurements of the complex acoustic impedance of porous materials, INTER-NOISE 2007

[12] H-E de Bree et al, Broad band method to determine the normal and oblique reflection coefficient of acoustic materials, SAE 2005

[13] Finn Jacobsen et al, A note on the calibration of pressure-velocity sound intensity probes, Jasa, 2006

[14] Yang Liu and Finn Jacobsen, Measurement of absorption with a p-u sound intensity probe in an impedance tube, ASA, 2005

[15] T.E. Vigran et al., Prediction and measurements of the influence of boundary conditions in a standing wave tube, Acta Acustica, 83, 419-423 (1997).

[16] Acoustic absorption measurements of moving structures and under influence of flow,E. Tijs et al, ISMA 2008

[17] PU surface impedance measurements on liner materials in the presence of a grazing flow, E. Tijs et al, CEAS 2008

SYMPOSIUM ON THE ACOUSTICS OF PORO-ELASTIC MATERIALS
Dec. 17-19, 2008, BRADFORD (UK)

Unified Analysis Model and Topology Optimization of an Acoustical System including a Poro-Elastic Material

Yoon Young Kim* and Joong Seok Lee

National Creative Research Initiatives Multiscale Design Center,

School of Mechanical and Aerospace Engineering, Seoul National University,

Shinlim-Dong San56-1, Kwanak-Gu, Seoul 151-742, Korea

Jung Soo Kim and Yeon June Kang

Advanced Automotive Research Center

School of Mechanical and Aerospace Engineering, Seoul National University,

Shinlim-Dong San56-1, Kwanak-Gu, Seoul 151-742, Korea

Corresponding to yykim@snu.ac.kr

Abstract

This presentation introduces a unified analysis model and a topology optimization formulation for an optimal configuration design of a poroelastic acoustical system to improve its acoustical performance such as sound absorption and transmission loss. Although many works have contributed to foam configuration design for improvement of acoustical performance, most of them were based on a given configuration of poroelastic foams. Therefore, their configuration designs were conducted by slight changes of the configuration or by comparisons of acoustical performance for some kinds of typical configurations with repeat analyses or experiments. The difficulties in the configuration design of a poroelastic acoustical foam were due to the absence of a systematic design method based on an iterative optimization process. For a poroelastic acoustic system consisting of an air region and a poroelastic foam region, two different physical regions and their interfaces are continuously changed in an iterative design process. In a common analysis model, different governing equations represent the different physical regions (e.g., the scalar Helmholtz equation for an air region and Biot's equation [1] for a poroelastic foam region, respectively), and coupling between them at interfaces are considered. Since any common analysis model has to repeat construction of the two regions and modification of the coupling between them manually at every iteration step, it is very time consuming to reflect continuously changing interfaces using common analysis model automatically. Therefore, a general analysis model is not proper to implement a foam configuration design to a systematic process. To cope with the difficulties, we proposed a new unified model to apply the foam configuration design in a systematic iterative optimization process [2, 3]. The

unified analysis model is based on Biot's theory and a material property interpolation concept from a topology optimization method modifies Biot's equation to express an air region as well as a poroelastic foam region. The material properties of a layer or an element are formulated as functions of real-valued material state variables, which have a continuous value between 1 and 0. Therefore two different physical regions can be expressed with the same governing equation by controlling the value of the real-valued material state variables. Moreover, changing interfaces between the two regions are automatically constructed with credible accuracy using the proposed unified analysis model. Consequently, the unified analysis model makes it possible to set a configuration design of a poroelastic acoustical foam as a topology optimization problem. Two types of poroelastic acoustical systems were considered to apply the developed unified analysis model and topology optimization setting. Optimal layer sequencing of one-dimensional multilayered acoustical foam maximizing the sound transmission loss were designed for several single and ranges of frequencies [2]. Under the total amount of a poroelastic material is restricted, the optimized sequences turned out to consist of alternating layers of air and a poroelastic material of different number and thickness according to target frequencies. Also, two-dimensional foam shape design for maximizing the absorption coefficient in low and middle ranges of frequencies were carried out [3]. Differently from the well-known wedge shape which is good for the sound absorption in high frequencies, the obtained foams for the sound absorption in low and middle ranges of frequencies had unusual shapes and showed a big improvement in their absorption performance compared with a nominal shape.

References

[1] M. A. Biot, "Theory of propagation of elastic waves in a fluid-saturated porous solid. I. Low-Frequency Range," *J. Acoust. Soc. Am.* **28**, 168-178 (1956).

[2] J. S. Lee, E. I. Kim, Y. Y. Kim, J. S. Kim and Y. J. Kang, "Optimal poroelastic layer sequencing for sound transmission loss maximization by topology optimization method," *J. Acoust. Soc. Am.* **122**(4), 2097-2106 (2007).

[3] J. S. Lee, Y. Y. Kim, J. S. Kim and Y. J. Kang, "Two-dimensional poroelastic acoustical foam shape design for absorption coefficient maximization by topology optimization method," *J. Acoust. Soc. Am.* **123**(4), 2094-2106 (2008).

The effect of flow resistivity on sound absorption and sound transmission loss of film-faced poroelastic foam

Jeong-Woo Kim
United Technologies
East Hartford, USA

ABSTRACT

The present work[1] was focused on the effect of flow resistivity in foam only and film (0.032 kg/m^2)-faced foam. Three different ranges of flow resistive film-faced foam sheets were carefully selected from the same product line and used to measure the sound absorption coefficient, flow resistivity and sound transmission loss (STL) successively. Using exactly the same specimen for all measurements is important in order to minimize discrepancies due to variations in the foam itself. These measurements were repeated in three samples (A, B and C) and the range of flow resistivity is listed in table 1.

Table 1 Measured flow resistivity range of poroelastic foam samples

Sample ID	Flow resistivity (MKS Rayls/m)
A	18000 – 26000
B	28000 – 35000
C	26000 – 44000

Sample A particularly shows a lower value than the others, which explains the lower sound absorption of A in the measured normal absorption coefficient of the foam-only. However, the flow resistivity factor is less contributive to the sound absorption performance if there is film on the surface. In addition, the discrepancy of sound absorption between samples of film-faced foam was not as large as that of foam-only cases. Interestingly, in the comparison of measured STLs, Sample A showed better sound barrier performance at around 1.3 to 2 KHz before the coincidence dropped. That is, lower flow resistive foam shows a little better sound barrier performance when the film is faced on the foam. This observation is consistent with previous work[2]. To more precisely understand the above experimental observation, isotropic poroelastic theory[3,4] was used to construct prediction models for sound absorption and sound transmission loss of the foam only and film-faced foam. These two analytic models provided quantitative information on how much sound can be absorbed or transmitted through such poroelastic media. However, in order to see how sound propagates within the media and to identify coincidence frequencies associated with drops in the transmission loss, a free wave propagation analysis[1,2,5] is needed. The characteristic dispersion equations can be extracted from the sound transmission model by first eliminating the contributions of the incident, reflected and transmitted plane waves, thus making it possible to find the propagation characteristics of freely propagating waves in the poroelastic media.

To see the effect of flow resistivity, three different values, 20000, 30000 and 40000 MKS Rays/m were used, without changing other parameters, for the analysis of free wave propagation and STL. By solving the determinant condition in a characteristic equation[1], for the complex

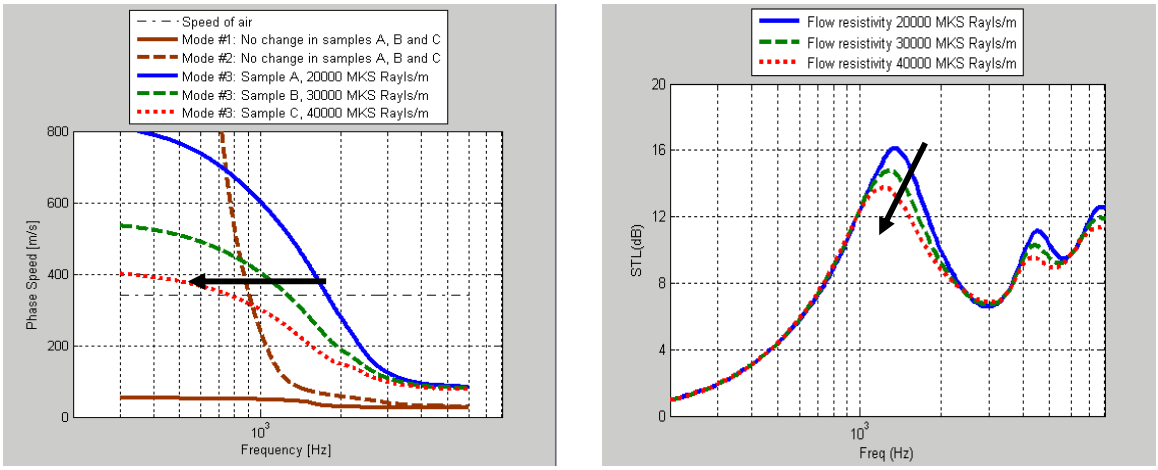

(a) Phase speed (b) Sound transmission loss

Figure 1: Flow resistivity effect on film-faced porous foam

wave number k_x, root trajectories for first three modes were identified up to 6 KHz starting from the initial values at 300 Hz for three different flow resistivity values. The real part of k_x is associated with the wave speed, while the imaginary part is related to the damping of the propagation. Those corresponding phase speeds derived from the real part of k_x are displayed in Figure 1 (a), showing that the turning frequency from supersonic to subsonic at mode #3 was decreased as the flow resistivity was increased from 20000 to 40000 MKS Rays/m. These changes of turning frequency are well matched with the changes of maximum peak location in STLs shown in Figure 1 (b). Normally, when the mode speed is changed from supersonic to subsonic and it converges to the existing subsonic mode, this causes a primary coincidence drop in sound transmission loss. In the comparison of STLs in Figure 1 (b), mode #1 and mode #2 converged at the location around 3KHz and additionally mode #3 converged at a similar speed. Therefore this coincidence drop was primarily determined by the convergence of mode #1 and mode #2; then, the different turning frequencies due to mode #3 contributed to the change of maximum peak between 1 KHz and 2 KHz. Our observation in measured STLs that the lower flow resistive sample shows the better sound barrier performance around 1 KHz to 2 KHz, was reproduced in predicted STLs in Figure 1 (b) and is reasonably explained by identifying the free propagation wave mode #3 for the film-faced poroelastic foam in the work.

REFERENCES

[1]Jeong-Woo Kim, "Flow resistivity effect on sound absorption and sound transmission loss of film-faced foam", *Proc. NOISE-CON*, RENO, USA, 2007.

[2]Jeong-Woo Kim, "Sound absorption and sound transmission loss of polyurethane porous foam and its film-faced composite", *Proc. INTER-NOISE*, HAWAII, USA, 2006.

[3]M.A. Biot, "Theory of propagation of elastic waves in a fluid-saturated porous solid I. Low frequency range. II. Higher frequency range," *J. Acoust. Soc. Am.*, Vol. 28, pp. 168-191 (1965).

[4]N.-M. Shiau, Y. J. Kang and J. S. Bolton, 1996, "Sound transmission through multi-panel structures lined with elastic porous materials," *J. Sound Vib.*, Vol. 191, pp. 317-347.

[5]Jeong-Woo Kim, Ph.D. Thesis, *School of Mechanical Engineering, Purdue University* "Sound transmission loss through lined, composite panel structures: Transversely isotropic poro-elastic model" (2005).

Fabrication of Novel Microcellular Acoustical Foams with Controlled Structure and Morphology

M. Y. Serry Ahmed and Chul B. Park

Microcellular Plastics Manufacturing Laboratory (MPML), University of Toronto

Noureddine Atalla

Groupe d'Acoustique De l'Université de Sherbrooke (GAUS), Université de Sherbrooke

This paper discusses three different fabrication approaches to the control of microcellular structures and morphologies for novel acoustical foams. Since most available open-cell foams are proprietary to the production companies, it is not easy to optimize the acoustical properties by controlling the cell structures and morphologies. Moreover, the relationships between the open-porous structures and the acoustical properties are not established yet. In this context, the aim of this research is to develop foaming technologies to control the cell number density, the expansion ratio, and the open-cell content for the purpose of varying the acoustical properties of the resultant foams.

The first approach focuses on the direct control of the foaming process parameters. The variability is achieved mainly through the control of cooling rates during the foaming process and saturation pressures at the saturation stages. Cross-linked LDPE was used as a base foam material. High open-cell contents (ranging between 43 - 95%), high microcellular cell densities (9E8 – 1.6E9 cells/cm^3) and desired expansion ratios (3 - 9 folds) were successfully obtained.

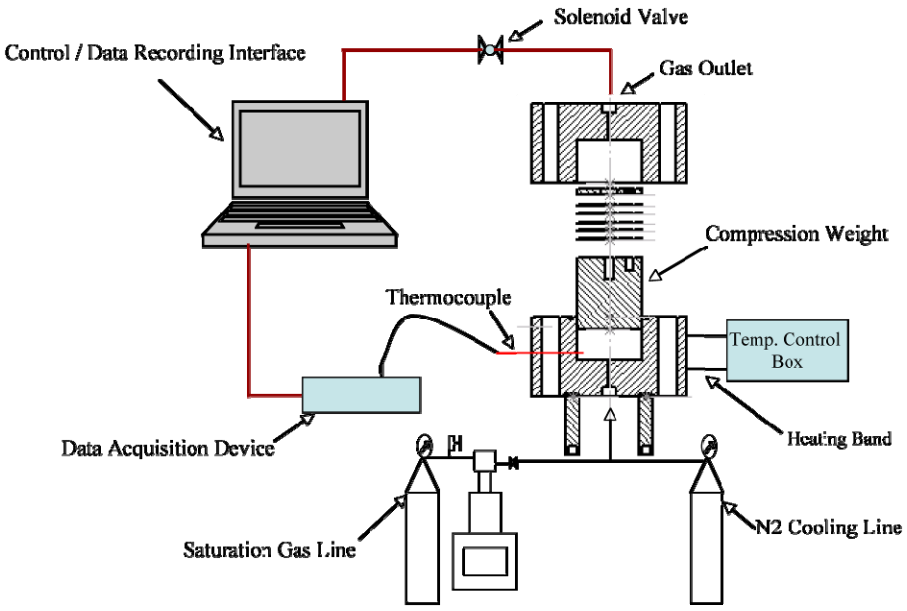

Figure 1: Schematic illustration of the designed batch foaming experimental system

In the second approach, a high internal phase emulsion (HIPE) polymerization foaming process is controlled for production of novel foams with various microcellular structures and morphologies. As an attempt to reduce the cell size and increase the microcellular density and the open cell content without sacrificing the mechanical properties, viscosity improvers were

combined into the conventional formulation of a styrene and water system via high internal phase emulsion polymerization.

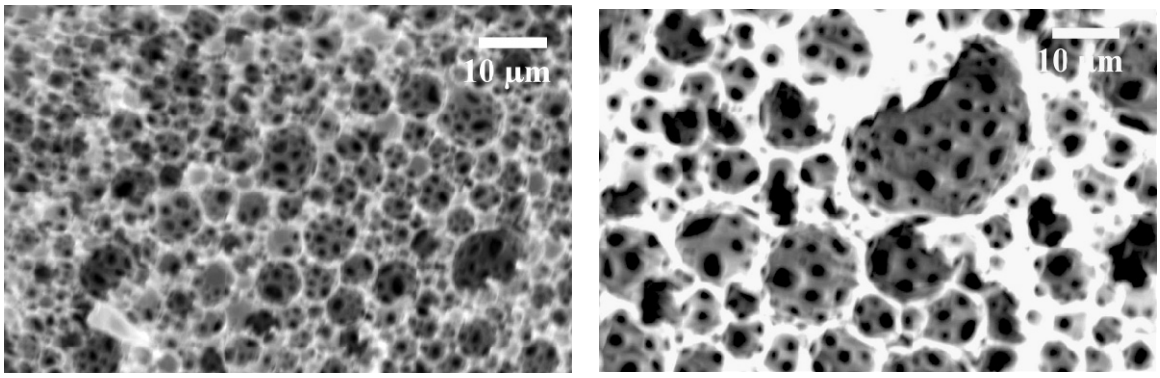

Figure 2: SEM picture illustrating the effect of increasing the viscosity of the mixture (a) 10% DVB mixture (b) 30% DVB mixture

In the third approach, organclay, C10A and C20A and natural clay, sodium montmorillonite (NaMMT) were introduced to the foams at various concentrations to control the microcellular morphology, cell size and open cell content. It was found that the open cell content increased as the organoclay content increased due to a non-homogeneous structure before foaming [1]. We attempted to derive a correlation for the open cell content and volume expansion ratio while varying the clay content and the result was quite satisfactory.

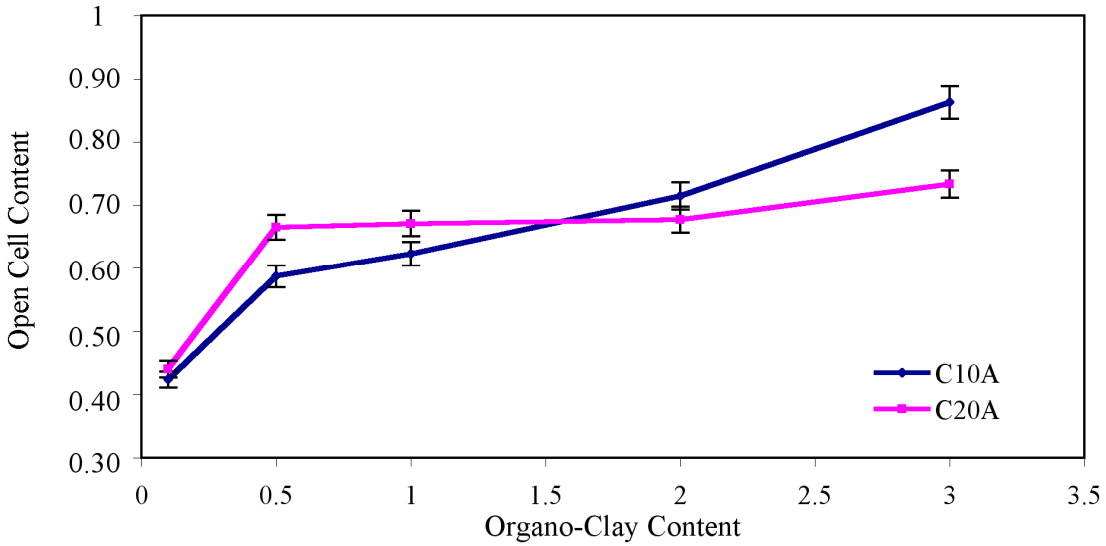

Figure 3: Effect of organoclay on the porosity of HIPE foams - (points represent average and extreme values)

The sound absorption behaviors of the produced samples showed significant variations with the change in the microstructure and morphology. A discussion of the effect of various mircostructural and morphological factors on the sound absorption behaviors of this class of materials is presented. Finally, some mircostructural design configurations are suggested to improve the sound absorption behaviors of microcellular foams.

[1] Park, C.B., Padareva, V., Lee, P.C. and Naguib, H.E., "Extruded Open-Celled LDPE and LDPE/PS Foams Using Non-Homogeneous Melt Structure,"*Journal of Polymer Engineering*, Vol. 39, No. 3, pp. 239-260, June 2004.

Progress in Micro-Perforated Panel Absorbers Research

Fenglei JIAO, Ke LIU
Institute of Acoustics, Chinese Academy of Sciences, Beijing 100190, China

Abstract: Theoretical and experimental investigations on the performance of micro-perforated-panel absorbers are reviewed in this paper. By reviewing recent research work, this paper reveals a relationship between the maximum absorption coefficient and the limit of the absorption frequency bandwidth. It has been demonstrated that the absorption frequency bandwidth can be extended up to 3 or 4 octaves as the diameters of the micro-holes decrease. This has become possible with the development of the technologies for manufacturing micro-perforated panels, such as laser drilling, powder metallurgy, welded meshing and electro-etching to form micrometer order holes. A new absorbing structure based on micro-perforated-panel absorbers demonstrates experimentally high sound absorption capability. This review shows that the micro-perforated-panel absorber has potentials to be one of ideal absorbing materials in the 21st century.

Keywords:
Micro-Perforated-Panel Absorber
Sound Absorbing Material

The interaction of finite amplitude acoustic pulses with rigid porous materials can not be performed using conventional frequency domain models due to nonlinearity induced interactions between different frequency components. A significant amount of literature is devoted to time domain numerical and experimental study of pulse propagation in porous materials [1] assuming Forchheimer's filtration law. In [2] for instance the propagation of the moderate amplitude acoustical pulse in a rigid porous material has been studied assuming Forchheimer's correction to Darcy's law and quadratic nonlinearity. However this approximation assumes that the viscous boundary layer thickness exceeds the characteristic pore size and hence neglects the early stages of the boundary layer formation. The approximation is valid when most of the acoustic energy is concentrated in the lower frequency range, $\omega \ll \omega_{crit} = \frac{\sigma^2 \phi^2 \Lambda^2}{4 c_{\infty}^2 \rho_0^2}$, which implies relatively long pulses. For shorter pulses the transient (or history) effects which account for the non-instantaneous response of the medium need to be taken into consideration. Analysis of the transient effects have been performed in the past [3], [4] and are valid for short pulses with most of the energy concentrated in the higher frequency range, $\omega \gg \omega_{crit}$. . The aim of this work is to investigate the propagation of the intermediate duration pulses, so that $\omega \approx \omega_{crit}$. In this case both contributions to the viscous force have to be taken into account together with nonlinearity which becomes noticeable for higher amplitude pulses. The model assumes that all contributions to the viscous force are additive in time domain. Strictly speaking this approximation is valid only for some simplified geometries, such as for instance fluid flow around isolated sphere [5]. For rigid porous materials of arbitrary geometry the approximation is equivalent to using the following expression

$$\alpha(\omega) = \alpha_{\infty} + \frac{\sigma\phi}{-i\omega\rho_0} + \frac{2c_{\infty}}{\Lambda}\sqrt{\frac{\eta}{-i\omega\rho_0}}$$

for dynamic tortuosity function in the frequency domain. Although different from the conventional scaling function [6], it still satisfies correct low and high frequency limits. With account of quadratic nonlineary, the following equation has been derived for the particle velocity of the plane acoustic wave in an infinite layer of porous material

$$\sqrt{\alpha_{\infty}}\rho_0 \frac{\partial v}{\partial x} - \varepsilon\rho_0 v \frac{\partial v}{\partial \tau} = -\frac{\sigma}{2c}(1 + \xi|v|)v - \frac{c_{\infty}}{\Lambda c}\sqrt{\frac{\eta}{\pi\rho_0}}\int_{-\infty}^{\tau} \frac{\frac{\partial v}{\partial \tau'}}{\sqrt{\tau - \tau'}} d\tau',$$

where $\tau = t - \frac{x\sqrt{\alpha_{\infty}}}{c}$, ε is an air nonlinearity parameter and ξ is Forchheimer's nonlinearity parameter.

Without the history term, this equation can be solved analytically [2]. To investigate the transient effects the above equation is solved numerically using a finite difference scheme. The approach described in [7], [8] is used which allows to consider the contribution of each term in the equation separately and to estimate their relative importance.

Numerical results will be compared with data available in the literature and with shock tube measurements on granular materials.

References

1. S.Sorek, A.Levy, G.Ben-Dor, D.Smeulders, "Contribution to theoretical/ experimental developments in shock wave propagation in porous media", Transport in Porous Media, 36, 63-100 (1999).
2. O.Umnova, K.Attenborough, A.Cummings, "High amplitude pulse propagation and reflection from a rigid porous layer", Noise Control Eng. 50, 204-210 (2002).
3. Z.E.A.Fellah, C.Depolier, "Transient acoustic wave propagation in rigid porous media: a time domain approach", J.Acoust.Soc.Am. 107, 683-688 (2000).
4. Y.M.Shtemler, I.R.Shreiber, A.Britan, "Shock induced flows through packed beds: transient regimes", Acta Acustica united with Acustica, 92, 612-617 (2006).
5. L.D.Landau, E.M.Lifshitz, "Fluid mechanics",p.91, Pergamon Press, 1987
6. D.L.Johnson, J.Koplik, R.Dashen, "Theory of dynamic permeability and tortuosity in fluid saturated porous media", J.Fluid Mech. 176, 379-402 (1987).
7. Y.-S.Li, M.F.Hamilton, "Time-domain modelling of pulsed finite amplitude sound beams", J.Acoust.Soc.Am. 97, 906-917 (1995).
8. R.O.Cleveland, M.F.Hamilton, D.T.Blackstock, "Time-domain modelling of finite-amplitude sound in relaxing fluids", J.Acoust.Soc.Am. 99, 3312-3318 (1996).

Biot model for transverse porous materials (Abstract proposal for SAPEM 2008)

G. Lielens and J.P. Coyette
Free Field Technologies S.A.,
Axis Parc Louvain-la-Neuve, Rue Emile Francqui 1, B-1435 Mont-Saint-Guibert, Belgium
e-mail: **jean-pierre.coyette@fft.be**

Abstract

The model developed by Biot for porous materials has been extensively used in vibro-acoustic simulations. Various implementations of the Biot model have been developed over the years. Usually a conventional isotropic model is selected although many applications are characterized by some anisotropy. Such an anisotropy can be induced by the manufacturing process or can result from particular design options. The present contribution is precisely devoted to the extension of the Biot model for problems involving a particular form of anisotropy. Such behavior is characterized by anisotropic elastic properties for the skeleton and a specific anisotropic flow resistivity for the fluid phase. Since an arbitrary anisotropic flow resistivity rules out the attractive $u - p$ formulation, one restricts the investigations to a special class of porous materials where the flow resistivity can be considered as infinite along transverse directions. The so-called *transverse* Biot model is further elaborated starting from the original isotropic model. The weak variational form related to the transverse Biot model is derived within the context of a displacement-potential formulation.

1 Introduction

The Biot model [1], [2], [3] is extensively used for modeling porous materials in a vibro-acoustic context [4], [5], [6]. Earlier finite element models have been using displacement formulations (for the skeleton and the fluid phase). This last decade has seen the emergence of displacement-pressure [6] and displacement-potential [7], [8] formulations. Compared to full displacement formulations, such models have the advantage of a reduced number of degrees of freedom (4 instead of 6 for 3-D applications) and offer easier coupling conditions with acoustic models. This feature is particularly attractive for acoustic transmission studies. In most of the applications, an isotropic model is selected for the porous material. The present contribution aims to further extend this model to a special class of transverse isotropic porous materials. This kind of material is characterized by a finite flow resistivity along an isotropy axis while the resistivity can be considered as infinite along the transverse directions. The elastic properties of the skeleton, on the other hand, retain a full anisotropic characterization. The derivation of a suitable displacement-pressure or displacement-potential model is described. The related weak, symmetric, variational form is also described in order to support the development of a particular class of poro-elastic finite elements.

2 Biot model for transverse porous materials

2.1 Main hypothesis

The so-called *transverse* Biot model is based on the following main assumptions:

- The heterogeneous medium is treated as an equivalent homogeneous medium where the solid phase occupies a fraction $(1-\Omega)$ of the volume while the fluid phase (air) occupies a fraction Ω of the volume;
- Elastic stress and pressure are defined at every point;
- The wave length λ is much greater than any feature of the porous material (pore size, fiber diameter);
- Displacements are small so that the theory of linear elasticity applies;
- The air phase is continuous while closed pores are considered as part of the skeleton (effects related to the movement of air inside closed pores are not taken into account);
- The material possess an isotropic transverse symmetry;
- Fluid displacements relative to the skeleton occur only along the isotropy axis direction (in other words, the flow resistivity is infinite in directions perpendicular to the isotropy axis).

The state variables are the displacement vectors **u** and **U** of the solid phase and the fluid phase, respectively.

2.2 Equilibrium equations

The equilibrium equation for the skeleton writes:

$$\partial_j \sigma_{ij}^S = (1-\Omega)\,\rho_s \ddot{u}_i + f_i^{FS} \ , \tag{1}$$

where σ_{ij}^S is the elastic stress tensor in the skeleton and f_I^{FS} is an interaction term representing the force exerted by the fluid on the structure. Similarly, the equilibrium equation for the fluid writes:

$$\partial_j \sigma_{ij}^F = \Omega \rho_f \ddot{U}_i + f_i^{SF} \ , \tag{2}$$

where $\sigma_{ij}^F = -\Omega p \delta_{ij}$ is the isotropic stress tensor in the fluid and f_i^{SF} is an interaction term representing the force exerted by the skeleton on the fluid.

The fluid-structure interaction term $f_i^{FS} = -f_i^{SF}$ is the sum of three terms:

$$f_i^{SF} = -f_i^{FS} = \rho_{12}\left(\ddot{u}_i - \ddot{U}_i\right) - \tilde{b}\left(\dot{u}_i - \dot{U}_i\right) + T_i \ . \tag{3}$$

The first term represents a mass coupling term proportional to the difference in acceleration between the air and the skeleton. The second term is a viscous force resulting from the velocity difference. Both of those forces are directed along the isotropy axis. The third term T_i is perpendicular to the isotropy axis and enforces the constraint that no relative displacement occur perpendicular to the isotropy direction **r**:

$$(\mathbf{U} - \mathbf{u}) \times \mathbf{r} = 0 \ , \tag{4}$$

where $\times$ denotes the vector cross-product.

For convenience, in the following, the index r is relative to the isotropy direction **r** while the indices s and t are relative to the directions perpendicular to the isotropy direction, referred as *transverse* directions. Indices i, j, k and l are relative to any direction. Einsteinian convention of sum over repeated indices is used.

One can express that the force T_i has a zero component along **r** direction:

$$T_r = T_i r_i = 0 \ , \tag{5}$$

while the fluid and solid displacements have equal components in a direction perpendicular to **r**:

$$U_s = U_i - U_j r_j r_i = u_s = u_i - u_j r_j r_i \ . \tag{6}$$

The global interaction forces along r direction, one one side, and s and t directions, on the other side, can therefore be written as:

$$f_r^{SF} = -f_r^{FS} = \rho_{12}\left(\ddot{u_r} - \ddot{U_r}\right) - \tilde{b}\left(\dot{u_r} - \dot{U_r}\right) \tag{7}$$

$$f_s^{SF} = -f_s^{FS} = T_s \ . \tag{8}$$

The two constants ρ_{12} and $\tilde{b}$ are related to the classical Biot parameters (R is the resistivity while α_∞ is the tortuosity):

$$\rho_{12} = \Omega\rho_f\left(1 - \alpha_\infty\right) \ , \tag{9}$$

$$\tilde{b} = \Omega R \ . \tag{10}$$

Considering an harmonic field at circular frequency ω, one can write the equilibrium equations as:

$$\partial_j \sigma_{ij}^S + \underbrace{\left[\underbrace{\left(1-\Omega\right)\rho_s - \rho_{12}}_{\rho_{11}} - \frac{i\omega\tilde{b}}{\omega^2}\right]}_{\tilde{\rho}_{11}} \omega^2 u_i + \underbrace{\left[\rho_{12} + \frac{i\omega\tilde{b}}{\omega^2}\right]}_{\tilde{\rho}_{12}} \omega^2 U_i - T_i = 0 \ , \tag{11}$$

$$\partial_j \sigma_{ij}^F + \underbrace{\left[\underbrace{\Omega\rho_f - \rho_{12}}_{\rho_{22}} - \frac{i\omega\tilde{b}}{\omega^2}\right]}_{\tilde{\rho}_{22}} \omega^2 U_i + \underbrace{\left[\rho_{12} + \frac{i\omega\tilde{b}}{\omega^2}\right]}_{\tilde{\rho}_{12}} \omega^2 u_i + T_i = 0 \ , \tag{12}$$

or

$$\partial_j \sigma_{ij}^S + \tilde{\rho}_{11}\omega^2 u_i + \tilde{\rho}_{12}\omega^2 U_i - T_i = 0 \ , \tag{13}$$

$$\partial_j \sigma_{ij}^F + \tilde{\rho}_{22}\omega^2 U_i + \tilde{\rho}_{12}\omega^2 u_i + T_i = 0 \ . \tag{14}$$

Note that:

$$\tilde{\rho}_{12} + \tilde{\rho}_{22} = \Omega\rho_f \ . \tag{15}$$

Replacing σ_{ij}^F by its definition in terms of the pressure p, the second equation becomes:

$$-\Omega\partial_i p + \tilde{\rho}_{22}\omega^2 U_i + \tilde{\rho}_{12}\omega^2 \ u_i + T_i = 0 \ , \tag{16}$$

yielding:

$$U_i = \frac{\Omega}{\tilde{\rho}_{22}\omega^2}\partial_i p - \frac{\tilde{\rho}_{12}}{\tilde{\rho}_{22}} u_i - \frac{T_i}{\tilde{\rho}_{22}\omega^2} \ . \tag{17}$$

This expression involves the unknown T_i and does not allow apparently for a direct elimination of **U** in terms of p. This elimination is however possible since $T_i = 0$ along the isotropy direction while $U_i = u_i$ for components i orthogonal to the isotropy direction. This leads to the following equations:

$$U_r = \frac{\Omega}{\tilde{\rho}_{22}\omega^2}\partial_r p - \frac{\tilde{\rho}_{12}}{\tilde{\rho}_{22}} u_r \ , \tag{18}$$

$$U_t = u_t \ . \tag{19}$$

This allows for the elimination of **U** (expressed in terms of by p) in the first equilibrium equation along the isotropy direction:

$$\partial_j \sigma_{rj}^S + \omega^2 \underbrace{\left[\tilde{\rho}_{11} - \frac{\tilde{\rho}_{12}^2}{\tilde{\rho}_{22}}\right]}_{\tilde{\rho}} u_r + \frac{\Omega\tilde{\rho}_{12}}{\tilde{\rho}_{22}}\partial_r p = 0 \ , \tag{20}$$

or

$$\partial_j \sigma^S_{rj} + \omega^2 \tilde{\rho} u_r + \frac{\Omega \tilde{\rho}_{12}}{\tilde{\rho}_{22}} \partial_r p = 0 \ . \tag{21}$$

In the transverse directions, adding the skeleton and the fluid equilibrium equations allows for the elimination of T_s:

$$\partial_j \sigma^S_{tj} - \Omega \partial_t p + \omega^2 (1-\Omega) \rho_s u_t + \omega^2 \Omega \rho_f U_t + T_s - T_s = 0 \ , \tag{22}$$

or

$$\partial_j \sigma^S_{tj} + \omega^2 \rho u_t - \Omega \partial_t p = 0 \ , \tag{23}$$

where $\rho = \Omega \rho_f + (1-\Omega)\rho_s$ is the total density of the porous material.

Equations (21) and (23) can re rewritten in term or i, j indices as:

$$\partial_j \sigma^S_{ij} + \omega^2 (\rho u_i + (\tilde{\rho} - \rho) u_r r_i) + \Omega(-\partial_i p + (1 + \frac{\tilde{\rho}_{12}}{\tilde{\rho}_{22}}) \partial_r p r_i) = 0 \ . \tag{24}$$

2.3 Constitutive relations

2.3.1 Acoustic fluid

The constitutive equation for the fluid expresses the fact that the pressure variation in an infinitesimal sample is related to the volumetric deformation of the sample and the net flow of fluid through the sample. This leads to the expression:

$$-p = Q \epsilon_V + \alpha Q \epsilon_S \ , \tag{25}$$

where Q is the mixture's bulk modulus, $\epsilon_V = \Omega \partial_j \left(U_j - u_j \right)$ is the net flow of fluid through the sample, $\epsilon_S = \partial_j u_j$ is the volumetric deformation of the sample and α is the Biot constant equal to one in most cases. One usually writes this first constitutive equation as:

$$-\Omega p = \underbrace{Q \Omega^2}_{\tilde{R}} \partial_j U_j + \underbrace{\Omega Q \left(\alpha - \Omega \right)}_{\tilde{Q}} \partial_j u_j \ , \tag{26}$$

or

$$-\Omega p = \tilde{R} \partial_j U_j + \tilde{Q} \partial_j u_j \ . \tag{27}$$

This equation can be rewritten as

$$\begin{aligned} -\Omega p &= \tilde{R}(\partial_j U_j - \partial_j u_j) + (\tilde{R} + \tilde{Q}) \partial_j u_j & (28) \\ &= \tilde{R} \partial_r U_r + \alpha \Omega Q \partial_j u_j - \tilde{R} \partial_r u_r \ . & (29) \end{aligned}$$

2.3.2 Elastic skeleton

The constitutive equation for the elastic skeleton is

$$\begin{aligned} \sigma^S_{ij} &= \left(C_{ijkl} + \delta_{ij} \delta_{kl} Q (\alpha - \Omega)^2 \right) \epsilon_{kl} + \underbrace{\Omega Q \left(\alpha - \Omega \right)}_{\tilde{Q}} \partial_k U_k \delta_{ij} \ , & (30) \\ &= \tilde{C}_{ijkl} \epsilon_{kl} + \tilde{Q} \partial_k U_k \delta_{ij} \ , & (31) \end{aligned}$$

where the coefficient $\tilde{Q}$ is identical to the coefficient $\tilde{Q}$ involved in the acoustic constitutive equation (27) due to energy considerations.

2.3.3 Elimination of U

U can be eliminated from the constitutive relations. Starting from the acoustic fluid constitutive equation, one can write:

$$\partial_k U_k = -\frac{\Omega}{\tilde{R}} p - \frac{\tilde{Q}}{\tilde{R}} \partial_k u_k \ , \tag{32}$$

which can be introduced in the constitutive relation for the solid phase and yields:

$$\begin{aligned} \sigma_{ij}^S &= \tilde{C}_{ijkl}\epsilon_{kl} - \frac{\tilde{Q}^2}{\tilde{R}}\partial_k u_k - \frac{\tilde{Q}\Omega}{\tilde{R}} p\delta_{ij}\delta_{ij} \ , \\ &= \left(\tilde{C}_{ijkl} - \frac{\tilde{Q}^2}{\tilde{R}\delta_{ij}\delta_{kl}}\right)\epsilon_{kl} - \frac{\tilde{Q}\Omega}{\tilde{R}} p\delta_{ij} \ , \end{aligned} \tag{33}$$

but

$$\frac{\tilde{Q}^2}{\tilde{R}} = Q(\alpha - \Omega)^2 \ , \tag{34}$$

and

$$\tilde{C}_{ijkl} - \frac{\tilde{Q}^2}{\tilde{R}}\delta_{ij}\delta_{kl} = \left(C_{ijkl} + \delta_{ij}\delta_{kl}Q(\alpha-\Omega)^2\right) - \delta_{ij}\delta_{kl}Q(\alpha-\Omega)^2 = C_{ijkl} \ , \tag{35}$$

so that

$$\sigma_{ij}^S = \underbrace{C_{ijkl}\epsilon_{kl}}_{\hat{\sigma}_{ij}^S} - (\alpha - \Omega)\, p\delta_{ij} \ . \tag{36}$$

$\hat{\sigma}_{ij}^S$ is the stress tensor that would exist in an elastic solid having the same composition and undergoing the same displacements as the skeleton.

2.4 Displacement-pressure model for transverse poroelastic materials

2.4.1 Basic equation for the solid phase

- Isotropy direction: Let us introduce equation (36) into equation (21):

$$\partial_j \hat{\sigma}_{rj}^S + \omega^2 \tilde{\rho} u_r + \underbrace{\left(\frac{\Omega\tilde{\rho}_{12}}{\tilde{\rho}_{22}} - (\alpha - \Omega)\right)}_{\tilde{\gamma}} \partial_r p = 0 \ , \tag{37}$$

  or

$$\partial_j \hat{\sigma}_{rj}^S + \omega^2 \tilde{\rho} u_r + \tilde{\gamma}\partial_r p = 0 \ . \tag{38}$$

- Transverse directions: Let us introduce equation (36) into equation (23):

$$\partial_j \hat{\sigma}_{tj}^S + \omega^2 \rho u_t + (-\Omega - (\alpha - \Omega))\, \partial_t p = 0 \ , \tag{39}$$

  or

$$\partial_j \hat{\sigma}_{tj}^S + \omega^2 \rho u_t - \alpha\partial_t p = 0 \ . \tag{40}$$

Rewriting this equation using i, j indices leads to

$$\partial_j \hat{\sigma}_{ij}^S + \omega^2(\rho\delta_{ij} + (\tilde{\rho} - \rho) r_i r_j) u_j + (-\alpha\delta_{ij} + (\alpha + \tilde{\gamma}) r_i r_j)\partial_j p = 0 \ . \tag{41}$$

This equation is very similar to the equilibrium equation for an elastic solid but with an adapted isotropic transverse density and an additional term coupling skeleton's deformations to the pore pressure. Note that:

$$\tilde{\gamma} = \frac{\Omega\tilde{\rho}_{12}}{\tilde{\rho}_{22}} - (\alpha - \Omega) = \Omega\left(\frac{\tilde{\rho}_{12}}{\tilde{\rho}_{22}} + 1\right) - \alpha = \frac{\Omega^2\rho_f}{\tilde{\rho}_{22}} - \alpha \ . \tag{42}$$

2.4.2 Basic equation for the fluid phase

Let us take the derivative of equation (17) along the isotropy direction:

$$\partial_r U_r = \frac{\Omega}{\tilde{\rho}_{22}\omega^2}\partial_{rr}p - \frac{\tilde{\rho}_{12}}{\tilde{\rho}_{22}}\partial_r u_r \ , \tag{43}$$

and let us solve equation (29) for $\partial_r U_r$:

$$\partial_r U_r = -\frac{\Omega}{\tilde{R}}p - \frac{\alpha}{\Omega}\partial_i u_i + \partial_r u_r \ . \tag{44}$$

Equating the right-hand sides of both equations, after multiplication by $\omega^2\Omega$, yields

$$\frac{\Omega^2}{\tilde{\rho}_{22}}\partial_{rr}p + \omega^2\frac{\Omega^2}{\tilde{R}}p + \omega^2\alpha\partial_i u_i - \omega^2\Omega\left(\frac{\tilde{\rho}_{12}}{\tilde{\rho}_{22}+1}\right)\partial_r u_r = 0 \ , \tag{45}$$

or

$$\frac{\Omega^2}{\tilde{\rho}_{22}}\partial_{rr}p + \omega^2\frac{\Omega^2}{\tilde{R}}p - \omega^2\partial_i\left(-\alpha\delta_{ij} + (\alpha+\tilde{\gamma})r_i r_j\right)u_j = 0 \ . \tag{46}$$

2.5 Displacement-potential model for poroelastic materials

Equations (41) and (46) can be rewritten in a more convenient form using a velocity potential ψ. For poroelastic materials in harmonic regime, this velocity potential is defined as:

$$p = -i\omega\psi \ . \tag{47}$$

For the solid phase, equation (41) becomes

$$\partial_j\hat{\sigma}^S_{ij} + \omega^2(\rho\delta_{ij} + (\tilde{\rho}-\rho)r_i r_j)u_j - i\omega\left((\alpha+\tilde{\gamma})r_i r_j - \alpha\delta_{ij}\right)\partial_j\psi = 0 \ . \tag{48}$$

For the fluid phase, introducing ψ in equation (46) and multiplying by i/ω yields:

$$\frac{\Omega^2}{\tilde{\rho}_{22}}\partial_{rr}\psi + \omega^2\frac{\Omega^2}{\tilde{R}}\psi - i\omega\partial_i\left((\alpha+\tilde{\gamma})r_i r_j - \alpha\delta_{ij}\right)u_j = 0 \ . \tag{49}$$

This last equation is a 1D Helmholtz equation (along the isotropy direction) using a modified wave number:

$$\tilde{k} = \frac{\omega}{\sqrt{\frac{\tilde{R}}{\tilde{\rho}_{22}}}} \ , \tag{50}$$

and an additional term coupling the pressure in the pores to skeleton's displacement.

Introducing the tensorial quantities $\tilde{\varrho}$ and $\tilde{\kappa}$

$$\tilde{\varrho}_{ij} = (\rho\delta_{ij} + (\tilde{\rho}-\rho)r_i r_j) \ , \tag{51}$$

$$\tilde{\kappa}_{ij} = ((\alpha+\tilde{\gamma})r_i r_j - \alpha\delta_{ij}) \ . \tag{52}$$

For the solid phase, equation (48) becomes

$$\partial_j\hat{\sigma}^S_{ij} + \omega^2\tilde{\varrho}_{ij}u_j - i\omega\tilde{\kappa}_{ij}\partial_j\psi = 0 \ . \tag{53}$$

For the fluid phase, equation (49) becomes

$$\frac{\Omega^2}{\tilde{\rho}_{22}}\partial_{rr}\psi + \omega^2\frac{\Omega^2}{\tilde{R}}\psi - i\omega\partial_i\tilde{\kappa}_{ij}u_j = 0 \ . \tag{54}$$

3 Variational statements

In order to build a finite element model for transverse porous materials, one must provide a variational statement equivalent to equations (53) and (54).

3.1 Variational statement for the poroelastic subdomain

3.1.1 Elastic skeleton

The variational form of equation (53) is:

$$\int_{V_P} \left(\partial_j \hat{\sigma}_{ij}^S + \omega^2 \tilde{\varrho}_{ij} u_j - i\omega \tilde{\kappa}_{ij} \partial_j \psi \right) \delta u_i dV = 0 \ . \tag{55}$$

The first term can be integrated by part:

$$\begin{aligned} \int_{V_P} \partial_j \hat{\sigma}_{ij}^S \delta u_i dV &= \int_{V_P} \left(\partial_j \left(\hat{\sigma}_{ij}^S \delta u_i \right) - \hat{\sigma}_{ij}^S \partial_j \left(\delta u_i \right) \right) dV \ , \\ &= \int_{S_P} \left(\hat{\sigma}_{ij}^S n_j \right) \delta u_i dS - \int_{V_P} \hat{\sigma}_{ij}^S \delta \epsilon_{ij}^S dV \ , \end{aligned} \tag{56}$$

yielding the weak form:

$$\int_{V_P} \left(\hat{\sigma}_{ij}^S \delta \epsilon_{ij}^S - \omega^2 \tilde{\varrho}_{ij} u_j \delta u_i \right) dV + \int_{V_P} i\omega \tilde{\kappa}_{ij} \partial_j \psi \delta u_i dV = \int_{S_P} \left(\hat{\sigma}_{ij}^S n_j \right) \delta u_i dS \ . \tag{57}$$

3.1.2 Fluid in the open pores

Similarly, the variational form of equation (54) is:

$$\int_{V_P} \left(\frac{\Omega^2}{\tilde{\rho}_{22}} \partial_{rr} \psi + \omega^2 \frac{\Omega^2}{\tilde{R}} \psi - i\omega \partial_i \tilde{\kappa}_{ij} u_j \right) \delta \psi dV = 0 \ . \tag{58}$$

The first term can be integrated by part:

$$\begin{aligned} \int_{V_P} \frac{\Omega^2}{\tilde{\rho}_{22}} \partial_{rr} \psi \delta \psi dV &= \int_{V_P} \frac{\Omega^2}{\tilde{\rho}_{22}} \left(\partial_r \left(\partial_r \psi \delta \psi \right) - \partial_r \psi \partial_r \delta \psi \right) dV \\ &= -\int_{V_P} \frac{\Omega^2}{\tilde{\rho}_{22}} \partial_r \psi \partial_r \delta \psi dV + \int_{S_P} \frac{\Omega^2}{\tilde{\rho}_{22}} n_i r_i \partial_r \psi \delta \psi dS \ . \end{aligned} \tag{59}$$

The third term can also be integrated by part:

$$\begin{aligned} \int_{V_P} -i\omega \partial_i \tilde{\kappa}_{ij} u_j \delta \psi dV &= \int_{V_P} -i\omega \left(\partial_i \left(\tilde{\kappa}_{ij} u_j \delta \psi \right) - \tilde{\kappa}_{ij} u_j \partial_i \delta \psi \right) dV \ , \\ &= \int_{V_P} i\omega \tilde{\kappa}_{ij} u_j \partial_i \delta \psi dV - \int_{S_P} i\omega n_i \tilde{\kappa}_{ij} u_j \delta \psi dS \ , \end{aligned} \tag{60}$$

yielding the weak form:

$$\begin{aligned} &\int_{V_P} \left(-\frac{\Omega^2}{\tilde{\rho}_{22}} \partial_r \psi \partial_r \delta \psi + \omega^2 \frac{\Omega^2}{\tilde{R}} \psi \delta \psi + i\omega \tilde{\kappa}_{ij} u_j \partial_i \delta \psi \right) dV \ , \\ &\qquad = \int_{S_P} \left(-\frac{\Omega^2}{\tilde{\rho}_{22}} n_i r_i \partial_r \psi + i\omega n_i \tilde{\kappa}_{ij} u_j \right) \delta \psi dS \ . \end{aligned} \tag{61}$$

3.2 Alternative form of the poroelastic variational statement

The boundary integrals appearing in equations (57) and (61) can be rewritten in a more suitable form for the imposition of classical boundary conditions:

3.2.1 Elastic skeleton

The total stress in the poroelastic material is the sum of the fluid pressure and the solid stress:

$$\begin{aligned} \sigma_{ij}^P &= \sigma_{ij}^S - \Omega p \delta_{ij} = \hat{\sigma}_{ij}^S - (\alpha - \Omega) p \delta_{ij} - \Omega p \delta_{ij} \ , \\ &= \hat{\sigma}_{ij}^S - \alpha p \delta_{ij} = \hat{\sigma}_{ij}^S + i\omega\alpha\psi\delta_{ij} \ . \end{aligned} \tag{62}$$

This allows to write the boundary contribution in equation (57) as:

$$\begin{aligned} \int_{S_P} \left(\hat{\sigma}_{ij}^S n_j\right) \delta u_i dS &= \int_{S_P} \left(\sigma_{ij}^P n_j\right) \delta u_i dS - \int_{S_P} i\omega\alpha\psi\delta u_i n_i dS \\ &= \int_{S_P} \left(\sigma_{ij}^P n_j\right) \delta u_i dS - \int_{V_P} i\omega\alpha\partial_i \left(\psi\delta u_i\right) dV \\ &= \int_{S_P} \left(\sigma_{ij}^P n_j\right) \delta u_i dS - \int_{V_P} i\omega\alpha\partial_i\psi\delta u_i dV - \int_{V_P} i\omega\alpha\psi\partial_i\delta u_i dV \ , \end{aligned} \tag{63}$$

and the weak form given by equation (57) becomes:

$$\begin{aligned} \int_{V_P} \left(\hat{\sigma}_{ij}^S \delta\epsilon_{ij}^S - \omega^2 \tilde{\varrho}_{ij} u_j \delta u_i\right) dV + \int_{V_P} i\omega(\tilde{\kappa}_{ij} + \alpha\delta_{ij})\partial_j\psi\delta u_i dV \\ + \int_{V_P} i\omega\alpha\psi\partial_i\delta u_i dV = \int_{S_P} \left(\sigma_{ij}^P n_j\right) \delta u_i dS \ . \end{aligned} \tag{64}$$

3.2.2 Fluid in the open pores

Equations (18) and (47) allow to rewrite the gradient of ψ along the isotropy direction:

$$\partial_r\psi = \frac{i\omega\tilde{\rho}_{22}}{\Omega} U_r + \frac{i\omega\tilde{\rho}_{12}}{\Omega} u_r = \frac{i\omega}{\Omega} r_j(\tilde{\rho}_{22} U_j + \tilde{\rho}_{12} u_j) \ . \tag{65}$$

This, together with the definition of $\tilde{\gamma}$ given by equation (42), allows to write the boundary term in equation (61) as:

$$\begin{aligned} &\int_{S_P} \left(-\frac{\Omega^2}{\tilde{\rho}_{22}} n_i r_i \partial_r\psi + i\omega n_i \tilde{\kappa}_{ij} u_j\right) \delta\psi dS \\ &\quad = \int_{S_P} -i\omega n_i \left(\Omega r_i r_j \left(U_j + \frac{\tilde{\rho}_{12}}{\tilde{\rho}_{22}} u_j\right) - \left(\Omega\left(1 + \frac{\tilde{\rho}_{12}}{\tilde{\rho}_{22}}\right) r_i r_j - \alpha\delta_{ij}\right) u_j\right) \delta\psi dS \\ &\quad = \int_{S_P} -i\omega n_i \left(\Omega r_i r_j (U_j - u_j) + \alpha\delta_{ij} u_j\right) \delta\psi dS \\ &\quad = -\int_{S_P} \left(i\omega\Omega n_i r_i \left(U_r - u_r\right) + i\omega\alpha u_n\right) \delta\psi dS \\ &\quad = -\int_{S_P} \left(i\omega\Omega n_i r_i \left(U_r - u_r\right) \delta\psi dS - \int_{S_P} i\omega\alpha n_i u_i\right) \delta\psi dS \ . \end{aligned} \tag{66}$$

Rewriting the second surface contribution in term of volume integral yield:

$$\begin{aligned} &\int_{V_P} \left(-\frac{\Omega^2}{\tilde{\rho}_{22}} \partial_r\psi\partial_r\delta\psi + \omega^2 \frac{\Omega^2}{\widetilde{R}} \psi\delta\psi\right) dV \\ &+ \int_{V_P} \left(i\omega(\tilde{\kappa}_{ij} + \alpha\delta_{ij}) u_j \partial_i\delta\psi + i\omega\alpha\partial_i u_i \delta\psi\right) dV \\ &= -\int_{S_P} i\omega\Omega n_i r_i \left(U_r - u_r\right) \delta\psi dS \ . \end{aligned} \tag{67}$$

Both weak forms given by equations (57) and (61), on one side, and by equations (64) and (67), on the other side, are symmetric. The second weak form given by equations (64) and (67) is preferred because it leads to more convenient natural boundary conditions, and compatibility condition with classical solid, fluid and porous media that are easier to enforce.

3.3 Preferred weak formulation for transverse porous material

Introducing the relation

$$\tilde{\kappa}_{ij} + \alpha\delta_{ij} = ((\alpha + \tilde{\gamma})r_i r_j - \alpha\delta_{ij}) + \alpha\delta_{ij} = (\alpha + \tilde{\gamma})r_i r_j \ , \tag{68}$$

into equations (64) and (67), one get:

$$\begin{aligned}\int_{V_P} \left(\hat{\sigma}_{ij}^S \delta\epsilon_{ij}^S - \omega^2 \tilde{\varrho}_{ij} u_j \delta u_i\right) dV + \int_{V_P} i\omega(\alpha + \tilde{\gamma})\partial_r\psi\delta u_r dV \\ + \int_{V_P} i\omega\alpha\psi\partial_i\delta u_i dV = \int_{S_P} \left(\sigma_{ij}^P n_j\right)\delta u_i dS \ ,\end{aligned} \tag{69}$$

$$\begin{aligned}&\int_{V_P} \left(-\frac{\Omega^2}{\tilde{\rho}_{22}}\partial_r\psi\partial_r\delta\psi + \omega^2\frac{\Omega^2}{\tilde{R}}\psi\delta\psi\right) dV \\ &+ \int_{V_P} \left(i\omega(\alpha + \tilde{\gamma})u_r\partial_r\delta\psi + i\omega\alpha\partial_i u_i\delta\psi\right) dV \\ &= -\int_{S_P} i\omega\Omega n_i r_i \left(U_r - u_r\right)\delta\psi dS \ .\end{aligned} \tag{70}$$

4 Conclusion

The derivation of a particular Biot model for transverse isotropic materials has been performed. The resulting model is formulated in terms of the skeleton's displacement components and the fluid scalar potential. A symmetric weak variational form has been set up in order to support the related finite element model. Boundary and interface conditions with visco-elastic and acoustic materials will be presented at the conference together with numerical applications.

References

[1] Biot M.A. Theory of propagation of elastic waves in a fluid-saturated porous solid. i. low-frequency range. *Journal of the Acoustical Society of America*, 28(2):168–178, 1956.

[2] Biot M.A. Theory of propagation of elastic waves in a fluid-saturated porous solid. i. higher-frequency range. *Journal of the Acoustical Society of America*, 28(2):179–191, 1956.

[3] Biot M.A. Mechanics of deformation and acoustic propagation in porous media. *Journal of the Acoustical Society of America*, 33(4):1482–1498, 1962.

[4] Allard J.F. *Propagation of sound in porous media: Modeling sound absorbing materials*. Elsevier, New-York, 1993.

[5] Coyette J.P. The use of finite element and boundary element models for predicting the vibro-acoustic behaviour of layered structures. *Advances in Engineering Software*, 30:133–139, 1999.

[6] Atalla N., Panneton R., and Debergue P. A mixed displacement-pressure formulation for poroelastic materials. *Journal of the Acoustical Society of America*, 104(3), 1998.

[7] Coyette J.P., G. Lielens, and J.L. Migeot. Numerical simulation of porous absorbing materials and multi-layered components. Technical report, Free Field Technologies, 2001.

[8] Coyette J.P. and Lielens G. ACTRAN Theoretical Manual. Technical report, Free Field Technologies, 2003.

Characterization of the ultrasonic waves in a water-saturated porous plate via its acoustic impulsive response.

Serge Derible[1], Hervé Franklin[1], Pierre Campistron[2], Bertrand Nongaillard[2].

[1] Laboratoire Ondes et Milieux Complexes,
LOMC GOA, FRE CNRS 3102, FANO FR CNRS 3110.

[2] Institut d'Electronique, de Microélectronique et de Nanotechnologie,
UMR CNRS 8520, FANO FR CNRS 3110.

Seldom is the acoustic impulsive response of a target implemented to determining some of its characteristics. It is an alternative means of revealing the slow wave even though it could not be located on the temporal signal emerging from a thin porous plate in which the fast and slow echoes overlap. The acoustic impulsive response is obtained performing the inverse Fourier transformation of the transmission coefficient of the plate. This coefficient is measured at normal incidence with the experimental arrangement presented in the following figure 1.

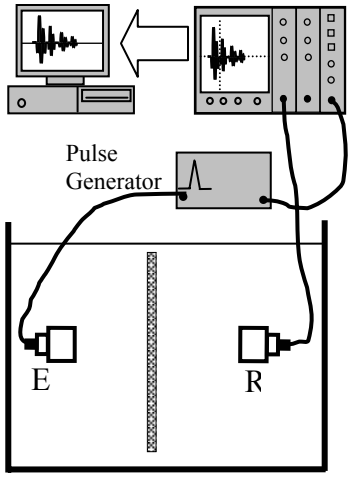

Fig. 1 Experimental set-up

The porous plate (300mm×200mm×5mm) is suspended between two identical wideband transducers in a water tank. The emitter is connected to a pulse generator which also triggers the recording apparatus chain.

The normalization signal is the direct one, launched from the emitter to the receiver and recorded under the same conditions, after the plate has been removed.

Two successive pairs of identical transducers, with central frequencies 0.5 MHz and 1 MHz, are used to give the system a wide frequency range (0.1 to 2 MHz).

The experimental transmission coefficient is the ratio of the Fourier transform of the transmitted signal to the Fourier transform of the relevant direct signal. The two spectra are then associated (figure 2).

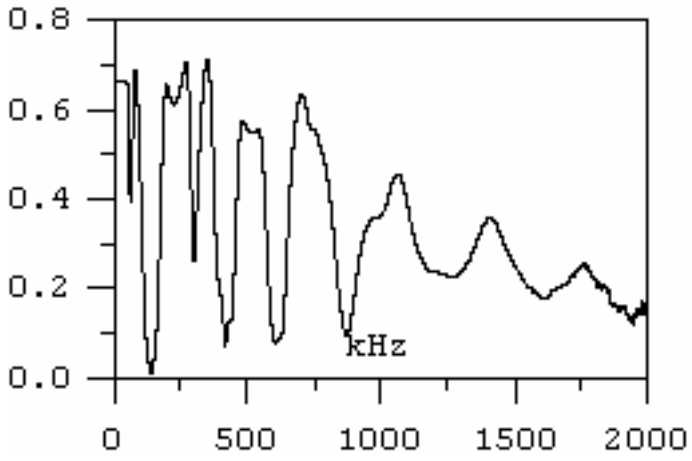

Fig. 2. Experimental spectrum of the transmission coefficient.

In order to obtain the real impulsive response given in figure 3, the inverse Fourier transformation is performed on the previous spectrum extended with its complex conjugate. One can first locate the successive decreasing fast pulses denoted F1, F3 and F5 where the integers indicate the number of times the wave has ran across the plate before it emerges. The first slow wave S1 is located between two smaller fast pulses.

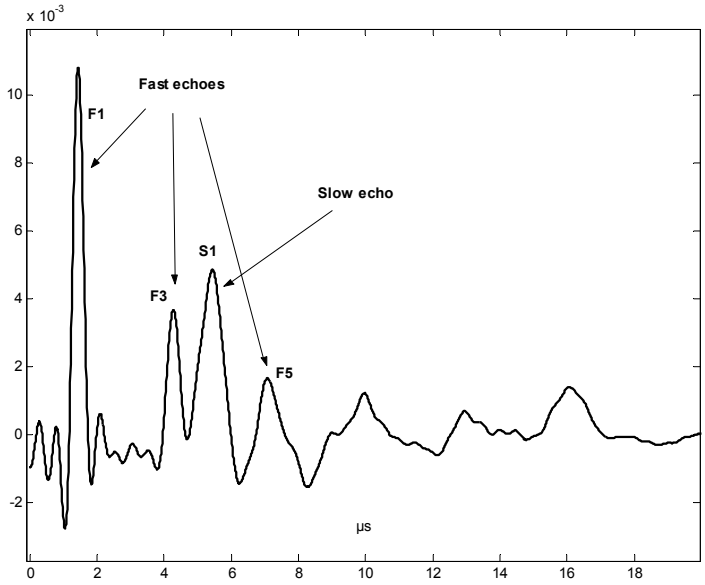

Fig. 3. Acoustic impulsive response.

This allows us to measure some of the characteristics of the fast and slow waves. There is a good agreement with the other previous determinations and the theoretical values.

Estimation of non Acoustical Parameters of Porous Materials Using Sensitivity Analysis and Global Minimisation Algorithms

M. Garoum, R. IdchabaniM. Rhachi

LEME Laboratory

Ecole Supérieure de Technologie de Salé Morocco

e-mail : garoum1@yahoo.fr

Abstract

In literature, various models have been proposed in order to predict characteristic impedance Z_c and wave number k_c of porous materials. To use these models their involved nonacoustical parameters (i. e. flow resistivity, tortuosity porosity…) are usually measured. Unfortunately measurements require specialised equipments and are often difficult on loose porous materials leading most often to erroneous values. Moreover, the inverse estimation of theses parameters from experimental data is not an easy task as believed. This is due to the non linearity of the available mathematical models containing often some parameters with weak and/or linearly dependent influences. In order to obtain a best estimation of non acoustical parameters, we propose in this work an approach based on two steps. First a trade-off between magnitude and linear independence of the sensitivity matrix components is developed to achieve an efficient ranking of parameters according to their inherent ease of estimation. Subsequently, the results obtained from the first step are associated to Global minimisation algorithms (i.e. Genetic Algorithms, Nelder-Mead, Differential Evolution and Random Research), to minimize the least squares norm between measured and modelled normal sound absorption coefficient.

To ensure the applicability off this approach, verification tests were carried out under various conditions on simulated data generated from some widely used models and fixed parameter values. The estimated parameter values were then compared with predetermined parameter values. The proposed approach was then applied on effective measured normal absorption coefficient of loose granular cork.

Results show that, unlike classical gradient methods, better estimation has been obtained.

References:

[1] **Biot MA**: Theory of propagation of elastic waves in a fluid-saturated porous solid. I. Low-frequency range. II. Higher frequency range. J Acoust Soc Am;**28** (19561).p. 68–91.

[2] **Hamet JF**: Modélisation Acoustique d'un enrobe´ Drainant. Bron: Rapport INRETS; 1992. p. 159.

[3] **K.Attenbborough**:"Models for the acoustical properties of air-saturated granular media" Acta acustica **1** (1993) 213-226.

[4] **Beck.J.V:** Parameters estimation in engineering and science. Wiley& sons, USA, 1989.

[5] **M.R. Stinson and Yvan Champoux**: Propagation of sound and the assignment of shape factors in model porous material having simple pore geometries. JASA **91(2)** (1992). 685-695.

[6] **D.L Johnson, J.Koplik, and Dashen**. Theory of dynamic permeability and tortuosity in fluid-saturated porous media. J.Fluid.Mech. **176**, (1987) .379-402.

[7] **M. Garoum**, **M. Tajayouti, M. Rhachi, F. Simón, A. Moreno:** Inverse estimation of non acoustical parameters of absorbing materials using genetic algorithms: 19th International Congress on Acoustics: Madrid, 2-7 September 2007.

[8] **M. Garoum, R. Idchabani(1), M. Tajayouti,M. Rhachi, A. Moreno:**Sensitivity analysis and non linear parameters estimation of porous materials from normal sound coefficient absorption measurements: Acoustics Paris 08 29 June Jully 2008.

Symposium on the Acoustics of Poro-Elastic Materials
December 17-18-19, 2008, Bradford (UK)

Using Micro-perforated absorbers for sustainable building envelop development

Jian Kang
School of Architecture, University of Sheffield
United Kingdom

INTRODUCTION

AIM

- to develop window systems that will reduce noise transmission whilst allowing natural ventilation, and enabling the efficient use of daylight.
  overall sustainability and green building

PREVIOUS STUDY

Active control

Passive control: seal the windows and use a silencer-type element.

- the use of fibrous materials
- rough surfaces increase air flow resistance
- minimum air exchange only
- non-transparent – daylighting/location affected

BASIC/GENERIC CONFIGURATIONS IN THIS RESEARCH

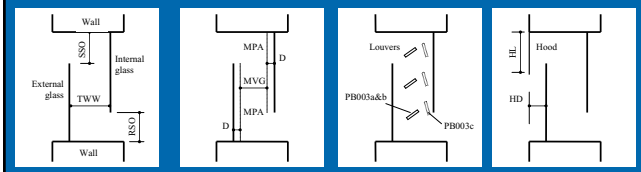

- using transparent micro-perforated absorbers (MPA)
- more freedom when designing the system
- useful for refurbishment projects
- maintain the integrity of the window form
- achieve occupant comfort by means of air movement

A parallel project

Acoustic ventilators for a supply-air window system, using MPA

BASIC THEORY: MPA

- Micro-perforated plate: acoustic resistance significant
- not necessary to provide extra acoustic resistance using porous materials.

- For normal incidence, the normalised specific acoustic impedance of the apertures

$$z_L = \frac{R_L + jM_L}{\rho c} = r + j\omega m = \frac{g_1}{d^2}\frac{t}{p}\left(\sqrt{1+\frac{k^2}{32}} + \frac{k\sqrt{2}}{8}\frac{d}{t}\right) + j\omega(0.294(10^{-3}))\frac{t}{p}\left(1+\frac{1}{\sqrt{9+\frac{k^2}{2}}}+0.85\frac{d}{t}\right)$$

where R_L and M_L are the specific acoustic resistance and reactance of the aperture, ρ is the density of air, c is the sound velocity in air, $\omega = 2\pi f$, f is the frequency (Hz), $k = g_2 d\sqrt{f}$, t is the panel/membrane thickness (mm), d is the aperture diameter (mm), p is the ratio of aperture area to panel/membrane area, and b is the distance between aperture centres (mm). g_1 and g_2 are constants. For non-metallic material, g_1=0.147 and g_2=0.316. For metallic material, g_1=0.335 and g_2=0.21.

Acoustic windows

NUMERICAL SIMULATION

Finite Element based software FEMLAB

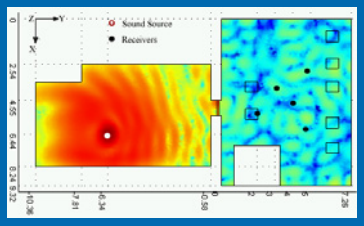

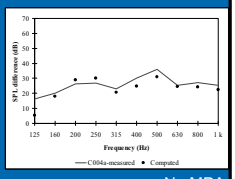

No MPA

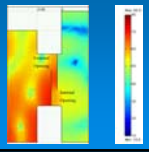

Comparison between simulation and measurement

A sound wave incident at an angle
the impedance of the air space?
apertures locally reacting

Parametric study: mainly no MPA

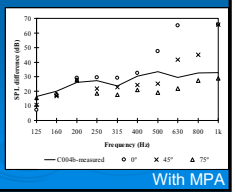

With MPA

Configuration used in parametric study

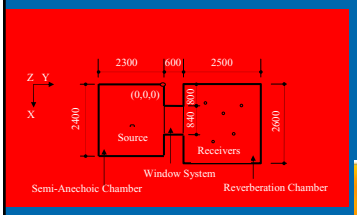

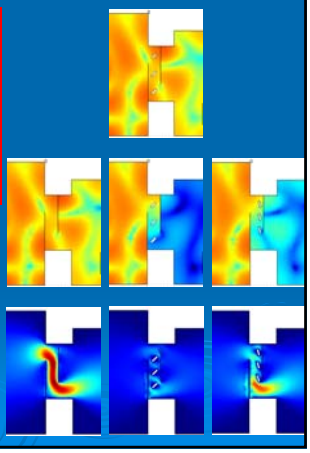

acoustic simulation

ventilation simulation

Velocity field map, with pressure difference 50Pa

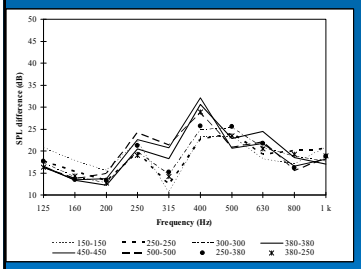

external and internal opening sizes

- with hard boundaries, the external and internal opening sizes affect the acoustic performance considerably at different frequencies
- there are peaks at certain frequencies due to the effects of resonance
- in terms of the average performance over the frequency range, difference rather small, within about 2dB.

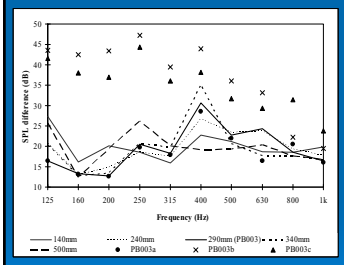

air gap

- with hard boundaries, air gap effect similar to opening sizes
- louvers with hard boundaries barely bring any acoustic benefit, but with absorbent surfaces performance significantly improved

- With absorbers between two sheets of glass, there is an optimal value of impedance and absorption coefficient for the maximum SPL difference.
- The ventilation simulation suggests that such window systems will provide sufficient ventilation for comfort.
  - Effect of the hood on ventilation negligible.
  - Louvers: optimal designs for acoustics and ventilation

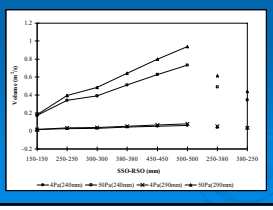

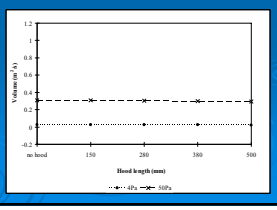

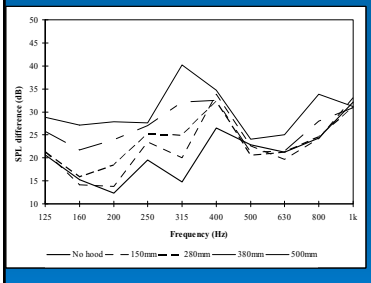

hood

- a hood hung outside the opening is very effective in increasing the SPL difference, especially at relatively low frequencies, and the effectiveness is improved by increased hood length

EXPERIMENTAL STUDY

An integrated acoustics, ventilation and lighting test facility

- Acoustics: a dodecahedral loudspeaker, a reference microphone, five receiving microphone positions.
- Ventilation: fans outside anechoic chamber
- Light transmission: using two large boxes

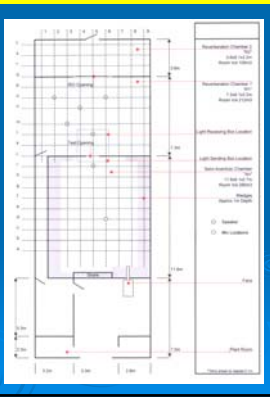

A ready-available micro-perforated membrane absorber: aiming at studying the effectiveness and feasibility of MPA in the window system.

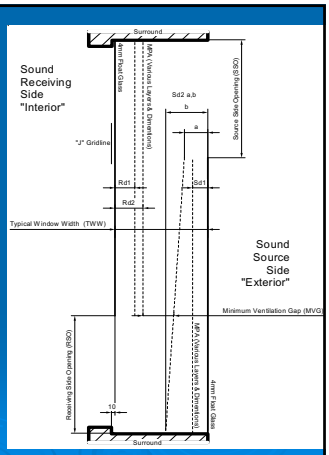

A typical test section

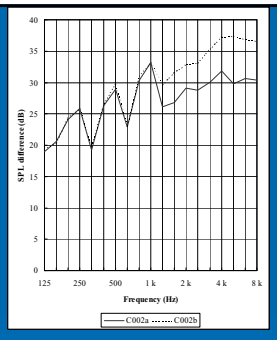

TWW of 145 mm:
(a single layer of MPA on each side with air space=10mm)

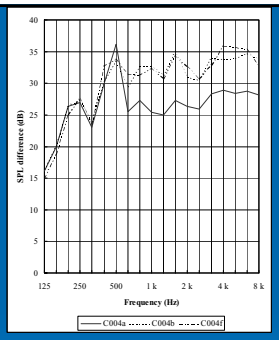

TWW of 290mm & Sd1=Rd1=80mm
MPA benefits significantly greater.
Better results using one of the sheets of MPA sloped away from the glass (C004f) - air space varies from 10mm to 40mm.

VENTILATION

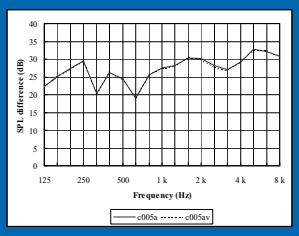

- Tests using forced ventilation during acoustic measurements suggest that, at normal air movement levels there is no adverse effect on MPA.

LIGHTING

- a single sheet glass in the opening : 100%
- no glass: 117%
- two sheets of glass with 380 mm: 89%
- Adding a single sheet MPA: 78%.
- Two sheets MPA: 70%
- Four sheets MPA: 63%

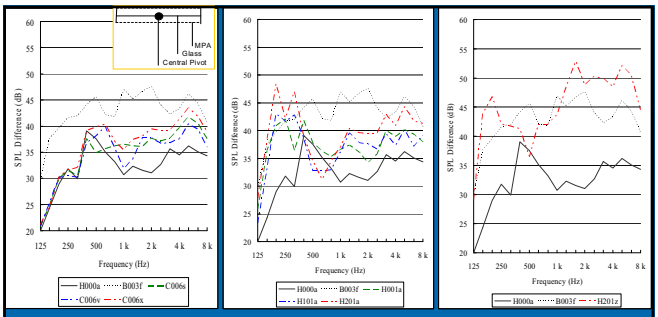

Acoustic louvers –

also control solar gain

H001a - internal hood,
H101a - external hood,
H201 - both

Both louvers and hoods

SPL difference achieved by a single pane of glass totally blocking the opening is shown by B003f.

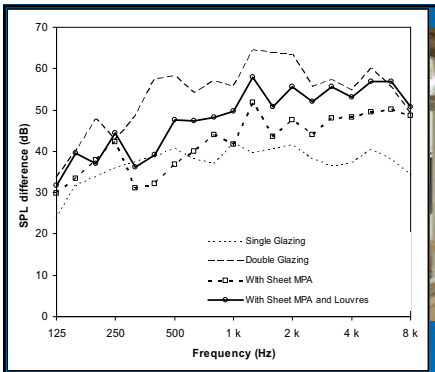

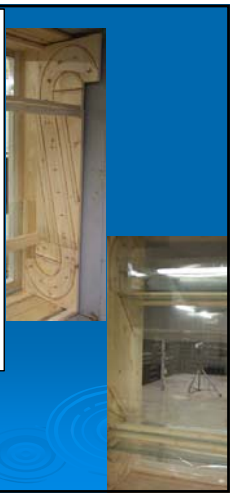

Strategically designed profiles

ACOUSTIC VENTILATORS

- low-energy whole-house ventilation system

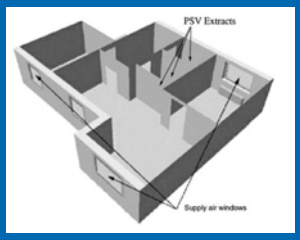

- 'regulated-flow supply-air' windows

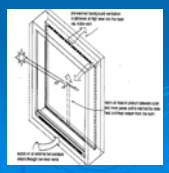

Laboratory tests

Site tests

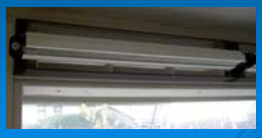

Measure results

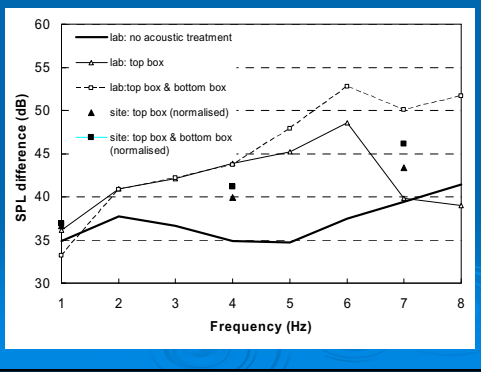

CONCLUSIONS

- Feasibility and effectiveness to use MPA in window systems
- Feasibility and effectiveness to use MPA in ventilator systems
- Usefulness of finite element method simulation
- Further potentials of strategic designs, also use better-adapted MPA

ACKNOWLEDGEMENTS

- The work was financially supported by the UK Engineering and Physical Sciences Research Council (EPSRC) and the European Commission. The author is indebted to the project partners for their contributions.

(2)Ultrasound impulse propagation in wet dense marine quartz sand in situ.

Has passed more than 20 years since publications results of ultrasound sounding of dense sandy massiv in situ [1].

Sandbanks sandy soils are under research. High uniformity of the sizes of grains and high density characterizes these marine sandsmassiv.It is formed as result of sedimentation and when the water level in a gulf goes down, shallows there are shaped. So formed natural marine sandy soils massiv have density close to the maximal density

High frequency,high velocity(25 kHz) and low frequansy, lov velocity wave propagations are observe simultaosly. If they are not waves Bio of 1 and 2 sorts they are waves of repacking (dilatnce) according to Nikolaevskii?

For finding-out of a question experiment with massiv sounding have been repeated, distance betveen sensors(resonance frequency 25 kHz) 1m: are seen high frequansy and low frequansy waves.

On the way of ultrasound impulse propagation the hole (20cm vide, 1 meter deep) has been dug: only low frequency waves are seen, high frequency waves disappear

the hole is filled in by water:only high frequansy wave are observe,

after an intensive filtration of water in surrounding massiv the hole partially has disappeared and after some consolidation there are high-frequency waves with the reduced amplitude and low-frequency waves.

Most interesting result of this extended experiment is that during an intensive filtration the low-frequency wave absolutely disappears.

That may be evidence of dilatants nature of low frequency wave and they are dominant frequencies waves. Resonant (dominant) frequencies in pure marine sandy soils known from 1980s[1,2,3,4,5]. Any influence - impact, explosion, an ultrasonic impulse and wind generates an acoustic field of resonant frequencies at a distance from the place of impact

References

[1] Vilchinskaja, N.A. Stress waves in sand and acoustic emission. *Dokladi Acad. Nauk SSSR*, vol.262, N3, pp.568-572 (1982).

[2] Vilchinskaja, N.A. and Nikolajevskiy, V.N.. The Acoustical Emission and Spectrum of Seismic Signals. Izvestiya, *Earth Physics* pp. 393 - 400 Vol. 20, No. 5,(1984).

[3] Vilchinska, N., Nikolajevskiy, V. and Lisin, V. Slow waves and natural oscillations in sandy marine soils. *Izvestiya Acad. Nauk SSSR, Oceanology* No. 4 (in Russian) (1985).

[4] Vilchinska, N. and Dzilna, I. Resonance frequencies in sands. Procs. *Field Measurements in Geotechnics*., edited by Geraldine Sörum, A.A. Balkema, Rotterdam, ISBN9054100257, pp. 927-935 (1991).

[5] Vilchinska N. Impulse induced wave propagation in quartz marine sands. *Forum Acusticum 2005*, Budapest, N7940 (2005).

A new set-up to measure the viscoelastic properties of porous media using a specific electrodynamic transducer

Nicolas DAUCHEZ, Olivier DOUTRES, Jean-Michel GENEVAUX, Guy LEMARQUAND

LAUM, CNRS, Université du Maine, Av. O. Messiaen, 72095 LE MANS, FRANCE
nicolas.dauchez@univ-lemans.fr

A new method for measuring viscoelastic properties of sound absorbing materials is presented. This method is derived from the quasistatic method [1,2] using a loudspeaker as actuator and sensor. Previous results carried out with a traditional electrodynamic loudspeaker were limited to 100 Hz because of transducer nonlinearities [3,4]. In this paper, viscoelastic properties are determined up to 500 Hz due to the design of a specific loudspeaker devoid of the main nonlinearities.

The proposed set-up is presented in Fig. 1. The porous sample is compressed in the top cavity using a specific electrodynamic transducer. The use of a cavity allows to carry out measurements in ambient conditions: it avoids a lateral airflow which can induce an overestimation of the porous material loss factor [5,6,7]. In opposition to the electrodynamic shaker used in the quasistatic method [1,2], the use of a loudspeaker as an actuator allows to excite the porous sample in the relevant frequency range for noise control applications. Indeed, such transducers are originally designed to radiate in the audible frequency range.

In the proposed method, the viscoelastic properties of the frame are derived from the mechanical impedance of the porous sample by inverse method using the Biot's model. This impedance is estimated from the measurement of the transducer electrical impedance and a model of its electro-mechanic behaviour [3,4]. The experimental set-up is thus considerably simplified but it requires in exchange a transducer as linear as possible to fit the Thiele and Small model [8].

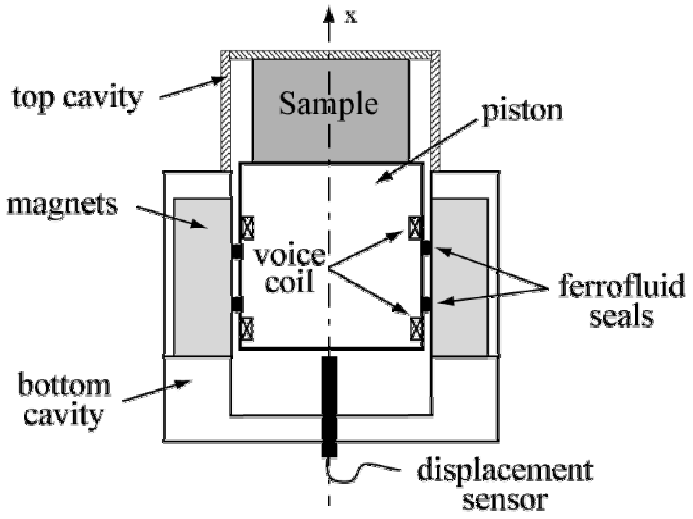

Fig. 1: set-up to measure the viscoelastic properties of porous materials

Thereto, the transducer presented in Fig. 1 is made of a voice-coil motor such as those used in traditional electrodynamic loudspeakers but with major improvements [9]:

- the magnetic structure is ironless and is designed to vanish the major electrical nonlinearities,
- the viscoelastic suspension is replaced by two ferrofluid-seals which help avoid nonlinearities in the movements of the piston.

The method has been applied to a polymer foam. Results obtained with this method are presented in Fig. 2. Results are given up to 500 Hz (square) and are compared to the results given by the classical compression quasistatic method (cross). Except around resonances in the system that mostly affect the estimation of the loss factor (void square), results are in good agreement. The optimization of the set-up will be performed from the evaluation of the uncertainties that will be presented further.

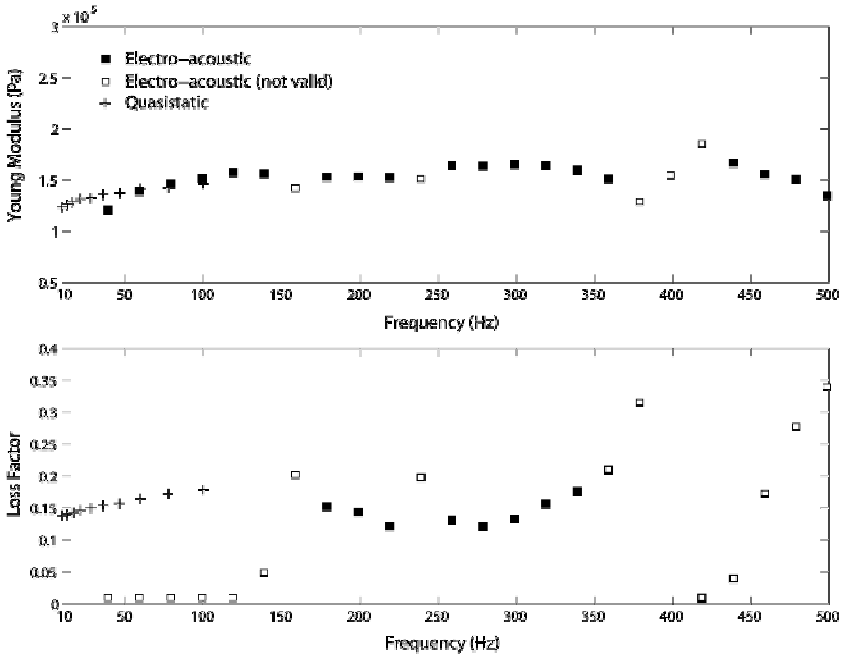

Fig. 2: Viscoelastic properties of a polymer foam estimated by a quasistatic and electro-acoustic techniques.

[1] DAUCHEZ N., ETCHESSAHAR M., SAHRAOUI S., *On measurement of mechanical properties of sound absorbing materials*, 2nd Biot conference on Poromechanics, 2002

[2] MARIEZ E., SAHRAOUI S., *Elastic constants of polyurethane foam's skeleton for Biot model*, Internoise Congress Proceedings, Liverpool, 951–954, 1996

[3] DOUTRES O., DAUCHEZ N., GENEVAUX J.M., LEMARQUAND G., *On the use of a loudspeaker for measuring the viscoelastic properties of sound absorbing materials*, JASA EL, Under Review, 2008

[4] DOUTRES O., DAUCHEZ N., GENEVAUX J.M., LEMARQUAND G., *A new set-up for measuring the mechanical properties of porous materials*, proceeding of Acoustics 08, Paris, 2008

[5] TARNOW V., *Dynamic measurements of the elastic constants of glass wool*, J. Acoust. Soc. Am. **118**(6), 3672-3678, 2005

[6] PRITZ T., *Transfert function method for investigating the complex modulus of acoustic materials: spring-like specimen*, J. Sound Vib. **72**(3), 317-341, 1980

[7] JAOUEN L., RENAULT A., DEVERGE M., *Elastic and damping characterizations of acoustical porous materials: Available experimental methods and applications to a melamine foam*, Appl. Acoust., doi:10.1016/j.apacoust.2007.11.008, 2008

[8] SMALL R.H., *Closed-box loudspeakers systems, part 1: analysis*, J. Audio Eng. Soc. **20**, 798-808, 1972

[9] LEMARQUAND G., *Ironless Loudspeakers*, IEEE Trans. Mag., **43** (8), 3371-3374, 2007

Active Multilayered Panels Based on Porous Materials for Improving Acoustic Performance

Azzedine Sitel[a], Ying Hu[a b] and Marie-Annick Galland[a]

[a]Centre Acoustique du LMFA, Ecole Centrale de Lyon, 36 avenue Guy de Collongue, 69134, Ecully cedex, France
[b]Department of Environmental Engineering, College of Marine Engineering, Northwestern Polytechnical University, Xi'an, 710072, China.

ABSTRACT

In this paper we present an active multilayered panel which is combined with passive means for reducing the sound reflection and transmission. A piezoelectric patch is added to the panel and behaves as a secondary vibrational source; meanwhile, some porous materials are applied for ensuring good performance throughout the whole frequency range because of its highly-dissipative character in high-frequency.

For reducing noise in both industry and civil engineering, it can be carried on three sides: sound source, transmission path and receiver. In traditional approaches, multilayered panels are widely used as a solution for limiting the transmission of acoustic waves [1]. These so-called 'sandwiches' are usually made up of two elastic plates and a core such as an air gap or highly-dissipative media like poro-elastic material. However, such passive multilayered panels are efficient enough at medium and high frequencies but exhibit a lack of performance at low frequencies, where resonance inherent to the layer distribution occurs. As an alternative to passive control, active control appears to be the right approach for remedying this problem. Therefore, an active multilayered panel combining porous materials is proposed in this paper.

Our analytical model is based on the concept of Ref [2]. A global framework is schematized in figure 1. The active multilayered panel under study consists of a MPP (micro-perforated panel), two elastic thin plates, two porous materials and several air gaps. A piezoelectric patch is adhered on the plate 1, which makes this plate vibrate as a secondary source. The modeling of the system is analyzed by two matrixes: transfer matrix and scattering matrix [3].

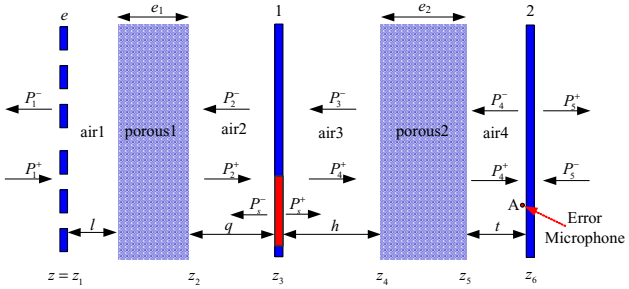

Figure 1: An active multilayered panel

We can describe the acoustical behavior of the active multilayered panel in equation (1), where the $\left\{P_1^+, P_5^-\right\}_2^T$ and $\left\{P_1^-, P_5^+\right\}_2^T$ represent the incoming and the out-coming pressure waves vector respectively, and $\left\{P_s^-, P_s^+\right\}_2^T$ is the pressure radiated by the piezoelectric patch on both sides.

$$\begin{Bmatrix} P_1^- \\ P_5^+ \end{Bmatrix}_2 = [D]_{2\times 2} \cdot \begin{Bmatrix} P_1^+ \\ P_5^- \end{Bmatrix}_2 + \begin{Bmatrix} P_s^- \\ P_s^+ \end{Bmatrix}_2, \tag{1}$$

Considering only one error sensor at point 'A', we can use the minimum pressure as the cost function for active control, that is, the pressure at point A is up to zero. Meanwhile, suppose $P_s^+ = -P_s^- = P_s$ and $P_1^+ = 1$, $P_5^- = 0$, we can calculate the optimal pressure of the secondary source, and then the absorption coefficient and transmission loss (TL) can be deducted.

The experiment is carried out in the Matisse tube proposed by LMFA with two source-location method [4], using a dSPACE-DS1103 controller implemented with Simulink® for finding the optimal value of the secondary sound source. Figure 2 displays the absorption coefficient and TL of this active multilayered panel with and without active control in simulation and experiment respectively.

For passive and hybrid cases, the agreement between theory and experiment is very good. Without active control, performances of the active multilayered panel are satisfactory on both absorption and acoustic insulation $(\alpha > 0.6; TL > 40\,dB)$ for the frequency range [500-2000Hz]. With active control, a significant gain (more than 15dB) has been obtained in transmission loss, but only around resonances (near of 400 Hz). The inefficiency of the active control far away resonances is due to the insufficient level of the pressure P_s^+ radiated by the piezoelectric patch far from its resonance frequency. This effect has also been shown by experiment.

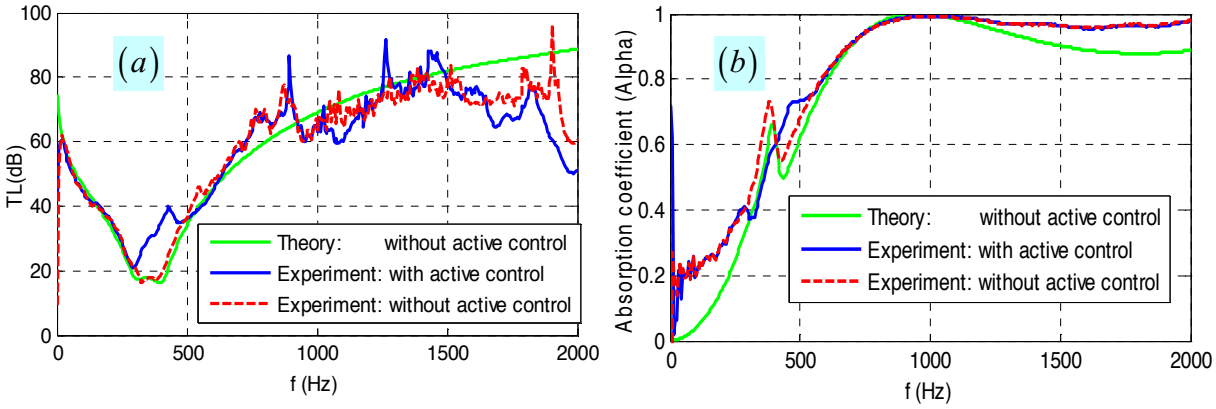

Figure 2: Performance parameters of the active multilayered panel.

(a) : Transmission Loss. (b) : Absorption coefficient.

Consequently, the active multilayered panel based on porous materials proposed in this paper can improve its performance in low-frequency range, especially around of resonance frequency. Experiments on the Matisse tube are in good agreement with simulation results and the transmission loss is increased on the frequency range where the piezoelectric patch works.

REFERENCES

1. C. Batifol, T.G. Zielinski, M.N. Ichchou and M.A. Galland, "A finite element study of a piezoelectric/poroelastic sound package concept", Smart Materials and Structures, **16**, 168-177 (2006).
2. M. A. Galland, B. Mazeaud, and N. Sellen, "Hybrid passive/active absorbers for flow ducts", Applied Acoustics, 66, 691-708 (2005).
3. Ying Hu, Azzedine Sitel, Marie-Annick. Galland, Kean Chen, Hybrid Sandwiches Panels for Reducing the Sound Reflection and Transmission, 37th International Congress and Exposition on Noise Control Engineering, 26-29 October 2008, Shanghai, China.
4. M. Aböm, "A note on the experimental determination of acoustical two-port matrices", J. Sound and Vibration, 155(1), 185-188 (1992.

Modeling of Multilayered Sound Insulators Including Poroelastic Material in Industrial Conditions

J. Monet-Descombey[1,2] M.A. Hamdi[2,3] C. Zhang[1]

1. Renault SA, Technocentre de Guyancourt, 1 Avenue du Golf, 78280 Guyancourt, France
2. Université Technologique de Compiègne, Laboratoire Roberval, 60205 Compiègne, France
3. ESI-Group, 20 rue du Fonds Pernant, 60471 Compiègne, France

Abstract

For the acoustic comfort of driver and passengers, the car cabin must be insulated from outside noise such as engine noise, road noise and wind noise. Trimmings materials are applied to the dashboard, the floor and the roof; these trimmings are made of layers of porous elastic materials covered or not by a heavy layer. Typical design of sound insulation treatment consists in two layers: a heavy layer and a foam (or felt) layer. The performance of such treatment depends on two factors, the mass of the heavy layer and the thickness of the foam (or felt). However, this design provides a good sound insulation performance with an important added mass to the car. During the past few years, sound package suppliers developed new insulation concepts to satisfy the weight reduction requirement from automotive companies and their new propositions include three, four or five layers components **[1-4]**. Typically, an automotive trimming is composed by wide and thin multilayer component.

To predict the vibro-acoustic behavior of a car with all its porous elastic trimmings (dash insulator, floor carpets, seats …) in middle frequency range, one can use a finite element software **[5-6]**, which is able to compute efficiently the vibro-acoustic response of large size fluid - structure - poroelastic media problem, as done for a fully trimmed car. However, because of the trimming dimensions and the number of thin layers with different materials, the finite element model of car trimmings can reach a large amount of nodes and elements. Computation of such large models can become very time consuming (between twelve and fifteen hours) and assuming that the computation server has enough memory to solve the problem. Because of these memory and time issues, some trimmings are poorly meshed: for example, it is common to detect elements with large aspect ratio in trimmings, to substitute a multilayer by a single layer of an approximate equivalent porous material, to use equivalent fluid element (one degree of freedom per node) instead of poroelastic element (four degrees of freedom per node - the enhanced (u,p) formulation **[7-9]** is used by the software for poroelastic elements) ... or to exclude some trimming components in the model.

The authors investigated an efficient method to save time and memory without losing the prediction's accuracy and without developing new functionalities in the used commercial finite element software **[5]**. This method is called "trim-cutting method" and the main idea is to consider the original trimming component as the assembly of smaller components. But the simulation software does not allow coupling between trimmings: with the trim-cutting method, a large and relatively thin multilayer is modeled by smaller pieces, which do not have any displacement or pressure continuity relations between each other, while continuity relations stay valid between each trim pieces and the fluid cavity and/or the structure. It will be shown that this hypothesis provides accurate results on both simple plate-cavity system and real sedan car when applied to the inner dash insulator and floor carpets.

The trim-cutting method has been successfully tested with different types of multilayers made of one simple porous layer with or without heavy layer and more complex trimmings such as porous - porous 2L-trimmings, porous - heavy layer - porous 3L-trimmings or porous - heavy layer 2L-trimmings including local air gaps. This

method has proved to be particularly relevant for modeling wide and thin multilayered sound insulators covering structure as complex as a car structure.

References

[1] A. Duval, *Faurecia Acoustic Light-Weight Concept*, SIA, Le Mans, France (2004).

[2] A. Duval, J.-F. Rondeau, G. Deshayes, F. Lhuillier, L. Bishoff, B. Teyssandier, *Generalized Light-Weight Concept: a Comprehensive Acoustic Package Weight Reduction* Strategy, SIA, Le Mans, France (2006).

[3] C. Zhang, *Numerical and Experimental Study on Three Layers Dash Inner Insulator,* Renault Technical Report (2007).

[4] C. Zhang, J. Monet-Descombey, O. Thuong, F. Lhuillier, A. Duval, *Numerical and Experimental Study of Light Weight Concept under Automobile Applications Conditions*, 5th International Styrian Noise, Vibration & Harshness Congress, Graz, Austria (2008).

[5] RAYON-VTM 2007 for I-deas 11 NX, User Manuel, ESI-Group.

[6] M. Anciant, L. Mebarek, C. Zhang, J. Monet-Descombey (2007) *Full Trimmed Vehicle Simulation by using RAYON-VTM*, 2007 JSAE Annual Congress.

[7] N. Atalla, R. Panneton, P. Debergue, *A Mixed Pressure-Displacement Formulation for Poroelastic Materials*, Journal of the Acoustical Society of America, 104(3), (1998).

[8] N. Atalla, M.A. Hamdi, R. Panneton, Enhanced *Weak Formulation for the Mixed (u,p) Poroelastic Equations*, Journal of the Acoustical Society of America, 109(6), (2001).

[9] P. Debergue, *Développement d'une Formulation Mixte en Déplacement-Pression pour les Matériaux Poroélastiques* (*Displacement-Pressure Mixte Formulation for Poroelastic Materials*), M.Sc. Thesis (in French), Université de Sherbrooke, Sherbrooke, Québec, Canada (1998).

NUMERICAL METHODOLOGY FOR DETERMINING THE CUT-OFF FREQUENCY OF THE ANECHOIC CHAMBER OF THE UNIVERSITY OF FERRARA

P. Bonfiglio, F. Pompoli
Engineering Department, University of Ferrara, ITALY

1. Introduction

In this paper a description of different numerical methodologies for determining the low cut-off frequency of anechoic and hemi-anechoic chambers will be presented.
In particular the methodology will be applied to the new anechoic chamber in Ferrara, having volumes of 800 m^3 and 650 m^3 in anechoic and hemi-anechoic configurations, respectively.
The qualification of the chamber has been carried out according to ISO Standard 3745 Annex A [1] by determining the deviation from inverse square law in different directions from a point sound source [2]. From the experimental tests the cut-off frequency has been found equal to 50 Hz in both the configurations.
Results will be compared in terms of sound decays along fixed directions and surfaces pressure distribution.

2. Description of the research

The anechoic chamber has been modelled as a cavity with proper surface impedance boundary conditions. In particular surfaces can be divided in three different categories:

- lateral walls made of polyester fiber wedges (having density of 40 kg/m^3 and total length equal to 1.71m), a rock wool layer (having density of 90 kg/m^3 and thickness equal to 0.1 m), a gypsum board layer (700 kg/m^3 – 12.5mm thick) and 0.9m air gap;
- ceiling made of the above-mentioned polyester fiber wedges and rock wool layer, a steel membrane (7850 kg/m^3 – 1mm thick) and 2 m air gap;
- floor made of polyester fiber wedges and 015 m air.

The afore-mentioned systems are tested by means of a finite element model in a “virtual” impedance tube when a plane wave field is impinging on them. The transfer function method is implemented and the normal incidence surface impedance and plane wave complex reflection coefficient are calculated. Fibrous material are modelled as equivalent dissipative fluid media (by using a complex density and sound velocity) for describing the propagation of sound within them. Gypsum board and steel laminate are modelled as elastic solids. A figure of the tube is shown in Figure 1a. Predicted normal incidence sound absorption coefficients of the three systems are depicted in Figure 1b.

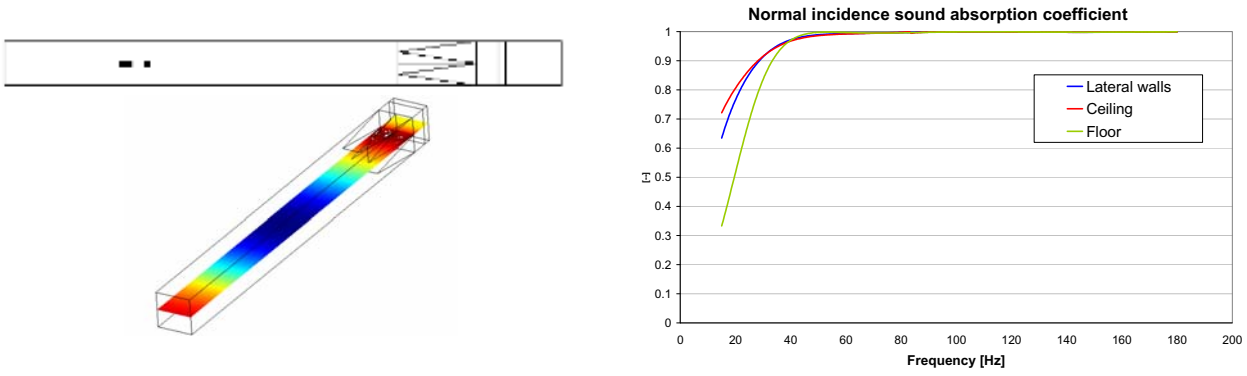

Figure 1 – a) The virtual impedance ; b) Predicted normal incidence sound absorption coefficients of the systems

Sound field within the chamber has been firstly predicted by means of a finite element model by using normal incidence surface impedance as boundary conditions.

It has to be emphasized the at very low frequency (i.e. lower then 100 Hz) the sound field emitted by the sound source is still spherical within the cavity.
For such reason an analytical approach has been used for calculating surface impedance for spherical waves from plane wave reflection [3]. In fact it has been demonstrated that, if $kR_i \gg 1$ the spherical reflection coefficient can be written as:

$$R_{sw}(\theta) = \left[R_{pw}(\theta) + \left(1 - R_{pw}(\theta)\right) F\left(p_e\right) \right] \qquad (1)$$

where k is the wave number, R_i is the path of the reflected wave and $R_{pw}(\theta)$ is the plane wave reflection coefficient at angle of incidence θ and:

$$F\left(p_e\right) = 1 + i\sqrt{\pi}\, p_e \exp\left(-p_e^2\right) erfc\left(-ip_e\right) \quad \text{and} \quad p_e = \left(ikR_1/2\right)^{1/2} \left(\rho_0 c_0 / Z_{pw} + \cos\theta\right) \qquad (2)$$

where $erfc(\cdot)$ is the complementary error function, ρ_0 and c_0 the air density and sound speed, respectively. From the spherical reflection coefficient the surface impedance can be calculated as:

$$Z_{sw}(\theta) = \frac{\rho_0 c_0}{\cos\theta} \frac{1 + R_{sw}(\theta)}{1 - R_{sw}(\theta)} \frac{1}{1 + i/kd} \qquad (3)$$

where d is the distance between the source and the surface.
From equation (3) it is possible to notice that the surface impedance depends on the angle of incidence and the distance from the source. For this reason a FEM model has been implemented by dividing each surface in several sub-surfaces where a different boundary conditions have been applied, as shown in Figure 2. Of course this is still an approximation and one should apply a surface impedance to each node of the boundary mesh.

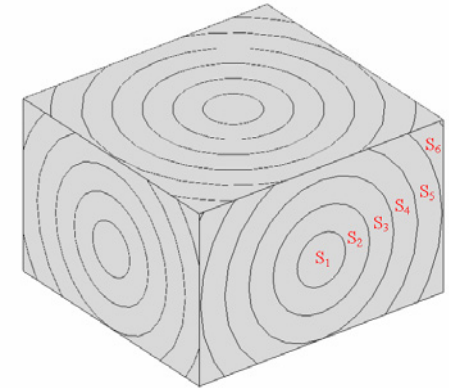

$$\begin{cases} S_1 \rightarrow Z_{sw}\left(\theta_1, d_1\right) \\ S_2 \rightarrow Z_{sw}\left(\theta_2, d_2\right) \\ S_3 \rightarrow Z_{sw}\left(\theta_3, d_3\right) \\ S_4 \rightarrow Z_{sw}\left(\theta_4, d_4\right) \\ S_5 \rightarrow Z_{sw}\left(\theta_5, d_5\right) \\ S_6 \rightarrow Z_{sw}\left(\theta_6, d_6\right) \end{cases}$$

Figure 2 – The "Multi-impedance" FEM model of the chamber

Finally an analytical model by using the complex mirror sources approach has been investigated for determining the sound field within the chamber. According to this method, the sound field in a certain point is the sum of the pressure from the source and reflections from the lateral walls (that one can be imaged as generated by virtual sources). Equation (1) will be used for calculating the reflection factor at each boundary. That is:

$$p_R = \frac{Ae^{ikR_0}}{R_0} + \sum_{n=1}^{6} \left(R_{sw}^{surface_i} \frac{Ae^{ikR_n}}{R_n} \right) + \sum_{n=7}^{18} \left(R_{sw}^{surface_i} R_{sw}^{surface_j} \frac{Ae^{ikR_n}}{R_n} \right) + \ldots \qquad i, j = 1 \ldots 6$$

The analysis has been limited at the second order of reflections.

3. Results

Analysis has been carried out in the frequency range between 15 Hz and 180 Hz and sound pressure level has been calculated in 1/3 octave bands from 20 Hz to 160 Hz. As an example in next figures the comparison between the experimental sound decay along a fixed direction (from the sound source to the upper corner of the Chamber) and decays predicted by means of the models before described is reported for the frequency bands of 40 Hz, 50 Hz, 80 Hz and 100 Hz.

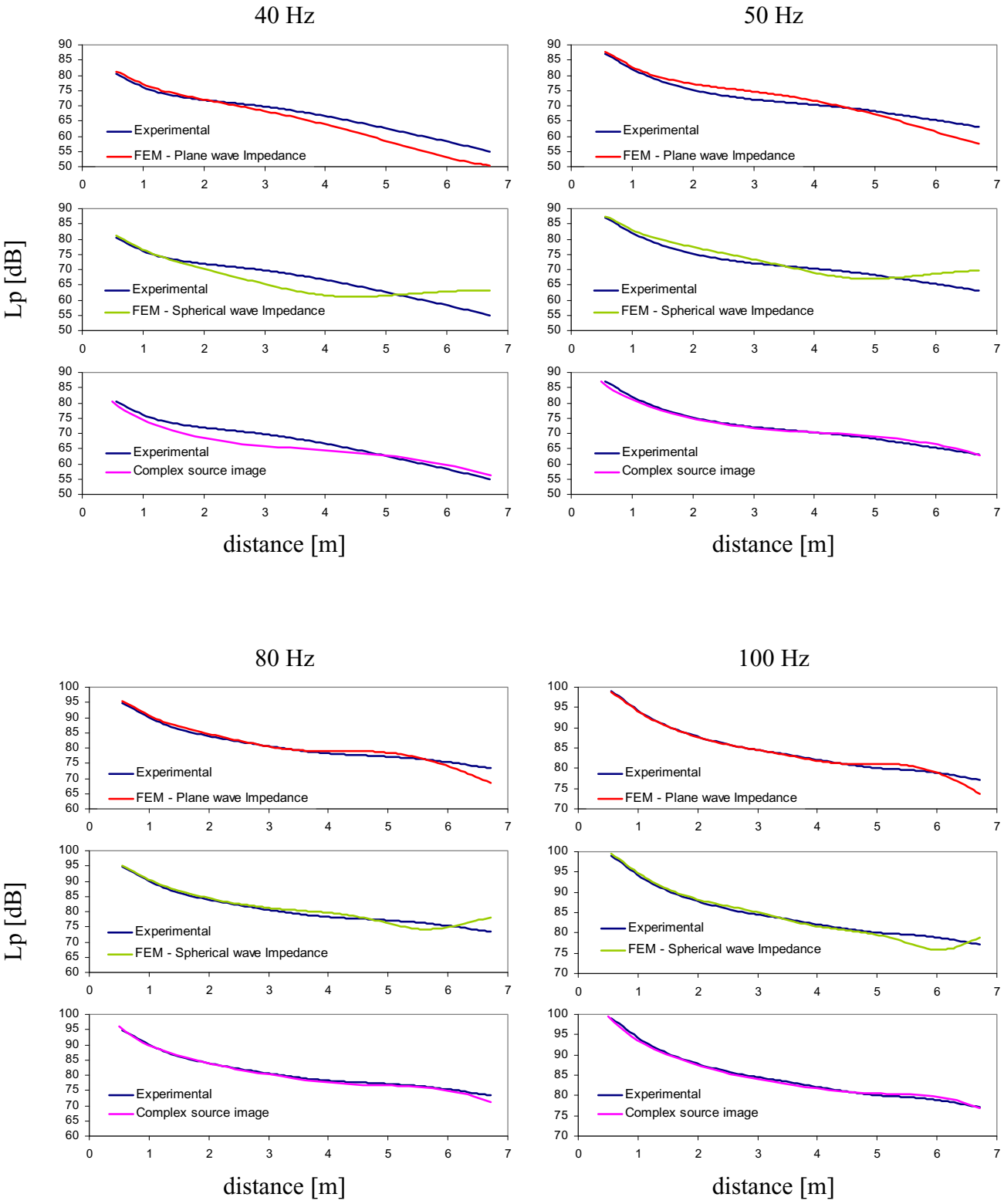

Figure 3 – Sound pressure level decay at different frequency bands

From the figures it can be possible to notice that finite element models exhibit fluctuations in the sound decay at distance close to the boundaries. The main reason of such effect is that in both the cases boundary conditions are not correct and impedances depending on the distance and angle of incidence should be applied at each point of the boundary mesh.
On the contrary the comparison between experimental decay and complex mirror sources method is quite satisfactory for all the frequency bands. In particular discrepancies at 40 Hz could be due to the low order of reflections (second order) when multiple reflections cannot be neglected.
Figure 4 shows the comparison between experimental tests and complex mirror sources method of the sound pressure distribution on the surface passing through the centre and corners at 100 Hz.

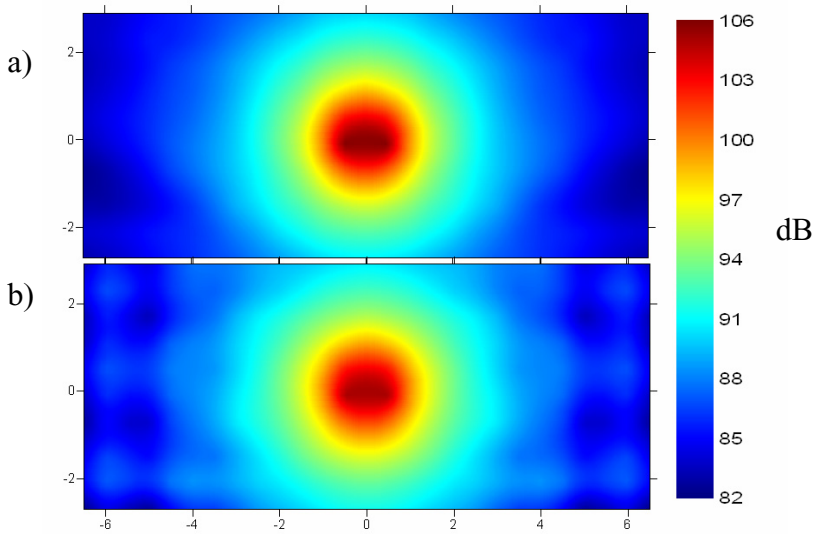

Figure 4 – Sound pressure distribution on the surface passing through the centre and corners at 100 Hz. a) Experimental b) Complex mirror sources method

4. Concluding remarks

In this research a numerical study for determining the cut-off frequency of an anechoic chamber has been proposed and discussed. Results of the predictions have been compared with experimental tests carried out at the anechoic chamber of the University of Ferrara. Among the investigated methodologies, the one based on the complex mirror sources method has shown a satisfactory correlation with the experimental tests.
Future effort will be devoted to improve the complex mirror sources method by increasing the order of reflection. Moreover a boundary element approach will be adopted for validating the formula (1) and the assumption of locally reagent boundary surfaces.

Bibliography

[1] ISO 3745:2003. Acoustics -- Determination of sound power levels of noise sources using sound pressure -- Precision methods for anechoic and hemi-anechoic rooms.
[2] Acoustical qualification of the new anechoic chamber of the University of Ferrara (*in Italian*). Proceedings of the 35th Conference of the Acoustical Society of Italy, Milan June 2008.
[3] C. F. Chien and W. W. Soroka, ‘‘Sound propagation along an impedance plane,’’ J. Sound Vib. 43, 9–20 (1975).

EXPERIMENTAL REPRODUCIBILITY INVESTIGATION ON PHYSICAL AND ACOUSTICAL CHARACTERIZATION OF POROUS MEDIA

Kirill V. Horoshenkov[1], Amir Khan[1], François-Xavier Bécot[2], Luc Jaouen[2], Franck Sgard[2], Amélie Renault[2], Nesrine Amirouche[2], Francesco Pompoli[3], Nicola Prodi[3], Paolo Bonfiglio[3], Giulio Pispola[4], Francesco Asdrubali[4], Jörn Hübelt[5], Noureddine Atalla[6], Celse K. Amédin[6], Walter Lauriks[7], Laurens Boeckx[7]

[1]School of Engineering, Design and Technology, University of Bradford, UK
[2]Laboratoire des Sciences de l'Habitat, Ecole Nationale des Travaux, Publics de l'Etat, France
[3]Department of Engineering (DIF), Universita di Ferrara, ITALY
[4]Industrial Engineering Department, University of Perugia, ITALY
[5]Gesellschaft für Akustikforschung Dresden mbH (AFD), GERMANY
[6]Acoustics and Vibration Group, Faculty of Applied Sciences
University of Sherbrooke CANADA
[7]Katholieke Universiteit Leuven, BELGIUM

Introduction

At the present the reproducibility of acoustical and physical characterization of porous materials has not been completely investigated. In particular regarding physical properties only the measurement of airflow resistivity is standardized and the inter-laboratory reproducibility was determined in [1]. Concerning the acoustical properties, authors of the present paper carried out a series of experiments to research the reproducibility in measuring normal incidence sound absorption coefficient and surface impedance; results have been published in [2]. As a result of the mentioned research, considerable differences have been observed between different laboratories.
In order to exclude the effect of inhomogeneity of the samples and the method of sample preparation, in the present research specimens of three porous materials were provided and both physical and acoustical properties were measured in some of the laboratories. The research activity is still in progress and preliminary results will be reported.

Description of the research

Three different porous materials have been provided. A short description of the tested material is reported in the following table.

Material	Description	Thickness [mm]	Density [kg/m^3]	Diameters [mm]	Number of samples
A	Reticulated foam	20	8,8	29/44/99	4
B	Consolidated flint	31	1500	29/44/99	6
C	Reconstituted porous rubber	28	242	29/44/99	6

At the present tests have been carried out in six laboratories which measured following parameters:

Parameters	Number of laboratories
Sound absorption coefficient and surface impedance	6
Complex acoustical properties	3
Airflow resistivity	5
Porosity	3
Tortuosity	1+1 (by means of inversion approach)
Viscous and thermal characteristic lengths	2 (by means of inversion approach)

Partners were asked to measure different specimen of the materials and to repeat measurements on one specimen of each material.
It is important to underline that each laboratory is using test-rigs having different diameters (i.e. 29mm, 44mm or 99mm) and this could lead to differences in terms of homogeneity and mounting condition.

Results
Available acoustical and physical results will be compared and discussed. It has to be emphasized that collected data are not sufficient for calculating repeatability and reproducibility according to ISO 5725-1 [3].

Future work
Once complete set of data will be collected, systematic analysis will be carried out in order to calculate inter-laboratory reproducibility. Consequently revisions of existing standards [4, 5] will be proposed and new standardized procedures will be defined for remaining acoustical and physical parameters (that are characteristic impedance, complex wave number, porosity, tortuosity and viscous and thermal characteristic lengths).

Bibliography
[1] Garai M., Pompoli F., A European Inter-Laboratory Test of Airflow Resistivity Measurements, Acustica united with Acta Acustica 89 pp. 471-478 (2003).
[2] K. Horoshenkov *et al*, "Reproducibility experiments on measuring acoustical properties of rigid frame porous media (roundrobin tests)", J. Acoust. Soc. Am. Volume 122, Issue 1, pp. 345-353 (2007).
[3] ISO 5725-1: Accuracy (trueness and precision) of measurement methods and results – Part 1: General principles and definitions. 1994.
[4] ISO 10354-2:1996, Acoustics-Determination of sound absorption coefficient and impedance in impedance tubes - Part 2: Transfer-function method.
[5] ISO 9053:1991. Acoustics - Materials for acoustical applications - Determination of airflow resistance.

Characterization of the ultrasonic waves in a water-saturated porous plate via its acoustic transfer function.

Pierre Campistron[1], Bertrand Nongaillard[1],Serge Derible[2], Hervé Franklin[2].

[1] Institut d'Electronique, de Microélectronique et de Nanotechnologie,
UMR CNRS 8520, FANO FR CNRS 3110.

[2] Laboratoire Ondes et Milieux Complexes,
LOMC GOA, FRE CNRS 3102, FANO FR CNRS 3110.

This work deals with the ultrasonic spectroscopy of a water-saturated porous plate. Measurements are performed in frequency domain using a network analyzer and benefit of its large dynamic (100dBm). The efficiency of this method has been tested for liquids characterization[1,2]. We present here a signal processing method devoted to a porous plate characterization. The experimental setup is briefly presented in figure 1.

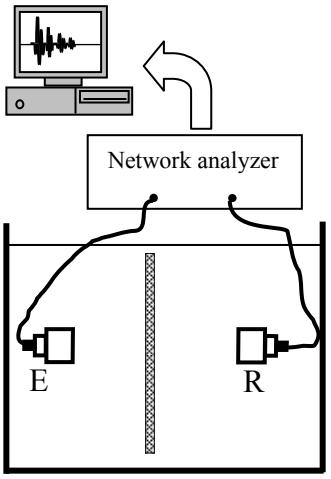

Fig. 1 Experimental set-up.

The porous plate (300mm×200mm×5mm) is suspended between two identical wideband transducers (200 kHz- 1.5 MHz) in a water tank. Emitter and receiver are connected to a network analyzer. The scattering parameter S_{21} is measured over 1601 points equally spaced within the frequency band. The intermediate frequency bandwidth is set to 300 Hz.

The normalization signal is the direct one, launched from the emitter to the receiver and recorded under the same conditions, after the plate has been removed.

The measured scattering parameter S_{21} is complex valued and contains interference terms of all possible ultrasonic paths from the emitter to the receiver. Its inverse Fourier transform is the impulse response of the system and can be more easily understood. We present an example of these two signals in figure 2.

[1] A continuous wave method for ultrasonic characterization of liquids materials, Y.Deblock, P.Campistron, B.Nongaillard, J. Acoust. Soc. Am. 118 (3), Pt 1, pp1388-1393, 2005

[2] High frequency ultrasonic spectrosmetry of viscoelastic liquids, P.Campistron, M.Toubal, F.Lefebvre, J.Carlier, D.Callens, B.Nongaillard, Y.Dubois, Proceedings of the International Congress on Ultrasonics, Vienna, 2007, doi:10.3728/ICUltrasonics.2007.Vienna.1683_campistron

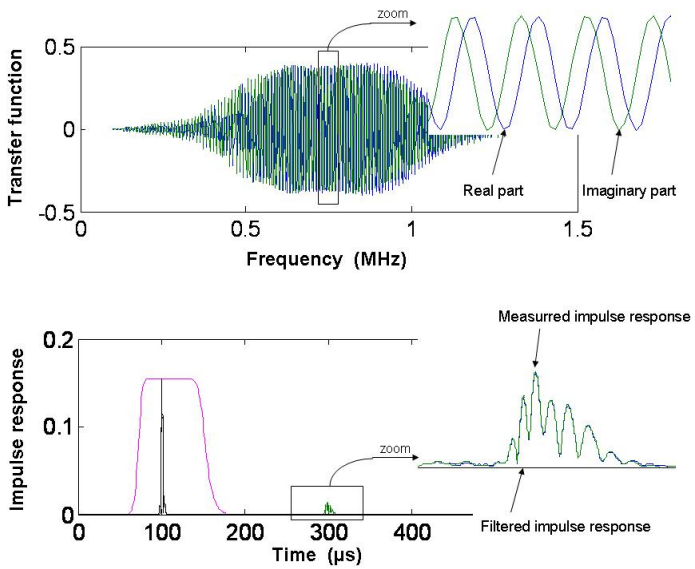

Fig. 2: Transfer function of the normalization signal and its associate impulse response.

The cornerstone of this work is the filtering of the transfer function used as a means to isolate some pulses of the impulse response. For doing that, we design an erasing window in time domain to conserve only the pulses we want to use. Then the transfer function is convoluated with the Fourier transform of the window. In this work we use Chebyshev type II windows which are free of ripple in the passband. An example is presented in figure 2. This filtered transfer function will be used to normalize the signal which propagates through the porous plate.

Then the ultrasonic transfer function of the porous plate is computed taking the ratio of the measured transfer function of the plate to the normalization transfer function. This ultrasonic transfer function (free of the effects of the transducers) is of great interest in porous plate characterization for it can be associated with a numerical inversion of the relevant theory of propagation. Figure 3 represents an example of this ultrasonic transfer function of the studied porous plate.

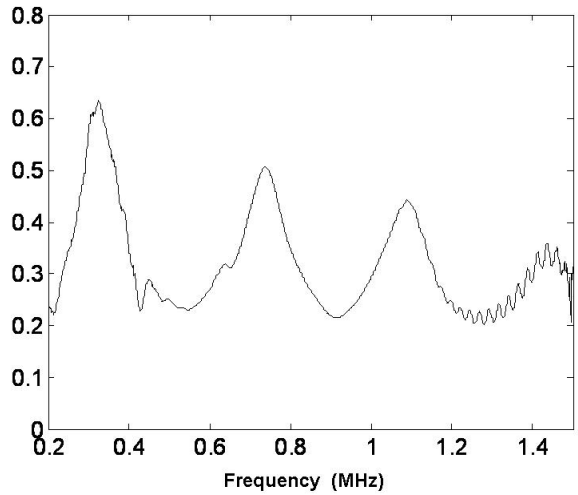

Figure 3: Modulus of the transfer function of a porous plate.

Analytical modelling of a novel acoustic absorber for space launcher fairings using modified BIOT Equations

Jamil KANFOUD, Prof. Mohamed Ali HAMDI
Laboratory of Mechanics-Acoustics and Materials
University of Technology of Compiègne (UTC, France)
BP20529, 60205 Compiègne-Cedex

Abstract

Space launchers are submitted to very high acoustic loads during lift-off, which may damage sensitive equipments inside the payload compartment. Helmholtz Acoustic Absorbers (HAA) have been previously developed by ASTRIUM Gmbh (Friedrishafen, Germany) and integrated inside Ariane V fairing to protect the equipments. The "Centre National d'Etude Spatiale (CNES,France)" decided to support a research program and a PhD thesis under the supervision of Professor M.A HAMDI from "Université de Technologie de Compiègne (UTC, France)" in cooperation with CONTRAVES Space AG, in order to design and develop a low cost Fairing Acoustic Protection (FAP) for Ariane V launcher. The new FAP is based on the use of optimized layer of foam covered by a very thin fabric screen. The fabric's main aim is to protect the payload against dust. But, it highly affects the acoustic behavior of the FAP.

The purpose of this paper is the modeling of the FAP using an analytical model. The analytical model describes wave propagation of acoustic waves within the multi-layers of porous media using mixed BIOT equations (written in terms of fluid phase pressure and skeleton displacement). Computed results have been validated by impedance tube measurements (absorption coefficient) performed by RIETER (Switzerland) and the ENTPE (France). Simulations show the effect of fabric on the acoustic behaviour of the FAP compared to the bare foam.

Parametric studies of Biot's parameters of the foam have been performed using the analytical model, especially in the very low frequency range. A parametric study has been conducted to determine optimal mechanical and acoustical material parameters of the FAP under dimensional constrains (layer thickness and weight) imposed by CNES. Typically, it has been shown that the flow resistivity can be optimized to achieve high absorption at the 63Hz third octave band. The maximum value of the absorption coefficient highly depends on the mechanical properties of the skeleton and on the mounting conditions of the FAP. The effect of the mounting conditions has also been studied experimentally and theoretically. Results reveal the importance of the lateral constraints on the absorption coefficient mainly at the low frequency range (for both porous material and fabric).

A transmission study has been carried out, where the structure of the fairing has been simulated by limp mass covered by the FAP. The Transmission Loss (TL) and Noise Reduction (NR) coefficients have been computed using Biot's theory and the Local Acoustic Impedance (LAI) approximation to represent porous layer effect. Comparison between the two models has been conducted showing the frequency domains of validity of the LAI model.

The presentation will be organized as following :

- *Presentation of the context (HAA vs FAP) ;*
- *Analytical model using mixed BIOT equations ;*
- *Validation of simulations by impedance tube measurements ;*
- *Absorption coefficient comparisons between bare foam and FAP (foam covered by fabric) ;*
- *Absorption coefficient sensitivity to the mounting conditions ;*
- *Parametric study of BIOT acoustical coefficients and skeleton mechanical coefficients highlights low frequency absorption sensitivity to static air flow resistivity and mechanical coefficients ;*
- *TL and NR simulations show Local Acoustic Impedance model limitations ;*
- *Conclusion and Perspectives.*

The references used for this work are the following :

1. M.A. BIOT, "Theory of propagation of elastic waves in a fluid-saturated porous solid I. Low-frequency range II. Higher frequency range", J. Acous. Soc. Am. **28**, 168-191 (1956).
2. J.F. ALLARD, *Propagation of sound in porous media : Modelling sound absorbing materials*, (Elsevier applied science, NEW YORK, 1993).
3. J.S. BOLTON, N.M. SHIAU, Y.J. KANG, "Sound transmission through multi-panel structures lined with elastic porous materials", J. Sound Vib. **191(3)**, 317-347 (1996).
4. J.S BOLTON, N.M. SHIAU, "Oblique incidence sound transmission through multi-panel structures lined with elastic porous material", 11th AIAA Aeroacoustics Conference, Sunnyvale CA,Oct, AIAA-87-2660, 19-21 (1987).
5. J.S BOLTON, N.M. SHIAU, "Random incidence sound transmission through multi-panel structures lined with elastic porous material", 12th AIAA Aeroacoustics Conference, San Antonio TX,Oct, AIAA-89-1048, 10-12 (1989).
6. G. BONNET**,** "Basic singular solutions for a poroelastic medium in the dynamic range", J. Acous. Soc. Am. **82(5)**, 1758-1762 (1987).
7. N. ATALLA, R. .PANNETON, P. DEBERGUE**,** "A mixed displacement-pressure formulation for poroelastic materials", J. Acous. Soc. Am. **104(3)**, 1444-1452 (1998)
8. P. DEBERGUE, R. PANNETON, N. ATALLA**,** " Boundary conditions for the weak formulation of the mixed (*u*,*p*) poroelasticity problem", J. Acous. Soc. Am. **106**, 2383-2390 (1999).
9. M.A. HAMDI, L. MEBAREK, A. OMRANI, N. ATALLA , "An efficient Formulation for the Analysis of Acoustic and Elastic Waves propagation in Porous-Elastic Materials", ISMA 25, International Conference on Noise and Vibration Engineering, 13-15 septembreSeptember 2000, Katholieke Universiteit Leuven, Belgium.
10. N. ATALLA, MA HAMDI, R. PANNETON**,** "Enhanced weak integral formulation for the mixed (U,p) porous-elastic equations", J. Acous. Soc. Am. **109(6)**, 3065-3068 (2001).
11. D. PILON, R. PANNETON, "Behavioral criterion quantifying the effect of circumferential air gaps on porous materials in the standing wave tube", J. Acous. Soc. Am. **116(1),** 344-356 (2004).
12. B. H. SONG, J..S. BOLTON, Y. J. KANG, "Effect of circumferential edge constraint on the acoustical properties of glass fiber materials", J. Acous. Soc. Am. **110(6),** 2902-2916 (2001).
13. A. CUMMINGS, ''Impedance tube measurements on porous media: The effect of air-gaps around the sample,'' , J. Sound Vib. **151**, 63–75 (1991).
14. J..S. BOLTON, E.R. GREEN, "Normal incidence sound transmission through double-panel systems lined with relatively stiff, partially reticulated polyurethane", Appl. Acoust. **39(1)**, 23-51 (1993).
15. F. X. BECOT, F. SGARD, "On the use of poroelastic materials for the control of the sound radiated by a cavity backed plate", J. Acous. Soc. Am. **120(4),** 2055-2066 (2006).
16. N. ATALLA, F. SGARD, C.K. AMEDIN, "On the modelling of sound radiation from poroelastic materials", J. Acous. Soc. Am. **120(4),** 1990-1995 (2006).
17. R. PANETON, N. ATALLA, "Numerical prediction of sound transmission through finite multilayer systems with poroelastic materials", J. Acous. Soc. Am. **100(1),** 346-354 (1996).
18. H.DEFOSSE, M.A HAMDI, "Vibro-Acoustic study of Ariane V launcher during lift off", Proceeding of the 29th International Congress on Noise Control Engineering, Inter-Noise 2000, 27th -30 Aug. 2000, Nice, France.

An efficient System Approach for Integration of Porous Elastic Materials in Finite Element Models of Vehicles

Prof.Mohamed Ali HAMDI

Laboratory of Mechanics-Acoustics and Materials

University of Technology of Compiègne (UTC, France)
BP20529, 60205 Compiègne-Cedex

The author presents recent progresses made during the last decade in numerical modeling of viscous and porous elastic materials [1] and in development of computer aided engineering software tools allowing the prediction of the vibro-acoustic performance of fully trimmed vehicles. A special attention will be made to description of sub-system solving approaches [2], facilitating the cooperation between vehicle and sound-package makers (OEM's, Supplier's) to predict and optimize the acoustic performance of trimmed vehicles at the early stage of the design cycle. Thanks to sub-structuring techniques [4], Suppliers are able to characterize separately their material samples and calculate complex surface impedance matrices of their sound package components, which will interact with the vehicle body-structure at connected interfaces and with acoustic cavities designed by OEM's. Impedance matrices representing viscous elastic layers or porous elastic components can be transferred by Suppliers to OEM's in appropriate file formats. Thanks to automated field transfer and projection techniques, OEM's will are capable to easily detect coupled interfaces, manage incompatible meshes and assemble imported impedance matrices on the algebraic coupled-system representing the vehicle body-structure and internal acoustic cavities. In addition OEM's can easily compare the performance of sound insulation solutions proposed by different Suppliers. Validation cases and industrial examples will be presented showing the performance of developed methods and software tools integrating sub-system approaches to predict the acoustic performance of fully trimmed vehicles [5].
Sensitivity of results to boundary conditions and to material properties will be highlighted in the perspective of developing Multi-Disciplinary Optimization (MDO) leading to cost and weight reduction of vehicles.

The author will present basics of modified Biot's equations, and associated mixed pressure displacement finite element formulation leading to natural satisfaction of boundary conditions at interfaces [3].

The second section of the presentation will explain principles of subsystem approaches for calculation of modal impedance matrices of viscous and porous elastic layers, and assembly with the modal impedance matrix of the vehicle body structure and with the modal acoustic impedance of internal cavities.

The third section of the presentation will be devoted to industrial applications in automobile [5] and aerospace [6].

References

[1] J.F Allard: "*Propagation of sound in porous media, Modelling of sound absorption*", Charpman & Hall, North Way Andover, Hampshire, SP105BE, England , (1993).

[2] M.A Hamdi & Coauthors: "*An Efficient Finite Element Formulation for the Analysis of Acoustic and Elastic Waves Propagation in Sound Packages*", SAE Noise Conference, May 2001, Traverse City, Michigan.

[3] N. Atalla, M.A Hamdi, R. Panneton:"*Enhanced weak formulation for mixed (U,p) poroelastic equations*", J. Acoust. Soc. Of America, 109(6), June 2001

[4] J.K Bennighof and R.B. Lehoucq, "*An Automated Mutilevel Substructuring Method for eigenspace computation in linear elasto-dynamics*", SIAM J.Sci. Comput., 25: 2084-2106, 2004.

[5] M.A HAMDI, L. MEBAREK, C. ZHANG & B. MAHIEUX, "*Analysis of vibro-acoustic performances of a fully trimmed vehicle using an innovative sub-system solving approach facilitating the cooperation between carmakers and sound-package suppliers*", EURODYN2005, Sixth European Conference on Structural Dynamics PARIS , 4-7 September 2005.

[6] A. OMRANI, M.A. HAMDI& J.S. PROWALD, *"Frequency responses of space structures excited by acoustic diffuse fields, development of an automatic procedure coupling NASTRAN and RAYON solvers",* EURODYN2005, Sixth European Conference on Structural Dynamics PARIS , 4-7 September 2005.

Corresponding Author:

Mohamed Ali HAMDI: Mohamed-ali.hamdi@utc.fr or Mohamed-ali.hamdi@esi-group.com

Phone +33-3-44304360; Mobile: +33612418746; Fax +33-3-4486877

Porous Foams with Active Implants Improving Acoustic Absorption

TOMASZ G. ZIELINSKI

Department of Intelligent Technologies
Institute of Fundamental Technological Research, Polish Academy of Sciences
ul.Swietokrzyska 21, 00-049, Warszawa, Poland
tzielins@ippt.gov.pl

1 Introduction

There are apparent reasons for an advanced modeling of porous media with distributed masses and solid implants which should be at the same time sufficiently accurate and efficient to allow a reliable optimization of such poroelastic composites. Recent experimental investigations report a significant improvement of the insertion loss of standard acoustic blankets at lower frequencies by the addition of randomly placed masses to the poroelastic layers [1]. They show that the improvement by distributed masses (implants) tend to be greater than the one due to the mass effect alone. The acoustic absorption of multi-layer absorbers with different inner structures has also become a subject of research [2]. The proposed modeling was accurate with respect to the geometry (thanks to the finite element approach), however, the porous medium was modeled by using the so-called fluid-equivalent approach which generally assumes that the frame (solid skeleton) of a porous medium is rigid. For many porous materials such approach gives good predictions in higher frequencies and for certain configurations.

The present work presents an accurate multiphysics modeling and analysis of active porous-composite sound absorbers composed of a layer of poroelastic material (a porous foam) with embedded elastic implants having active (piezoelectric) elements. The purpose of such active composite material is to significantly absorb the energy of acoustic waves in a wide frequency range. At the same time the total thickness of composites should be very small. The active parts of composites are used to adapt the absorbing properties of porous layers to different noise conditions by affecting the so-called solid-borne wave (originating mainly from the vibrations of elastic skeleton of porous medium) to counteract the fluid-borne wave (resulting mainly from the vibrations of air in the pores); the both waves are strongly coupled, especially, in lower frequencies. Passive and active performance of the absorbers is analysed to test the feasibility of this approach. Since the absorption should be actively improved by affecting the vibrations of the elastic skeleton of porous layers, it is apparent that the rigid-frame modelling cannot be used here. Instead, the advanced biphasic theory of poroelasticity (ref. [3, 4]) must be used to model porous material of the active absorbers. For time-harmonic analysis it is efficient to use the so-called mixed displacement–pressure formulation of the Biot's poroelasticity (ref. [5, 6]).

The examined application of active porous composites links several mathematical models of single- and multiphysics, namely:

- the Biot's theory poroelasticity – to model the material of porous layer (with the air-filled pores),
- the linear elasticity – to model elastic implants,
- the piezoelectricity – to model the active parts (piezo-actuators) of implants which affect the lower frequency vibrations of the elastic skeleton of a porous medium.

All these problems are strongly coupled and the consideration of this mutual interaction of different media is very important. Thus, a coupled multiphysics model of a system made up of poroelastic, elastic, and piezoelectric media was constructed using the Galerkin finite element method.

2 Acoustic absorption of poroelastic layers

The main purpose of the present analysis of poroelastic layers with solid implants is to asses how passive and active implants can influence the acoustic absorption of layers. The acoustic absorption of a poroelastic layer fixed to a rigid wall and subject to a plane acoustic wave propagating in the air onto the layer surface at normal incidence will be computed as follows [4]. First, the acoustic impedance at normal incidence is determined at the interface between the poroelastic layer and the air:

$$Z = \frac{p_0}{v}\,, \quad \text{where} \quad v = \mathrm{j}\,\omega\,u_1^{\mathrm{t}} = \mathrm{j}\,\omega\left[(1-\phi)\,u_1 + \phi\,U_1\right]. \tag{1}$$

Here, v is the velocity of the propagating wave at the layer–air interface (continuous across this boundary) whereas p_0 is the wave pressure. As a matter of fact the (complex) amplitudes are used here, (nb. $\mathrm{j} = \sqrt{-1}$). For time-harmonic vibrations the velocity v at the interface of a poroelastic material depends on the angular frequency $\omega = 2\pi f$ (f is the frequency), and on the total (normal) displacements of the poroelastic layer u_1^{t}, which by itself is composed of the porosity-dependent contributions of the displacements of solid phase u_1 and fluid phase U_1 (ϕ is the porosity).

Now, the reflection coefficient in is computed:

$$R = \frac{Z - Z_0}{Z + Z_0}\,, \tag{2}$$

where $Z_0 = \varrho_0\,c_0$ is the characteristic impedance of the air (ϱ_0 is the air density and c_0 the speed of sound). Finally, knowing the reflection coefficient, the acoustic absorption coefficient can be determined:

$$A = 1 - |R|^2\,. \tag{3}$$

This final property is real-valued (unlike the reflection coefficient R, and the impedance Z, which are complex).

Figure 1 presents a layer of porous foam with *T-shaped* implants made up of stripes of 0.3 mm-thick aluminium foil fixed to the the active PZT-elements. The analysis consisted in determining the acoustic absorption of such active/passive poroelastic composites. To this end, the results of finite-element analysis (especially, u_1^{t} at the layer's surface) were used by the analytical formulas for the impedance, the reflection and absorption coefficients. These formulas result from a one-dimensional analysis of the plane wave propagation which is slightly violated if the solid implants are present (notice, however, that the implants are set approximately 7 mm form the surface of the free-interface). Therefore, the absorption coefficient was computed in two points of the layer surface: at $x_2 = 0$ mm and $x_2 = 5$ mm (see Figure 1), providing two limit-values. It was checked that in the considered frequency range the two values are almost always very similar and thus, for the sake of clearness, only the average curve is plotted in the graph presented below.

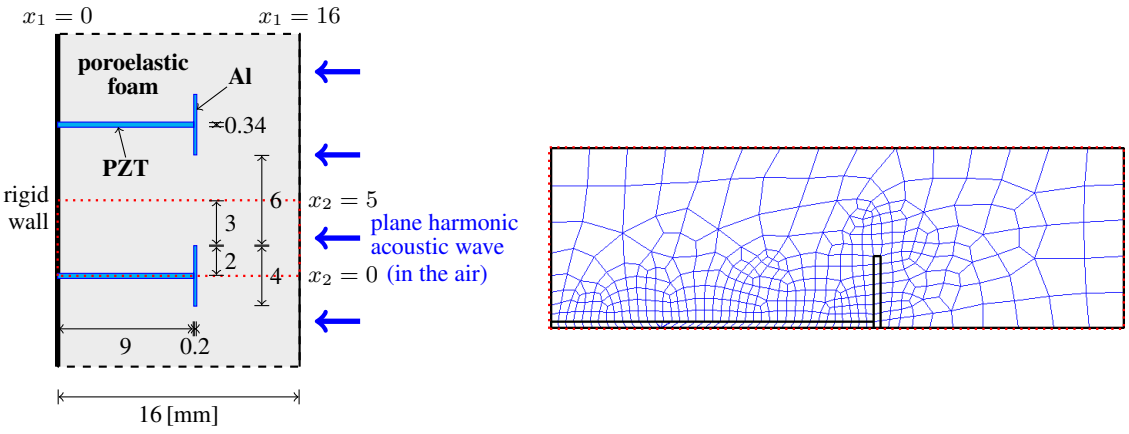

Figure 1: *Active composite configuration and the finite-element mesh of the modeled representative subdomain*

3 Active improvement of the acoustic absorption of poroelastic composites

The general idea of active improvement of the acoustic absorption of poroelastic composites can be explained as follows:

- A harmonic acoustic wave propagates in the air onto the interface between the air and a poroelastic layer (or composite). Higher frequency waves can be well absorbed by the layer but at lower frequencies the acoustic absorption of thin layers is very poor.

- Now, the acoustic wave continues to propagate in the porous medium and is reflected by the rigid wall. In fact, there are three waves: a slow longitudinal wave in the fluid phase (the so-called fluid-borne wave in the 'smeared' air of the pores), a fast longitudinal wave in the solid phase (the so-called solid-borne wave in the 'smeared' elastic skeleton) and a shear wave in the solid phase. At lower frequencies all these waves are strongly coupled so that the vibrations of elastic skeleton are coupled with the vibrations of the air in the pores.

- Because of this coupling the acoustic absorption may be actively modified by affecting the vibrations of the elastic skeleton. To this end, active implants are embedded into the porous layer and an appropriate harmonic excitation signal is applied onto the electrodes of the piezoelectric parts of the implants.

The results presented in this section show the feasibility of this approach.

The fixed parts of he T-shaped implants can be active – they are thin patches of piezoelectric ceramic PZT4, through-thickness polarized, 9 mm long and 0.34 mm thick (see Figure 1). It was checked that by applying a voltage onto their electrodes these piezo-patches would stretch almost 10^{-8} m/V, which means that, for example, a signal with the amplitude of 20 V would extend the active implant for nearly 2×10^{-7} m. Notice that this amplitude is of the same order of magnitude as the maximal amplitude of vibrations of the elastic skeleton of the considered porous layer subject to a harmonic noise of 100 dB. Thus, the active implants may affect the vibrations of elastic skeleton in order to improve the acoustic absorption of the active poroelastic composite. The results presented below prove the feasibility of this assumption.

Figure 2 shows passive and active absorption curves of the porous layer with active and passive implants, or without implants. The frequency range reaches 2600 Hz – above this frequency the passive absorption of the layer with implants was very good (from 0.8 to 1.0) and almost identical with the

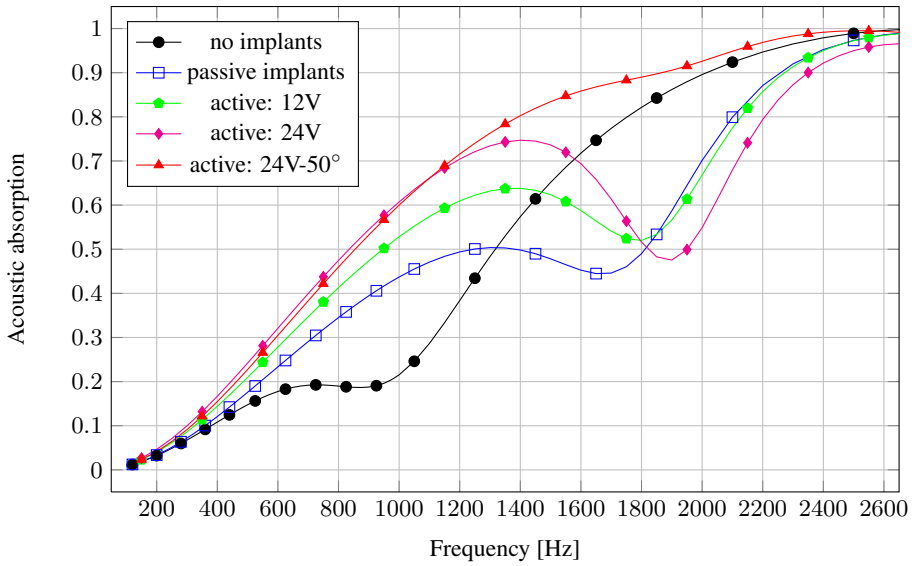

Figure 2: *Active and passive absorption curves for the porous composite/layer*

absorption of the layer with no implants. As mentioned above, to actively improve the absorption a harmonic excitation signal is applied onto the electrodes of the piezoelectric parts of the T-shaped implants. The frequency of the signal equals to the frequency of the acoustic wave, and for the considered range the same constant voltage amplitude is assumed. Three cases are presented which differ by the value of the amplitude and phase of voltage signals (the phase angle of 0° means the maximal extension of the implant): (1) 12 V (no phase shift), (2) 24 V (no phase shift), (3) 24 V with the phase of 50°. In general, all signals improve the acoustic absorption of the composite, however, only the one with the phase shift gives always better absorption than the layer without implants. For lower frequencies the improvement is very weak, and for very low frequencies the absorption is very poor which is obvious when one remembers that the porous layer has only 16 mm. Another interesting observation is that the phase shift effect tends to be visible only when the frequency increases.

4 Conclusions

The obtained results allow to draw the following general conclusions:

- The proposed T-shaped implants (in the passive state) improve the acoustic absorption of a thin porous layer in some range of lower frequencies (where the absorption is poor), but can decrease it in another range of higher frequencies (where altogether, the absorption is better). Similar statement is also valid for stripes of aluminium foil embedded inside the porous layer. For the lowest frequencies and above some high frequency there is no difference in the absorption curves of the porous layer with or without implants.
- The actuators in the form of thin patches of PZT ceramic are able to extend enough to affect the vibrations of the elastic skeleton of polyurethane foams induced by acoustic waves. This influence is better for the proposed T-shaped implants.
- At lower frequencies the coupling between the solid-borne waves (of the elastic skeleton) and the fluid-borne wave (of the air in the pores) is strong enough to allow the exploitation for the improvement of acoustic absorption by the proposed active approach.
- Electric signals with the amplitudes of the order of magnitude of 10 or 20 V, applied to the active piezoelectric parts of the implants, give significant improvement of the acoustic absorption of porus composites subject to the acoustic pressure excitation of 100 dB. A phase shift in the signal is necessary to achieve this improvement in the whole frequency range of interest, although it is important only above some frequency (below its effect is insignificant).

References

[1] M. R. F. Kidner, C. R. Fuller, and B. Gardner. Increase in transmission loss of single panels by addition of mass inclusions to a poro-elastic layer: Experimental investigation. *J. Sound Vib.*, 294:466–472, 2006.

[2] F.-C. Lee and W.-H. Chen. On the acoustic absorption of multi-layer absorbers with different inner structures. *J. Sound Vib.*, 259(4):761–777, 2003.

[3] M. A. Biot. The theory of propagation of elastic waves in a fluid-saturated porous solid. *J. Acoust. Soc. Am.*, 28:168–191, 1956.

[4] J. F. Allard. *Propagation of Sound in Porous Media. Modelling Sound Absorbing Materials*. Elsevier, 1993.

[5] N. Atalla, R. Panneton, and P. Debergue. A mixed displacement-pressure formulation for poroelastic materials. *J. Acoust. Soc. Am.*, 104(3):1444–1452, September 1998.

[6] P. Debergue, R. Panneton, and N. Atalla. Boundary conditions for the weak formulation of the mixed (u,p) poroelasticity problem. *J. Acoust. Soc. Am.*, 106(5):2383–2390, November 1999.

Evaluation of simplified poroelastic models

B. Nennig, J.-D. Chazot, E. Perrey-Debain and M. Ben Tahar
Université de Technologie de Compiègne, Lab. Roberval UMR 6253,
Dept. Acoustique, BP 60319, 60203 Compiègne, France

1 Introduction

In poroelastic modeling, several simplified models can be derived from the full Biot's model. In the case of rigid materials, the solid phase can for example be neglected leading then to the bulk reacting model. The inertial part of the skeleton can however be taken into account thanks to the Limp model. It is also possible to take into account the solid phase without the shear stress thanks to a fluid fluid model. This model was first developed for light and non cohesive materials such as expanded polystyrene beads with a fluid like behaviour. In the present work we tested these different models in two practical cases in order to evaluate their range of validity. First we worked on the transmission loss of a multilayered infinite panel including a porous material with the Transfer Matrix Method. Then we studied the transmission loss of a duct treated with a poroelastic liner with and without flow thanks to a finite element model.

2 Poroelastic models

For isotropic porous materials, Biot's model [4] is grounded on the superposition of a fluid phase and a solid phase which are coupled together. The original equations set involves the fluid phase displacement $\mathbf{U}$ and the solid phase displacement $\mathbf{u}$. For the numerical implementation, the equivalent Atalla's mixed formulation [2] can be used to simplify coupling conditions and to save computation time. Indeed, for linear element, only 4 degrees of freedom (dof) per node are needed instead of 6 in the $(\mathbf{u}, \mathbf{U})$ formulation. The Atalla's mixed formulation can be found in [2].

Different simplifications can be brought to the previous full Biot's theory depending on the studied material elastic characteristics. A simplification was hence proposed by Chazot *et al.* in [6] to model light and non cohesive porogranular materials. The basic idea of this model is to modify the elastic law of the solid phase to suppress shear stresses. The solid phase is then assumed to behave like a fluid. This simplification leads to a reduction of the degrees of freedom in finite element models.

An other classical simplification of Biot's model is to consider the skeleton as motionless [1]. The solid phase elasticity is then neglected, and only the fluid phase is modeled. Viscous and thermal effect are however still taken into account via an equivalent fluid density $\rho_e = \rho_{22}/\phi$, and an equivalent acoustic celerity $c_e = (K_f/\rho_e)^{1/2}$. Here, the same frequency dependent expressions of K_f and ρ_{22} used in Biot's model and based on Allard's formulation are employed in the bulk material modeling (BM).

The limp model introduced by Beranek [3] is very similar to the bulk reacting model since the poroelastic behaviour is described by a single compressional wave. However, this model enables also to take into account the inertia added by the limp solid phase via a modified effective density. The solid phase is hence considered with a solid motion but without elasticity. The validity of this model has been studied in details by Doutres et al.[7] with a criterion called the Frame Stiffness Influence. In practice, this model works well for materials with a very low shear modulus and when the solid phase elasticity is not directly excited as it can be the case in sandwich panels.

3 Transmission loss of infinite multilayered panels

The studied sandwich panel is composed of two external aluminium panels of 2mm and 1.5mm, and an internal poroelastic core of 1cm. Two poroelastic materials A (low density glass wool) and C (plastic foam) defined in [7] are used in the following simulations. Finally, using the Transfer Matrix Method described in [8, 10, 5], models are compared in figure 1. In this configuration, the effect of the solid phase elasticity is clearly identified. Indeed, for the material A with a very low shear modulus, the different simplified models lead to similar results. On the contrary, it is important to take into account the solid phase elasticity for material with higher shear modulus like material C. Indeed, in this case the Biot's model and the Fluid Fluid model lead to similar results while the Limp and the Bulk reacting models lead to very different results.

4 Transmission loss of ducts treated with a poroelastic liner

The TL of ducts treated with a poroelastic liner is calculated using the finite element model presented in [9] with the same configuration. Results are presented in figure 2. Once again the Fluid Fluid model with less degrees of freedom than the Biot's model leads to better results than the limp or the bulk reacting model in the case of rigid materials. However, when shear effects are predominant, the fluid fluid model is still inefficient compared to the full Biot's model.

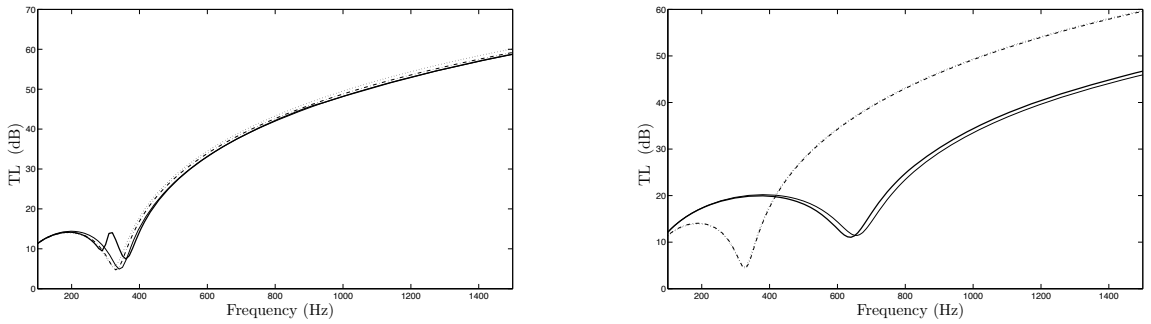

Figure 1: Confrontation of TL of a sandwich panel excited by a plane wave at 45° (foam A on the left and foam C on the rigth) calculated with four models : — Biot, — Fluid Fluid, – · – Limp, · · · Bulk reacting.

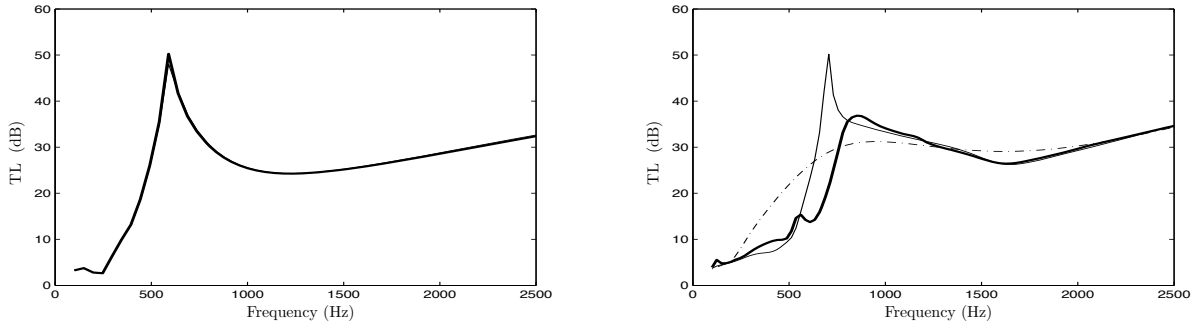

Figure 2: Confrontation of TL in a duct treated with a poroelastic liner (foam A on the left and foam C on the rigth) calculated with three models : — Biot sliding, — Fluid Fluid, – · – Limp.

5 Conclusion

Different simplifications of the Biot's model can be used to describe the behavior of a poroelastic material. It is however always important to know the range of validity of each model. In this work, model comparisons have been presented and some model limitations have been underlined.

References

[1] J.-F. Allard. *Propagation of Sound in Porous Media: Modeling Sound Absorbing Materials*. Chapman and Hall, 1993.

[2] N. Atalla, M. A. Hamdi, and R. Panneton. Enhanced weak integral formulation for the mixed (u, p) poroelastic equations. *J. Acoust. Soc. Am.*, 109(6):3065 – 3068, 2001.

[3] L. Beranek. *Noise Reduction*. New York : McGraw-Hill, 1960, 752 p.

[4] M.A. Biot. Theory of propagation of elastic waves in a fluid-saturated porous solid. i. low-frequency range. *J. Acoust. Soc. Am.*, 28(2):168–178, 1956.

[5] B. Brouard, D. Lafarge, and J.F. Allard. Validity of the limp model for porous materials: A criterion based on the biot theory. *Journal of Sound and Vibration*, 183(1):129–142, 1995.

[6] J. D. C. Chazot and J. L. G. Guyader. Characterization of light and non cohesive poro-granular materials with a fluid/fluid model. *Acta Mech.*, 195(1-4):227–247, 2008.

[7] O. Doutres, N. Dauchez, J.-M. Genevaux, and O. Dazel. Validity of the limp model for porous materials: A criterion based on the biot theory. *J. Acoust. Soc. Am.*, 122(4):2038–2048, 2007.

[8] M.L. Munjal. Response of a multi-layer infinite plate to an oblique plane wave by means of transfer matrices. *Journal of Sound and Vibration*, 162(2):333–343, 1993.

[9] B. Nennig, J.-D. Chazot, E. Perrey-Debain, and M. Ben Tahar. Influence of solid phase elasticity in poroelastic liners submitted to grazing flows. In *Proceedings of Acoustics08*, 2008.

[10] J.S. Sastry and M.L. Munjal. A transfer matrix approach for evaluation of the response of a multi-layer infinite plate to a two-dimensional pressure excitation. *Journal of Sound and Vibration*, 182(1):109–128, 1995.

Checking of an optimal sound absorbing microporous structure

Camille PERROT
Université Paris-Est, Laboratoire Modélisation et Simulation Multi Echelle, MSME FRE3160 CNRS, 5 bd Descartes, 77454 Marne-la-Vallée, France

Fabien CHEVILLOTTE
INSA de Lyon, Laboratoire Vibrations Acoustique, Batiment 303, 20 Avenue Albert Einstein, 69621 Villeurbanne Cedex, France

Raymond PANNETON
Université de Sherbrooke, Groupe d'Acoustique de l'Université de Sherbrooke, Département de génie mécanique, QC J1K 2R1, Canada

Corresponding author: camille.perrot@univ-paris-est.fr
Running title: Optimal porous structure assessment

Abstract

A variety of performance demands are increasingly being placed on sound absorbing material systems. A bottom-up approach for microstructure optimization of long-wavelength sound absorbing materials was recently presented using hybrid estimates based on direct numerical evaluation of macroscopic parameters and analytical models [J. Acoust. Soc. Am. 124, 940 (2008)]. To illustrate the potential of such an optimization method, this methodology was applied to study the sound absorption properties of a two-dimensional and manufacturable hexagonal-like porous structure of motionless solid fibers. Results of this paper tend to demonstrate the existence of a microstructural configuration maximizing the area under the sound absorption spectrum, together with the optimal range of local characteristic lengths. This is a crucial conclusion, notably for foam and fibrous materials manufacturers, which need to be confirmed with a more general formulation proposed by Lafarge and provided in terms of two independent permeabilities including a thermal analog of the well known viscous dynamic one. This paper reports and quantifies differences obtained with the simplified and refined models. It is found that the optimal microstructural configuration is correctly estimated from a simplified model with only 3 % of uncertainty on the global performances. However, for very dilluted (large porosities) porous structures, the simplified model underestimates significantly the material performances with uncertainties reaching up to 30 %.

Keywords: porous media, local geometry, microstructure, periodic unit cell, macroscopic parameters, optimization, sound absorption, acoustic materials.

Pacs numbers: 43.50.Gf, 43.58.Hq, 43.20.Wd

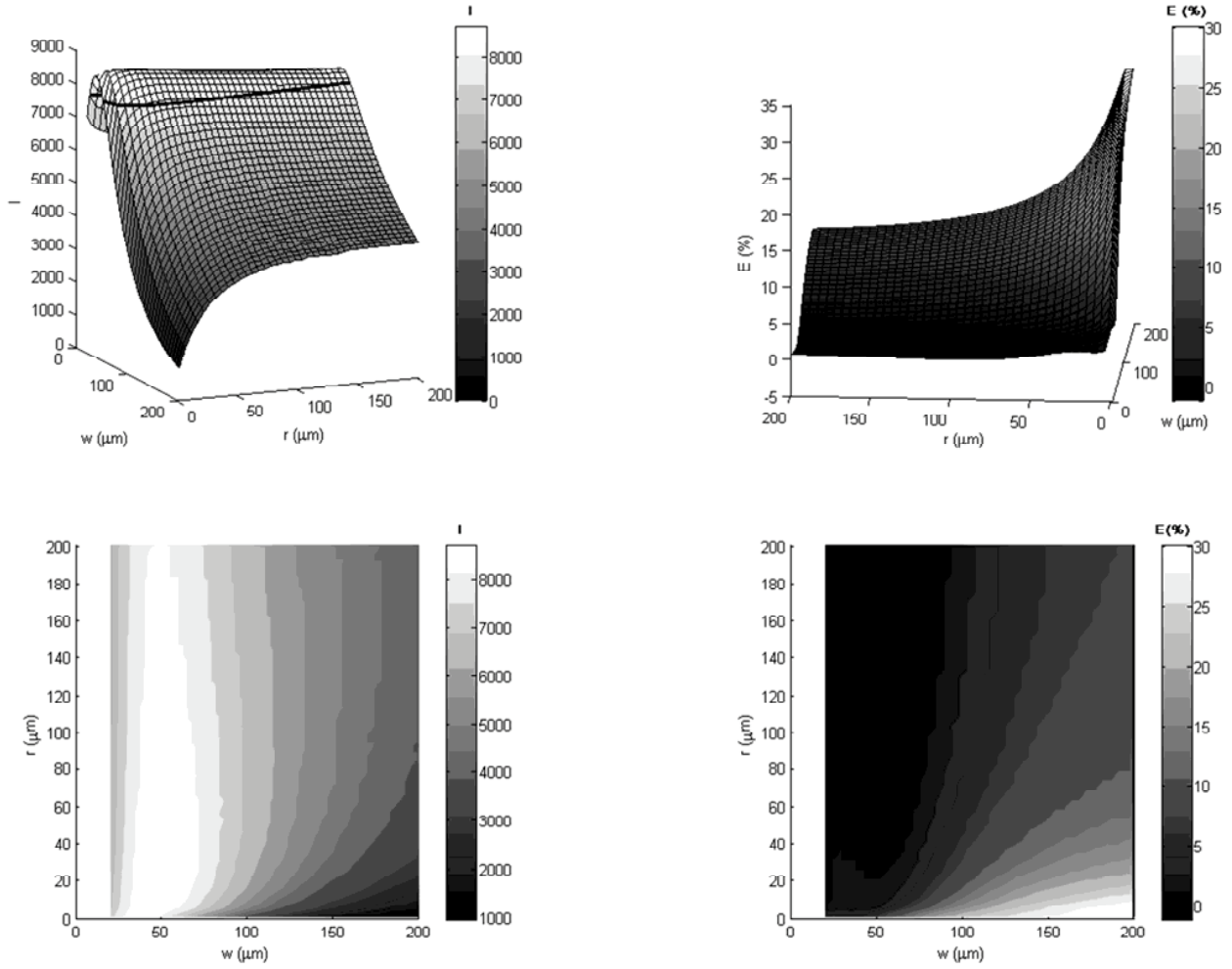

Figure 1. Response surface of the performance index I representing the area under the sound absorption curve in the frequency range 0 - 10 000 Hz for varying (w-throat size, r-fiber radius) couples (top-left); and associated 2D practicle chart (bottom-left). Response surfaces of the error E made on I when using the simplified model instead of the refined one (top-right); and corresponding practical chart (bottom-right).

Introduction of curved trims in Virtual SEA models using poroelastic finite elements in the middle frequency range

Arnaud Duval, Julien Baratier*, Ludovic Dejaeger

Faurecia, Acoustics and Soft Trim Division,
R&D Center Z.I. BP 13, 08210 Mouzon, France
arnaud.duval@faurecia.com
*Centre of Acoustic Technology, Dämmstoffwerk 100, 38524 Sassenburg, Germany
julien.baratier@faurecia.com

SAPEM 2008, Bradford, 17-19 December 2008

Two main parameters are driving the introduction of trims in SEA or Virtual SEA models: the Damping Loss Factors, which represent the damping induced by the trims to the structure or the absorption in a cavity and the Coupling Loss Factors, which represent the modified radiation efficiency of the structure induced by the trims coupled to a cavity or a semi-infinite fluid.

The determination of these adequate trim Damping Loss Factors and Coupling Loss Factors have been carried out for years using the Transfer Matrix Method (TMM) implementing the Biot-Allard theory calculating typically the dissipated power, the absorption coefficient and the Insertion Loss of the trims. This 1D approach for the simulation of the trims is giving good results when the structures are almost flat. This is not the case anymore for highly curved panels where a decrease of the Insertion Loss of poroelastic materials (like a foam - heavy layer complex) with the curvature or 3D shape of the supporting structure is observed experimentally ([1],[2]).

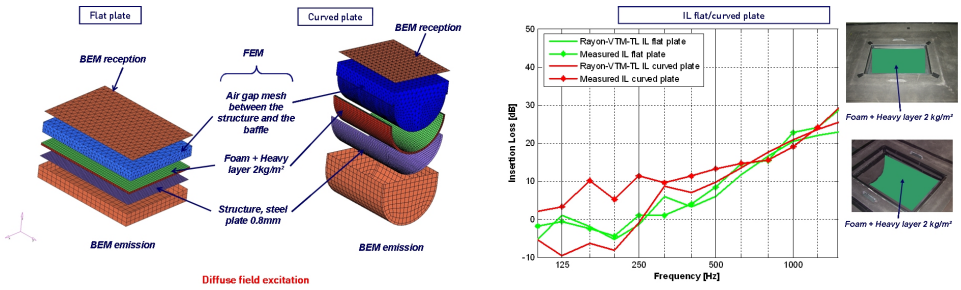

Figure 1: **Insertion Loss simulation of trimmed curved and flat panels**

This physical 3D coupling phenomenon (shear coupling mainly) is well reproduced using poroelastic FEM simulation (U-P formulation) in the low and middle frequency range for a simplified trimmed curved panel like a half-cylinder (cf. Figure 1). Compared to a flat panel, the Insertion Loss simulation slopes are decreased as expected for both structureborne and airborne excitations with a modal "small" cavity in reception as well as with a large reverberant room (Transmission Loss case) [3].

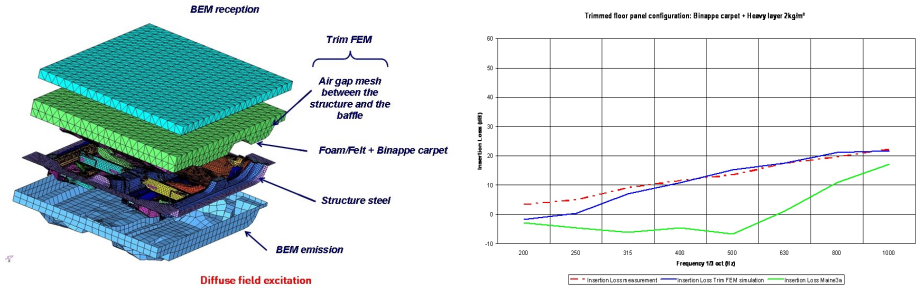

Figure 2: **Insertion Loss simulation of a trimmed floor module**

This work shows that poroelastic FEM simulation addresses the physics properly in the middle frequency range for an industrial case like a complete floor module (IL 9 dB/oct as measured), where the TMM, even with thickness 3D maps, is in difficulty not only in terms of slope after the respiration frequency (IL 12 dB/oct instead of 9 dB/oct) but also in terms of level in the low frequency range (cf. Figure 2) [4].

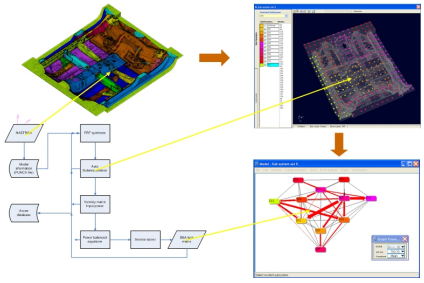

Figure 3: **Floor module Virtual SEA model**

For Virtual SEA modeling, where a bare structure FEM model is used for the automatic substructuration, the idea is to introduce the trims as User Defined IL using poroelastic FEM submodels capturing the curvature effects and to carry out an inverse SEA on the trimmed poroelastic FEM model of the structure with a limited number of load cases (cf. Figure 3). This new procedure will be illustrated in this paper on a floor module case.

References

1. A. Duval and al. Faurecia vehicle acoustic synthesis method: A hybrid approach to simulate interior noise of fully trimmed vehicles. In *Congrès SIA Confort automobile et ferroviaire, Le Mans*, 2004.

2. A. Duval, L. Dejaeger, and J. Baratier. Structureborne and airborne Insertion Loss simulation of trimmed curved and flat panels using an (u,p) poroelastic FEM formulation. In *VA User Conference, Cologne*, 2007.

3. A. Duval, L. Dejaeger, J. Baratier, and J.-F. Rondeau. Structureborne and airborne Insertion Loss simulation of trimmed curved and flat panels using Rayon-VTM-TL : implications for the 3 D design of insulators. In *Congrès SIA Confort automobile et ferroviaire, Le Mans*, 2008.

4. A. Duval and al. Trim FEM simulation of a dash and floor insulator cut out modules with structureborne and airborne excitations. In *Acoustics'08, Paris*, 2008.

ABSTRACT

Internal Mean Flow Effects on the Bulk Acoustic Properties of Rigid Porous Media

Alan Cummings, Department of Engineering, University of Hull

When a reticulated porous medium is employed as a sound absorbent it is usually assumed that there is no mean fluid flow through its pores, even if the surface of the bulk material may be exposed to a mean flow. This assumption might be reasonable, as in the case of porous material used as an absorbent to cover the walls of an internal building space. However, in other situations such as acoustically lined flow ducts where the absorbent can be subjected to mean static pressure gradients, it is not at all obvious whether the effects of 'internal' mean flow – induced within the porous medium itself by pressure gradients – on its bulk acoustic properties can be ignored.

There are two main parts to this issue: first, the question of whether there is likely to be any significant mean flow in the porous medium in a particular situation, and secondly what the effects of this mean flow, on the bulk acoustic properties of the medium, might be. These two aspects of the problem may be treated separately: the mean fluid flow within the material can be calculated to good accuracy, in most situations, by ignoring the acoustic field, and the effects of internal mean flow on the bulk acoustic properties of a given porous medium can be calculated – assuming a suitable predictive model is available – from knowledge of the internal mean flow distribution within this material.

It is, perhaps, rather surprising that so little attention has been paid to the effects of internal mean flow on the bulk acoustic properties of porous media, judging from the dearth of journal publications on the subject over the past two decades. Given the extremely widespread use of porous materials in road vehicle exhaust silencers of the 'dissipative' type – for example – one wonders whether this apparent lack of interest has come about because investigators and designers have been confident in believing that internal mean flow is generally of no importance, or that this rather specialised aspect of design has simply passed them by.

Some years ago, the author and a co-worker [1,2,3] carried out an investigation into internal mean flow effects on the bulk acoustic properties of rigid-framed reticulated porous media and the consequence of these effects on the sound attenuation of dissipative flow duct silencers. It was shown that the steady-flow Ergun (or Forchheimer) equation, relating the gradient of the mean pressure in a reticulated porous material to the average fluid velocity, could be combined with an existing formulation for sound propagation in porous media containing zero mean flow to yield expressions for the bulk acoustic properties of the material in the presence of internal mean flow. Substantial deviations from the zero-flow properties were measured and predicted [1], even with internal mean flow speeds as low as 1-2 m/s. The quadratic velocity term in the Ergun equation was shown to be responsible for the mean flow effects. A further result was that mean fluid flow introduced anisotropy into the acoustic properties of a porous medium having inherently isotropic geometric structure. Good agreement was noted between predictions and measured data. The model derived in [1] was applied [2] to 'bulk-reacting' acoustic wall liners in circular section flow ducts of effectively infinite length. Fairly accurate predictions of fundamental mode parameters were reported (attenuation rate per unit length and phase speed), and quite small internal mean flow speeds (e.g. 0.72 m/s) were shown to have a significant effect on liner performance. The liner employed in the experiments [2] was directly exposed to the mean flow. In a later paper [3], internal mean flow effects in the liner were modelled in the case of finite length dissipative flow duct silencers of circular section. Again, the prediction accuracy of silencer attenuation was good and internal mean flow effects were significant, even for small internal mean flow velocities. It should be noted that, in [1-3], the mean flow within the porous medium was taken to be uniform.

Theoretical and experimental results from [1-3] are discussed in this presentation and placed in a more general context.

In 1995 Peat and Rathi [4], in a numerical study of finite length dissipative flow duct silencers (acoustically lined expansion chambers), examined the effects of internal mean flow in the absorbent. By the use of finite element formulations, they were able to model both the mean flow and acoustic fields in much more detail than had been possible in the work reported in [1-3]. They presented velocity field vector plots within the absorbent for two circular section silencers. These were particularly illuminating: in a silencer with a relatively large length/diameter ratio, the internal mean flow velocity in the absorbent was shown to be essentially uniform and axial, apart from a region immediately downstream of the

silencer inlet whereas, in the case of a 'short, fat' silencer, significant radial velocity components were evident, directed away from the axis prior to the mid-point of the silencer and toward the axis downstream of this point. These data illustrate well the validity of the uniform flow assumption. One drawback in this work is that knowledge of the axial pressure gradient in the central flow channel was required before the steady internal velocity field could be computed. On the other hand, several detailed and very useful comparisons were made, for example that the uniform-flow assumption entails little loss of prediction accuracy in the silencer performance.

Following the work of Peat and Rathi there appears, from the literature, to have been little interest in the effects of internal mean flow on the acoustics of porous media.

In addition to the acoustical aspect of induced mean flow within porous media is the purely fluid-mechanical problem of the effect of porous liners on steady flow in channels. Between the mid to late 1960s and the early 1970s, several articles appeared in the literature, relating to the boundary condition at the interface between a planar two-dimensional flow channel and a region of permeable material exposed to the flow in this channel. A seminal piece of work is that by Beavers and Joseph [5], which led to the (later eponymous) boundary condition at the porous/ fluid interface. In this, the existence of a boundary layer *within* the porous material, adjacent to the interface, is postulated, and furthermore it is assumed that the 'slip velocity' in the free fluid, at the interface, is proportional to the velocity gradient, normal to the flow, at the interface. This is the essence of the B&J boundary condition. The various articles including, and following, the Beavers and Joseph paper, are all concerned with *laminar* flow. The correct boundary condition in the case where the flow in the channel is *turbulent* does not appear, at least to the author's knowledge, to have been firmly established. Swim [6], *circa* 1977, reported an experimental investigation of axial pressure losses in air-conditioning ducts containing turbulent flow and lined with glass fibre blanket. The relative roughness heights (related to the commonly-used 'Moody chart'), inferred from the data, generally appear to be very high compared to those expected from galvanised steel duct walls.

The results of [5,6] suggest that, in a straight length of uniform duct with a porous lining, the axial pressure gradient is likely to be significantly higher than it would be if only the central flow channel, surrounded by smooth impervious walls, were to carry the flow. Measurements conducted by the author and co-workers bear this out and it is possible that the cause is principally mean flow losses within the liner itself. These data also showed that, if a perforated tube is placed between the central flow channel and the liner (as is often the case in dissipative silencers), axial pressure gradients can be significantly reduced, thereby reducing the internal mean flow effects in the liner.

An 'overview' of the consequences of internal mean flow effects on the acoustical properties of porous media is included in this presentation, with reference to the aforementioned work. Where appropriate, quantitative data will be presented and their significance highlighted.

References

1. A. CUMMINGS and I.-J. CHANG 1987 *Journal of Sound and Vibration* **114**, 565-581. Acoustic propagation in porous media with internal mean flow.
2. A. CUMMINGS and I.-J. CHANG 1987 *Acustica* **64**, 169-178. Internal mean flow effects on the characteristics of bulk-reacting liners in circular ducts.
3. A. CUMMINGS and I.-J. CHANG 1988 *Journal of Sound and Vibration* **127**, 1-17. Sound attenuation of a finite length dissipative flow duct silencer with internal mean flow in the absorbent.
4. K. S. PEAT and K. L. RATHI 1995 *Journal of Sound and Vibration* **184**, 529-545. A finite element analysis of the convected acoustic wave motion in dissipative silencers.
5. G. S. BEAVERS and D. D. JOSEPH 1967 *Journal of Fluid Mechanics* **30**, 197-207. Boundary conditions at a naturally permeable wall.
6. W. B. SWIM *ASRHAE Paper No. 2505, circa 1977*. Flow losses in rectangular ducts lined with fiber glass.

Optimising Open Porous Foam for Acoustical and Vibrational Performance

Abstract

Flexible porous foams with open cells are often used as sound absorbers and play an important part when trying to achieve good noise, vibration and harshness (NVH) comfort. In vehicle industry the additional weight and volume caused by adding porous materials is an important factor to minimise and thus efforts are made to achieve the best possible performance out of the added material. Using multiple layers of various open cell foam materials is often an efficient way to achieve good NVH comfort within limited bounds of added mass and volume, although very time consuming due to the extensive testing needed [1] to achieve good results. The ability to predict and optimise the acoustical behaviour of such multi-layered structures is clearly much needed.

For flexible open cell porous foams the vibroacoustic energy is carried both through the fluid in the pores (e.g. air) and through the solid frame material itself. The waves are strongly coupled and propagate simultaneously along the two paths with different amplitude and relative phase. The differences in amplitude and phase will transform some of the mechanical-acoustical energy into heat, mainly due to viscoelastic and viscoacoustic phenomena in the solid frame and at the interface between the solid frame and the fluid in the pores. The macroscopic, space averaged properties of the foam, such as bulk density, porosity, flow resistivity and Young's modulus, are traditionally used when modelling acoustic wave propagation through a porous medium. Through the work and theories of Biot [2], Allard [3], and Zwicker & Kosten [4], the macroscopic properties are used to calculate macroscopic space averaged quantities such as acoustic pressure, elastic stress, solid and fluid displacement. The microscopic properties of foam, such as pore size, strut length and strut thickness as well as the material properties of the frame material will together determine the macroscopic properties of the foam. Since the macroscopic properties are closely linked to the microscopic properties the former cannot be changed independently of each other. Thus to optimise the macroscopic properties is pointless as it would most likely result in a foam that is physically impossible to create. This stresses the need of scaling laws that relate the macroscopic properties of the foam to the underlying microscopic structural properties, which can be changed independently. Scaling laws for some of the macroscopic parameters have been proposed by e.g. Warren & Kraynik [5] [6], Göransson [7], and Gibson & Ashby [8].

This presentation deals with a computational method for designing optimal arrangements of multi layer noise and vibration treatments based on flexible, open cell porous foam. The method is based on finite element solutions to Biot's equations for poroelastic materials which are used to evaluate cost functions and gradients. The FE-model is then connected to an MMA optimiser (Method of Moving Asymptotes) [9], a gradient based optimiser that finds a minimum while using relatively few iterations. The porous materials are parameterised using scaling laws linking the microscopic properties to the averaged elasticity, flow resistivity and characteristic viscous and thermal lengths. The

cost function used is either in terms of total weight of the added material or in terms of the variational pressure response in a finite cavity, complemented with constraints on the other. The pressure response at different frequencies is weighted with a factor corresponding to A- or C-weighting and then summed over the entire frequency range to give a total sound pressure level. The optimisation process implied a non-convex behaviour, however with a limited amount of minima within the parameter range of interest as well as beneficial continuity around these minima, thus enabling a meaningful optimisation, though care must be taken when choosing the cost function, as this will greatly affect the outcome of the optimisation. The results suggest that fairly small changes of the microscopic properties of the foam may be sufficient to adapt the foam to a specific environmental condition and thereby achieve improved acoustic behaviour as well as reduced weight.

References

[1] Simon, F., Pauzin, S. & Biron, D. 2005 Optimisation of sandwich trim panels for reducing helicopter internal noise. *30th European Rotorcraft Forum.* 2005;**2005**:1025-1033.

[2] Biot, M. A. 1956 Theory of propagation of elastic waves in a fluid-saturated porous solid. Part I: Low frequency range and Part II: Higher frequency range. *Journal of Acoustical Society of America.* 1956; **28**:168-178 and **28**:179-191.

[3] Allard, J.F. 1993 *Propagation of sound in porous media: modeling sound absorbing materials.* New York: Elsevier Applied Science. [ISBN 0-387-98319-8].

[4] Zwicker, C. & Kosten, C. 1949 *Sound absorbing materials,* ch. I and II. Amsterdam: Elsevier Publishing Company.

[5] Warren, W. E. & Kraynik, A. M. 1988 The linear elastic properties of open cell foams. *J. Appl. Mech.*, 1988:**55**(2):341-346.

[6] Warren, W. E. & Kraynik, A. M. 1997 Linear elastic behaviour of a low-density Kelvin foam with open cells. *J. Appl. Mech.*, 1997:**64**(4):787-794.

[7] Göransson, P. 2005 Acoustic and vibrational damping in porous solid. *Philosophical Transactions of the Royal Society A.* 2006; **364**:89-108.

[8] Gibson, L. J. & Ashby, M. F. 1988 *Cellular solids, structure and properties,* pp. 184-192. Oxford UK: Pergamon Press.

[9] Svanberg, K. 1987 The method of moving asymptotes – a new method for structural optimization. *International Journal for Numerical Methods in Engineering.* 1987; **24**:358-373.